AD-A236 241

(2)

ONR-307 Experiment on the Combined Release and Radiation Effects Satellite (CRRES)

DTIC

Interim Technical Report

Prepared for The Office of Naval Research
Space Physics Program
Under Contract N00014-83-C-0476

March 1, 1991

DEFENSE TECHNICAL INFORMATION CENTER
9100603

Lockheed
Research & Development Division
LOCKHEED MISSILES & SPACE COMPANY, INC.
Palo Alto, California 94304

91 5 28 056

DISCLAIMER NOTICE

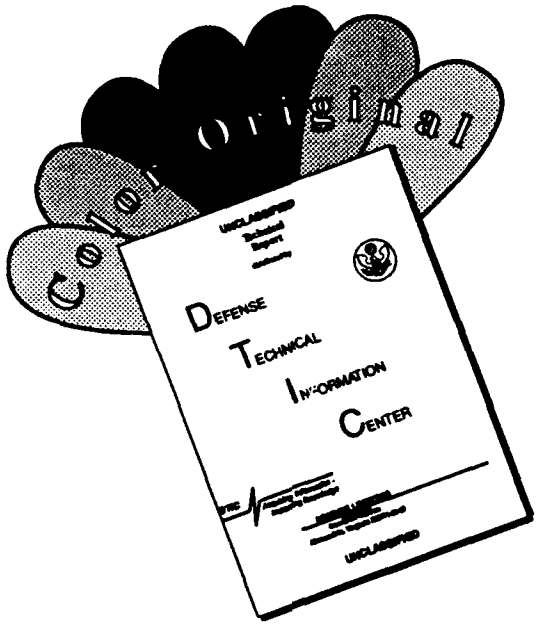

THIS DOCUMENT IS BEST QUALITY AVAILABLE. THE COPY FURNISHED TO DTIC CONTAINED A SIGNIFICANT NUMBER OF COLOR PAGES WHICH DO NOT REPRODUCE LEGIBLY ON BLACK AND WHITE MICROFICHE.

SECURITY CLASSIFICATION OF THIS PAGE (When Data Entered) UNCLASSIFIED

REPORT DOCUMENTATION PAGE

READ INSTRUCTIONS BEFORE COMPLETING FORM

1. REPORT NUMBER
2. GOVT ACCESSION NO.
3. RECIPIENT'S CATALOG NUMBER

4. TITLE (and Subtitle)
ONR-307 Experiment on the Combined Release and Radiation Effects Satellite (CRRES)

5. TYPE OF REPORT & PERIOD COVERED
INTERIM Technical Report
July 1988 - March 1991

6. PERFORMING ORG. REPORT NUMBER

7. AUTHOR(s)
R.M. Robinson
R.R. Vondrak

8. CONTRACT OR GRANT NUMBER(s)
N00014-83-C-0476

9. PERFORMING ORGANIZATION NAME AND ADDRESS
Lockheed Missiles and Space Co.
Dept. 91-20, Building 255
3251 Hanover St.
Palo Alto, CA 94304

10. PROGRAM ELEMENT, PROJECT, TASK AREA & WORK UNIT NUMBERS
4149169

11. CONTROLLING OFFICE NAME AND ADDRESS
R. Gracen Joiner
Office of Naval Research
800 North Quincy St.
Arlington, VA 22217

12. REPORT DATE
1 March 1991

13. NUMBER OF PAGES

14. MONITORING AGENCY NAME & ADDRESS(if different from Controlling Office)

15. SECURITY CLASS. (of this report)
Unclassified

15a. DECLASSIFICATION/DOWNGRADING SCHEDULE

16. DISTRIBUTION STATEMENT (of this Report)
Statement "A". Distribution unlimited.

17. DISTRIBUTION STATEMENT (of the abstract entered in Block 20, if different from Report)

18. SUPPLEMENTARY NOTES
CRRES is a joint NASA/DoD space experiment.

19. KEY WORDS (Continue on reverse side if necessary and identify by block number)
Radiation belts, CRRES satellite, energetic particles, magnetospheric storms

20. ABSTRACT (Continue on reverse side if necessary and identify by block number)
The Combined Release and Radiation Effects Satellite (CRRES) was successfully launched on July 25, 1990 on an Atlas I booster. Its geosynchronous transfer orbit with an apogee of 35,786 km makes it an ideal platform to study problems related to the radiation belts and its effects on spacecraft systems. The instrumentation on CRRES can be broadly divided into three categories: (1) engineering experiments, (2) radiation belt experiments, and (3) plasma and fields experiments. Over the past seven years the Lockheed Space Sciences Laboratory under sponsorship from The Office of Naval Research designed,

DD FORM 1 JAN 73 1473 EDITION OF 1 NOV 65 IS OBSOLETE

developed, tested and delivered a set of instruments referred to as ONR-307. The ONR-307 payload consists of three different types of instruments that acquire data on the composition of the plasma in the energy range from 0.5 to 1000 keV and on energetic electrons from 20 to 5000 keV and protons from 500 keV to 100 MeV. The data from these instruments provide important information for modeling radiation belt particle populations and understanding the sources and losses of these particles. The ONR-307 instruments were initialized by August 7, 1990 and have been operating flawlessly throughout the CRRES mission. Initial results show that the data quality is excellent. A period of high magnetic activity in late August has been selected for detailed study by the CRRES science team. Data analysis is continuing and future efforts will concentrate on the validation of the data and coordinated measurements with other CRRES instruments.

TABLE OF CONTENTS

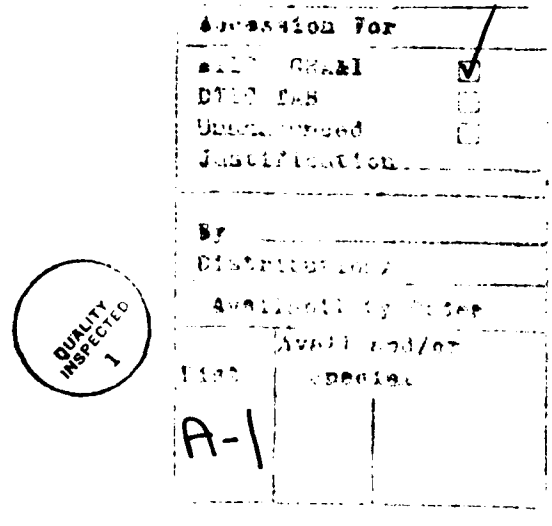

I. Introduction

The Combined Release and Radiation Effects Satellite (CRRES) was successfully launched on July 25, 1990 on an Atlas I booster, achieving a geosynchronous transfer orbit with an apogee of 35,786 km and a perigee of 350 km. The primary objectives of the CRRES mission are to determine the effects of the radiation environment on a broad range of microelectronics components and to make a comprehensive set of measurements that can be used in the development of improved radiation belt models. Additionally, the CRRES satellite carries chemical canisters that are released at various times during the mission to aid in the study of magnetospheric and ionospheric plasma processes. CRRES is a joint NASA/DOD program with the DOD primarily responsible for the radiation belt studies and NASA responsible for the chemical release campaigns.

Among the instruments on CRRES is the ONR-307 payload which consists of four instruments to be operated continuously in support of U. S. Navy objectives. Specifically, these objectives are to obtain the necessary plasma composition and energetic particle data over an extended period of time and with sufficient pitch angle resolution throughout Earth's radiation belts such that accurate environmental models, suitable for engineering purposes, can be constructed.

This report summarizes the operation of the CRRES satellite and ONR-307 payload during the first six months of the mission. The CRRES mission objectives are described in Section II. Section III describes the specific objectives of the ONR-307 experiment. The CRRES orbit, and spacecraft performance are discussed in Section IV. Section V reviews the initialization procedure and status of the ONR-307 payload and Section VI describes some of the data that have been obtained thus far. In Section VII we discuss future plans for the operation and data analysis of the ONR-307 experiment.

II. The CRRES Mission

One of the most important life-limiting elements of DoD reconnaissance, communication and manned platforms in space is the radiation environment. Current program requirements demand operational spacecraft lifetimes of 5 to 10 years in near-earth orbit. Such long operational lifetimes require that considerable attention be given to shielding and radiation-hardening of electronic parts. Military space systems must also be designed to survive the even more extreme radiation effects from nuclear weapon bursts in space. Radiation shielding creates significant weight and cost impacts on many DoD missions. Uncertainties in the

amount of shielding leads to conservative design practices which adversely impact available payload weight capability.

Our present understanding of the earth's radiation belts, based on three decades of measurements, has been synthesized by the National Space Science Data Center into models of the electron and proton populations that provide the principal threat to satellites. For several reasons the accuracy of these models in defining the environment that a particular satellite mission will encounter is only good to a factor of 3, i.e. a 300 percent uncertainty. Of the many factors responsible for this large uncertainty, the most significant are the dynamics of the radiation belts with solar activity, the limited region of space and temporal duration covered by the measurements, and the variability in the capabilities and accuracy of the measuring instrumentation. To significantly improve on the current radiation belt models, therefore, all of these limitations must be improved upon. The unique orbit of the CRRES mission, the comprehensive set of measurements to be made and the three-year mission duration provide great promise for substantial improvements in future radiation belt modeling.

It is important to clearly understand the elements necessary for the improvement of radiation modeling for DoD purposes. The first of these elements involves the type of orbits used by the military for photo and electromagnetic reconnaissance, for communications and for planned manned observatories. These orbits and their relationship to the earth's inner and outer trapped radiation belts are depicted in Figure 1. The principal orbit used by the United States and the Soviet Union for land and ocean reconnaissance is the low-altitude polar orbit, designated as LEO in the figure. Communications from earth-to-satellite heavily utilize the synchronous (SYNC) and high-earth orbits (HEO). The radiation dose received in each of these orbits comes from different regions of the trapped radiation belts. The type and energy of the particles providing the dose is also different in the respective orbits. For example, the principal natural threat to a SYNC orbit vehicle is from the intense flux of electrons, while the principal threat to the LEO orbit comes from the very energetic protons in the inner radiation belt in the vicinity of the South Atlantic Anomaly. The radiation intensity increases with altitude on a given field line and the maximum intensity is reached at the geomagnetic equator. In Figure 1 notice that the HEO orbit transits the same magnetic field lines as the SYNC orbit but at lower altitude. Because the particle distributions at geosynchronous orbit are not isotropic, the precipitating fluxes that reach low altitudes will be substantially less than those at high altitudes. On the other hand, the HEO orbit transits the inner belt at higher altitudes than the LEO orbit. The HEO orbit is therefore very complex in terms of the radiation environment and the modeling effects on spacecraft systems.

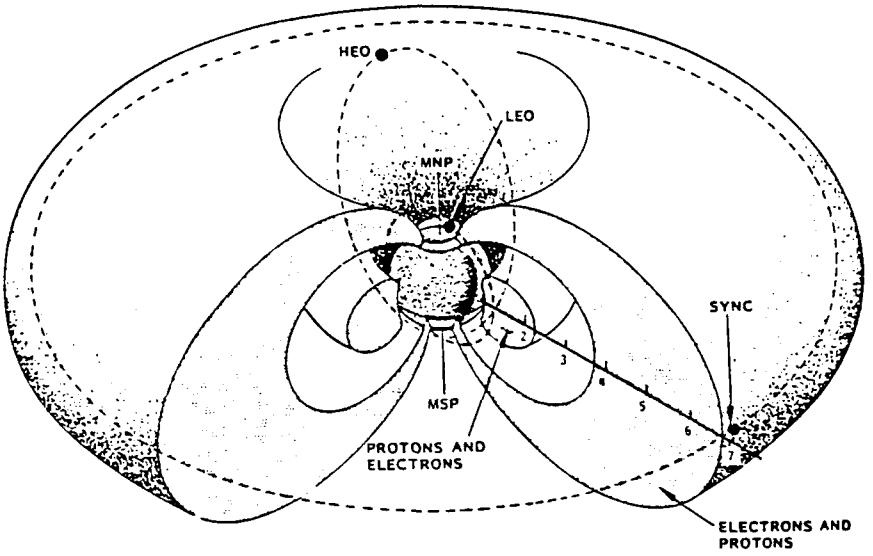

Figure 1 The earth's radiation belts showing the inner and outer portions, the locations at which radiation dose levels are most severe. The three common types of satellite orbits, HEO, LEO, and SYNCH, traverse these regions at different altitudes.

Because of the variety of orbits used by the DoD and the complexity of the radiations encountered it is essential that a comprehensive radiation-measuring payload include:

1) Discrimination of the various particle types and masses, i.e. electrons, protons, and heavy ions.

2) Measurement of the energy spectra of the various particle species since this directly translates into the penetrating power through shielding.

3) Complete pitch angle coverage with good angular resolution because this provides the ability to map particles down the field lines from the point of observation. Measurements of the complete pitch angle distribution at the geomagnetic equator from 0° (along the field line) to 90° (perpendicular to the field line) with good angular resolution completely define the entire particle population on that field line at all altitudes.

4) The ability to sample all of the magnetic field lines as close to the geomagnetic equator as possible since this will define the environment of the entire radiation belts.

5) Nearly continuous temporal coverage over a period of several years to provide statistically meaningful flux measurements over the highly dynamic variations experienced as a result of solar and geomagnetic storms and substorms.

CRRES was originally planned to be carried out in two phases following a shuttle launch. The NASA phase of the mission, planned for execution in low earth orbit, was to consist of several chemical releases in combination with onboard diagnostic instrumentation, measurements from other satellites, and ground-based observation. Following the NASA phase of the mission, the spacecraft was to be boosted to geosynchronous transfer orbit to initiate the DOD phase. After the Challenger accident the CRRES spacecraft was reconfigured to fit on an expendable launch vehicle in order to allow the earliest possible launch. Because of this the low earth orbit phase of the mission was eliminated and the number of NASA chemical releases was reduced from 48 to 24.

III. The ONR-307 Experiment

Under sponsorship from the Office of Naval Research, the Lockheed Space Sciences Laboratory designed, developed, tested and delivered a set of instruments referred to as ONR-307. The organization chart for the ONR-307 project at Lockheed is shown in Figure 2. Each instrument scientist with the aid of participating scientists is responsible for the operation, data analysis and science related to that instrument. The project scientist and co-principal investigators are responsible for seeing that the overall science objectives are realized.

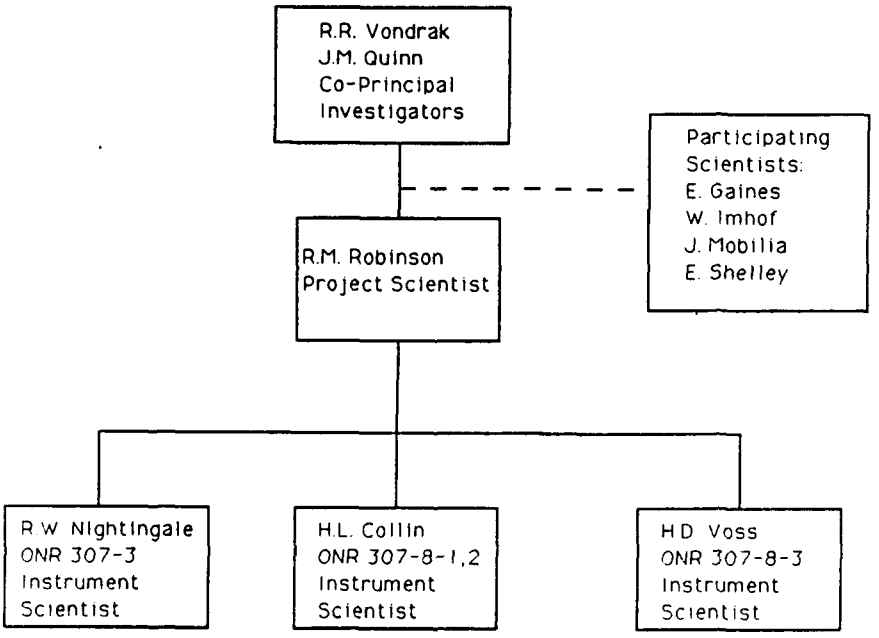

Figure 2: Key personnel responsible for ONR-307 at Lockheed.

The overall objective of the ONR-307 experiment is to obtain necessary data to construct predictive models, suitable for engineering purposes, of the energetic particle and plasma environment in those regions of space of primary interest to the Department of Defense satellite operations. Two critical components of that environment will be investigated:

1) The energetic magnetospheric plasma, including the composition of that plasma, in the energy range from 0.5 to 1000 keV. This component of the space environment is the principal cause of spacecraft surface charging, degradation of spacecraft thermal control surfaces and other sensitive surfaces, and ionospheric disturbance phenomena that disrupt critical communications paths. A critical parameter of this plasma is the composition of the ion component. Because of limitations in available satellite instrumentation, measurement of this parameter has only recently begun. The comprehensive data required for an environmental model are not yet available and a principal objective of this experiment is to provide a data base suitable for this purpose.

2) Energetic electrons in the energy range 20 to 5000 keV and protons in the range 500 keV to 100 MeV. These energetic trapped components of the radiation belts penetrate deeply into spacecraft systems where they cause degradation of microelectronic components, charging/discharging of internal dielectrics such as coaxial cables, CMOS devices etc., and ultimately limit mission lifetime. These electrons are precipitated out of the radiation belts into the atmosphere/ionosphere at varying rates as a result of resonant interactions with natural and man made electromagnetic waves. The precipitated component enhances the ionization of the D and E region ionosphere and can disrupt communications from ELF to HF of vital interest to the United States Navy. Electromagnetic waves from USN-operated high power VLF transmitters contribute to the precipitation of electrons from the inner magnetosphere in this energy range. These dynamical processes result in a high degree of variability in the electron population in the magnetosphere, making long-term predictive modeling difficult. A prime objective of this experiment is therefore to study these wave-particle interactions throughout the magnetosphere to acquire the data base for improved predictive models. To achieve the objectives of this investigation energetic electron and ion measurements of the entire particle distribution function must be acquired with good mass, temporal, spatial and energy resolution. For best results, the resolutions should be adjustable to optimize the data acquired over a broad range of satellite altitudes and source intensities.

The measurement capabilities of the ONR-307 instruments are summarized in Table 1. Weight, power, and other specifications are given in Table 2. The three instruments are described briefly in the following subsections and in more detail in Appendices 1,2, and 3.

TABLE 1: ONR-307 PAYLOAD SUMMARY

Instrument	Measured Quantity	Energy	Sensor Angle to Spacecraft Spin Axis
ONR-307-3 SEP	Electrons Protons	20 - 5000 keV 0.5 -100 MeV	40°, 60°, 80°
ONR-307-8-1,2 IMS-LO	Ion Composition Electrons	E/q = 0.1 -32 keV 0.05 - 25 keV	45°, 75°
ONR-307-8-3 IMS-HI	Ion Composition	EM/q^2 = 20 - 800 keV-AMU/e^2	75°

TABLE 2: ONR-307 SPECIFICATIONS

#	ITEM	307-3-1 (SENSOR)	307-3-2 (ANAL)	307-8-1	307-8-2	307-8-3	TOTALS
1	PACKAGE ONR DESIGNATION						
2	PACKAGE ACRONYM	SEP-SP	SEP-AP	IMS-L01	IMS-L02	IMS-HI	-
3	ENVELOPE DRAWING NUMBER	11503E	11404F	11405E	11405E	11759Ø D	-
4	LOOK DIRECTION(S) (SPIN AXIS = 0°)	40;60;80	-	45	75	75	-
5	WEIGHT (LBS)	15.0	8.5	14.4	14.4	23.6	75.9
6	POWER (W)	-	8.8	6.0	6.0	7.5	28.3
7	DATA						
	-SCIENCE WDS PER .128S MINOR FRAME	-	19	7	7	9	42
	-STATUS WDS PER 4.096S MAJOR FRAME	-	15	1	1	8	25
	-TOTAL DATA WDS PER 1.024S	-	155.75	56.25	56.25	74	342.25
	-TOTAL DATA WDS PER SECOND	-	152.10	54.93	54.93	72.27	334.23
	-TM BITS PER 1.024S	-	1246	450	450	592	2738
	-TM BITS PER SECOND	-	1216.8	439.45	439.45	578.12	2673.82
	-ANALOG	-	11	5	5	7	28
	-BILEVELS	-	5	4	4	5	18
8	COMMANDS						
	-16 BIT SERIAL	-	1	1	1	1	4
	-LOW LEVEL DISCRETES	-	7	2	2	4	15
	-HIGH LEVEL DISCRETES	-	2	2	2	2	8

III.1 ONR-307-3 Spectrometer for Electrons and Protons (SEP)

The Spectrometer for Electrons and Protons (SEP), designated ONR-307-3, measures electrons in the energy range 20 - 5000 keV and protons in the range 0.5 - 100 MeV. The energy ranges are covered with fine, programmable energy resolution. Very good pitch angle resolution is provided by 3 degree FWHM collimation. In order to obtain nearly complete pitch angle coverage over the CRRES orbit, the instrument uses three identical particle telescopes, mounted at carefully optimized angles to the spacecraft spin axis. Each telescope uses a stack of surface-barrier silicon detectors with active anticoincidence shielding. Various logic combinations of the detector elements determine the particle types and energy ranges that are measured. The SEP instrument is based on the highly successful SC-3 instrument developed for ONR and flown on SCATHA. The SC-3 instrument continues to operate after more than 13 years on orbit. Figure 3 shows the SEP instrument, consisting of the sensor package with three particle telescopes, the analyzer package, and the interconnect cable. A more detailed description of this instrument, its capabilities, and measurement goals is included as Appendix 1.

III.2 ONR-307-8-1, 2 Low Energy Ion Mass Spectrometer (IMS-LO)

The Low Energy Ion Mass Spectrometers (IMS-LO), designated ONR-307-8-1 and ONR-307-8-2, are two identical instruments which measure ion composition in the energy range E/q = 0.1 -32 keV/e. The two instruments are mounted at different angles to the spacecraft spin axis in order to optimize pitch angle sampling. The IMS-LO instruments use crossed electric and magnetic field Wien filters, followed by 180 degree electrostatic analyzers and channeltron sensors to determine ion energy/charge and mass/charge. Three parallel analyzers are used within each instrument to cover different segments of the full energy range. The instruments may be commanded to sweep through the full mass range to alternately lock on any four selected masses, or to alternate between the two modes. In addition to the ion measurements, IMS-LO uses magnetic analyzers to measure the electron background fluxes at eight energy steps between 50 eV and 25 keV.

The IMS-LO instruments are derived from the extremely successful instruments developed for the Office of Naval Research for flight on S3-3 and SCATHA. Figure 4 shows one of the two IMS-LO instruments. The three large circular openings are the entrance apertures to the ion collimators. Four smaller cylindrical electron collimators are visible on the right. The instrument is described in more detail in Appendix 2.

III.3 ONR-307-8-3 Medium Energy Ion Mass Spectrometer

The Medium Energy Ion Mass Spectrometer (IMS-HI), designated ONR-307-8-3, measures ion composition in the energy range EM/q^2 = 20 - 8000 keV-AMU/e^2. The instrument is a novel design based on ion momentum separation in a magnetic field. The ions are dispersed onto an array of six passively cooled silicon solid state detectors. Energy and mass defect analysis is performed in parallel processing electronics, allowing simultaneous measurements by each of the detectors. The instrument can be operated in two basic modes, providing full mass coverage every eight seconds or sampling of four selected ions every half second. Figure 5 shows the IMS-HI instrument. The top part of the instrument comprises the ion optics, detectors, and radiator surfaces. The square hole on the left of the figure is the entrance aperture. The bottom portion is processing electronics. A detailed description of the instrument is contained in Appendix 3.

IV. CRRES: Instrumentation, Orbital Operations, and Status

The instrumentation on CRRES can be broadly divided into three categories: (1) engineering experiments, (2) radiation belt experiments, and (3) plasma and fields experiments. The instruments in each category are listed in Table 3 along with the approximate date on which they began normal operations. A list of investigators and institutions involved with each of the experiments is given in Table 4.

The primary engineering experiment is the High Efficiency Solar Panel whose purpose is to test the tolerance of gallium arsenide solar cells to radiation and high temperature. Another important engineering experiment is the microelectronics package which monitors the performance of various electronic components to quantitatively assess their performance in the radiation belt environment. This environment is continuously monitored with the energetic particle experiments which are listed separately in Table 3. Figure 6 indicates the energy range over which the particles are detected. Note that many energy ranges are redundantly measured by two or more instruments. This enables the data to be verified through intercalibration. The plasma and field measurements provide information about the low energy particle fluxes and electric and magnetic fields that control the motion of magnetospheric particles. The vector magnetic field measured by the magnetometer is also used to determine the pitch angle of the particles.

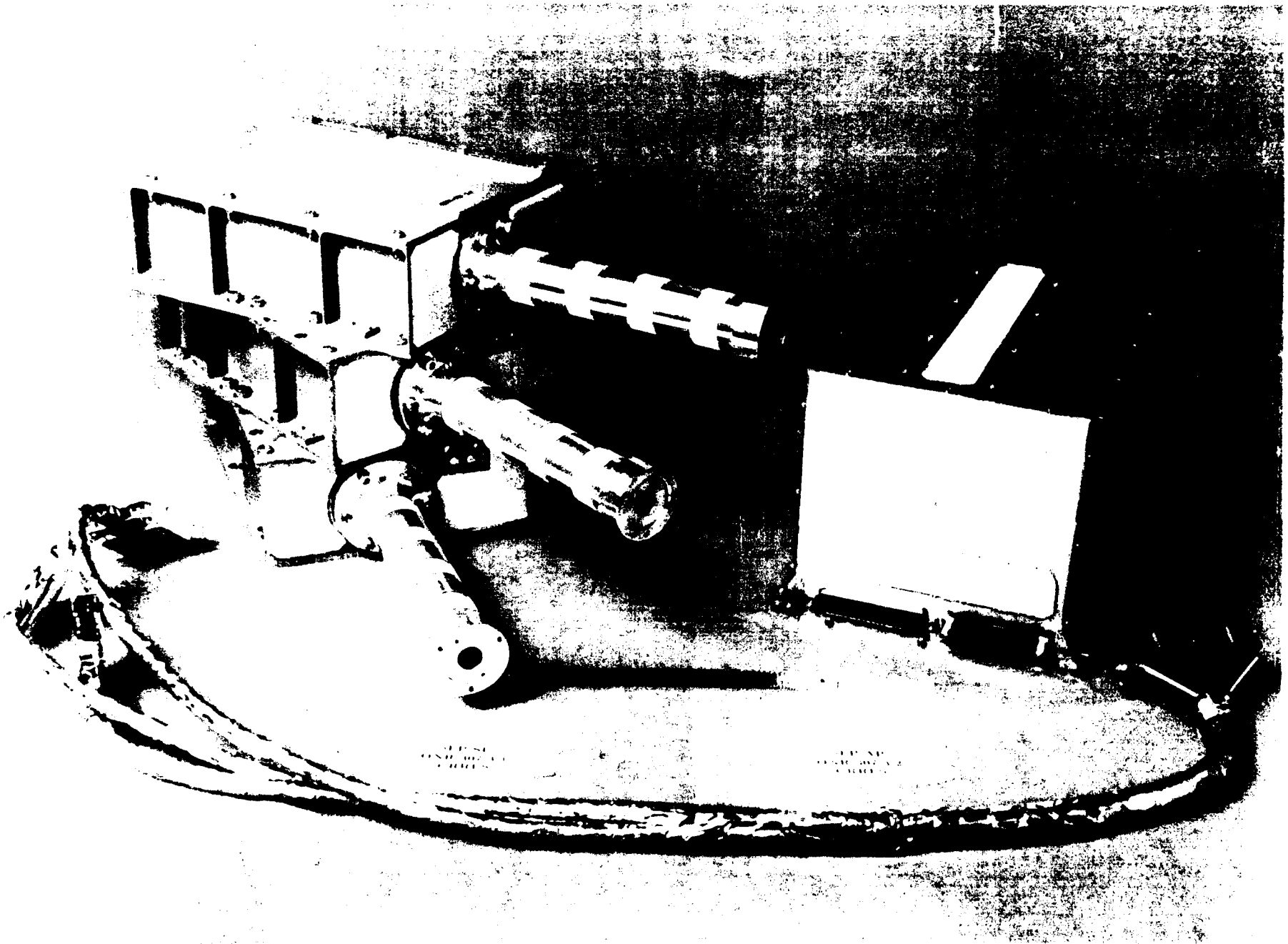

Figure 3 Spectrometer for Electrons and Protons

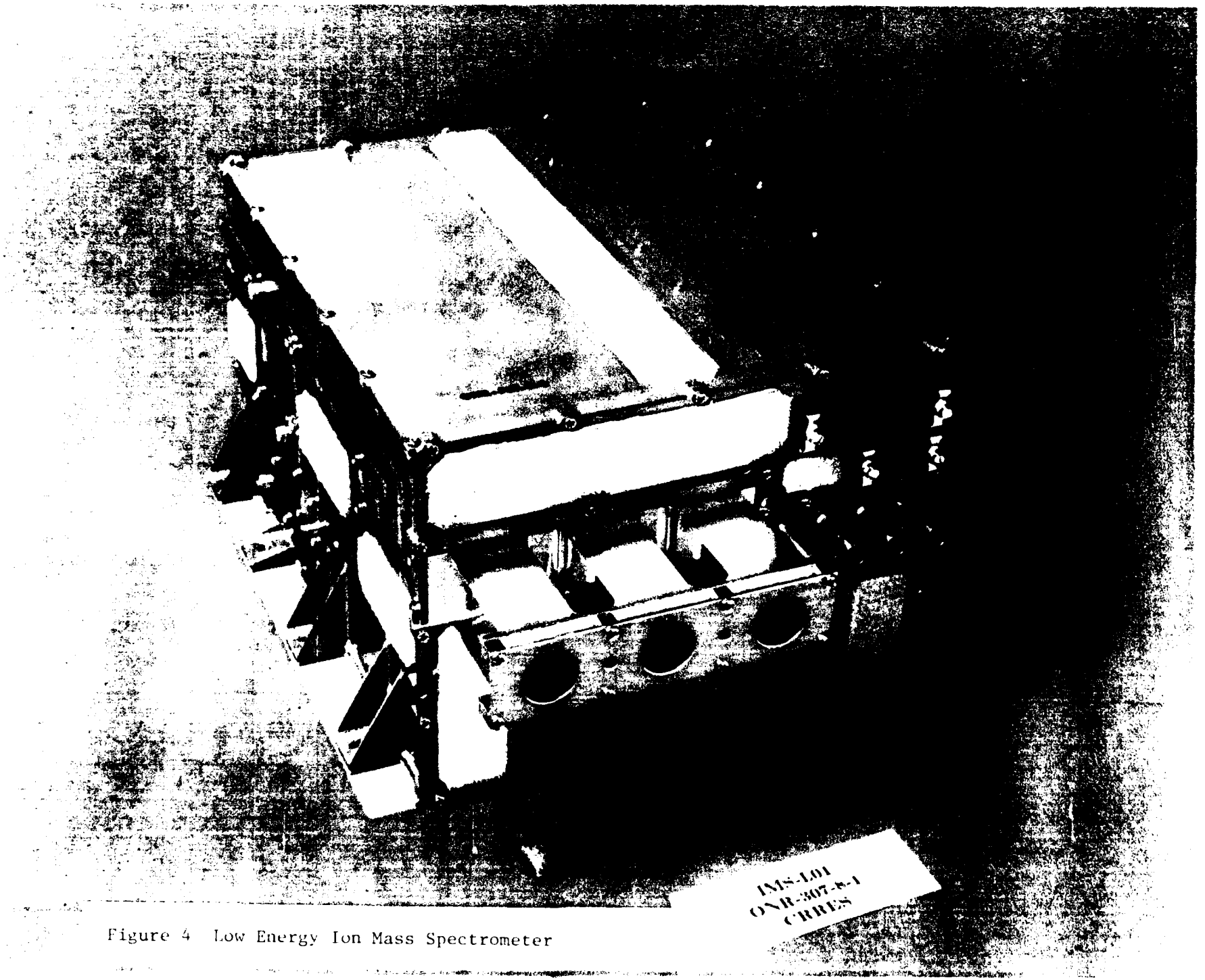

Figure 4 Low Energy Ion Mass Spectrometer

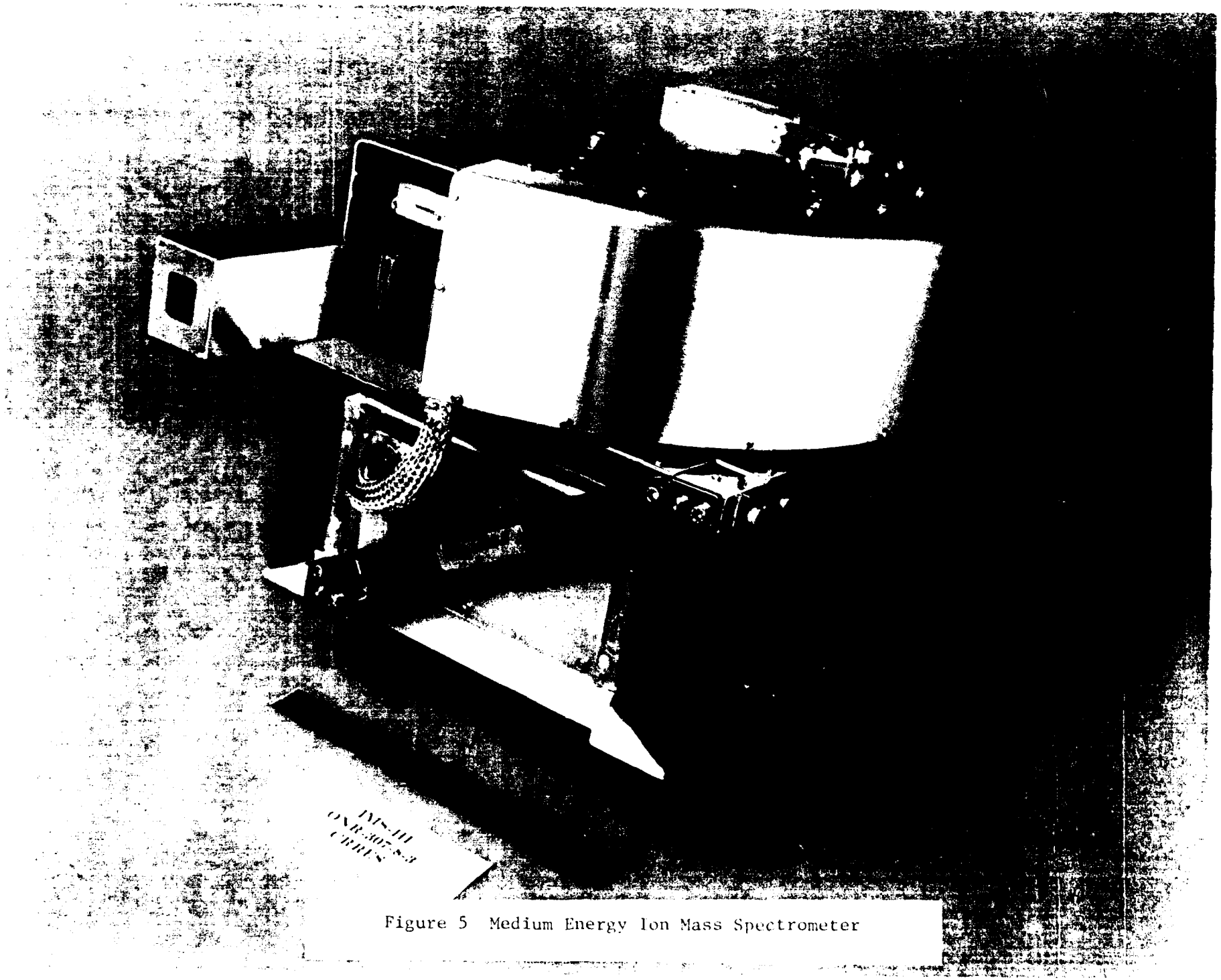

Figure 5 Medium Energy Ion Mass Spectrometer

TABLE 3: CRRES INSTUMENTATION

	Experiment	Date Initialized
Engineering Experiments		
AFGL-701-1A	Microelectronics Package	27 July
AFGL-701-1B	Internal Discharge Monitor	30 July
AFAPL-801	Gallium Arsenide Solar Cells	Launch
Energetic Particles		
AFGL-701-6	Low Energy Plasma Analyzer	21 Aug
AFGL-701-5A, B	Medium energy electron and proton spectrometers	30 July
AFGL-701-8, 9	Proton Telescope	30 July
AFGL-701-7a	Cerenkov Counter	21 Aug
AFGL-701-7b	Proton Switches	30 July
AFGL-701-11a	Heavy Ion Telescope	31 July
AFGL-701-11b	Medium energy mass ion composition spectrometer	1 Aug
AFGL-701-11c	Low energy mass ion composition spectrometer	21 Aug
AFGL-701-2	Space Dosimeter	27 July
AFGL-701-3	MOS Dosimeter	27 July
AFGL-701-4	High Energy Electron Spectrometer	27 July
ONR-307-3	Spectrometer for electrons and Protons	7 Aug
ONR-307-8-1,2	Low energy ion mass spectrometer	4 Aug
ONR-307-8-3	High energy ion mass spectrometer	4 Aug
Plasma, Fields, & Waves		
AFGL-701-13-1	Fluxgate Magnetometer	31 July
AFGL-701-14	Lanmuir Probe	1 Aug
AFGL-701-15	Passive Plasma Sounder	1 Aug

TABLE 4: CRRES INVESTIGATORS AND ORGANIZATIONS

AFGL 701 Space Radiation Experiment (SPACERAD)
P. I.: E. G. Mullen, Geophysics Laboratory, Hanscom Air Force Base

701-1B	Robb Fredrickson	Geophysics Laboratory
701-1A,-3	J. C. Ritter	Naval Research Laboratory
701-2,-4,-6, -8,-9	David Hardy	Geophysics Laboratory
	Alan Johnstone	Mullard Space Sciences Laboratory
01-5,-7,-11	Al Vampola	
	Theodore Fritz, David Young	Los Alamos National Laboratory
	Berand Wilken, Axel Korth	Max Planck Institute for Aeronomie
701-13,14,15	Bill Sullivan	Geophysics Laboratory
	Roger Anderson, Don Gurnett	University of Iowa
	Forrest Mozer	University of California at Berkeley
	Howard Singer	Geophysics Laboratory

ONR 307 Energetic Particles and Ion Composition
Co-P.I.'s: Richard Vondrak and Jack Quinn, Lockheed Palo Alto Research Laboratory

307-3	Richard Nightingale	Lockheed Palo Alto Research Laboratory
307-8-1,2	Harry Collin	Lockheed Palo Alto Research Laboratory
307-8-3	Hank Voss	Lockheed Palo Alto Research Laboratory

NRL 701 Low Altitude Satellite Studies of Ionospheric Irregularities (LASSII)
P. I.: Paul Rodriguez, Naval Research Laboratory

P3	Chung-san Lin	Naval Research Laboratory
QIMS	Don Hunton	Geophysics Laboratory
VLFWA	Harry Koons	The Aerospace Corporation

ONR 604 Isotopes in Solar Flares
P. I.: John Simpson, University of Chicago
Co-I.: Moises Garcia-Munoz, University of Chicago

AFAPL 801 High Efficiency Solar Panel Experiment (HESP)
P. I.: Terry Trumble, Air Force Wright Aeronautical Laboratories

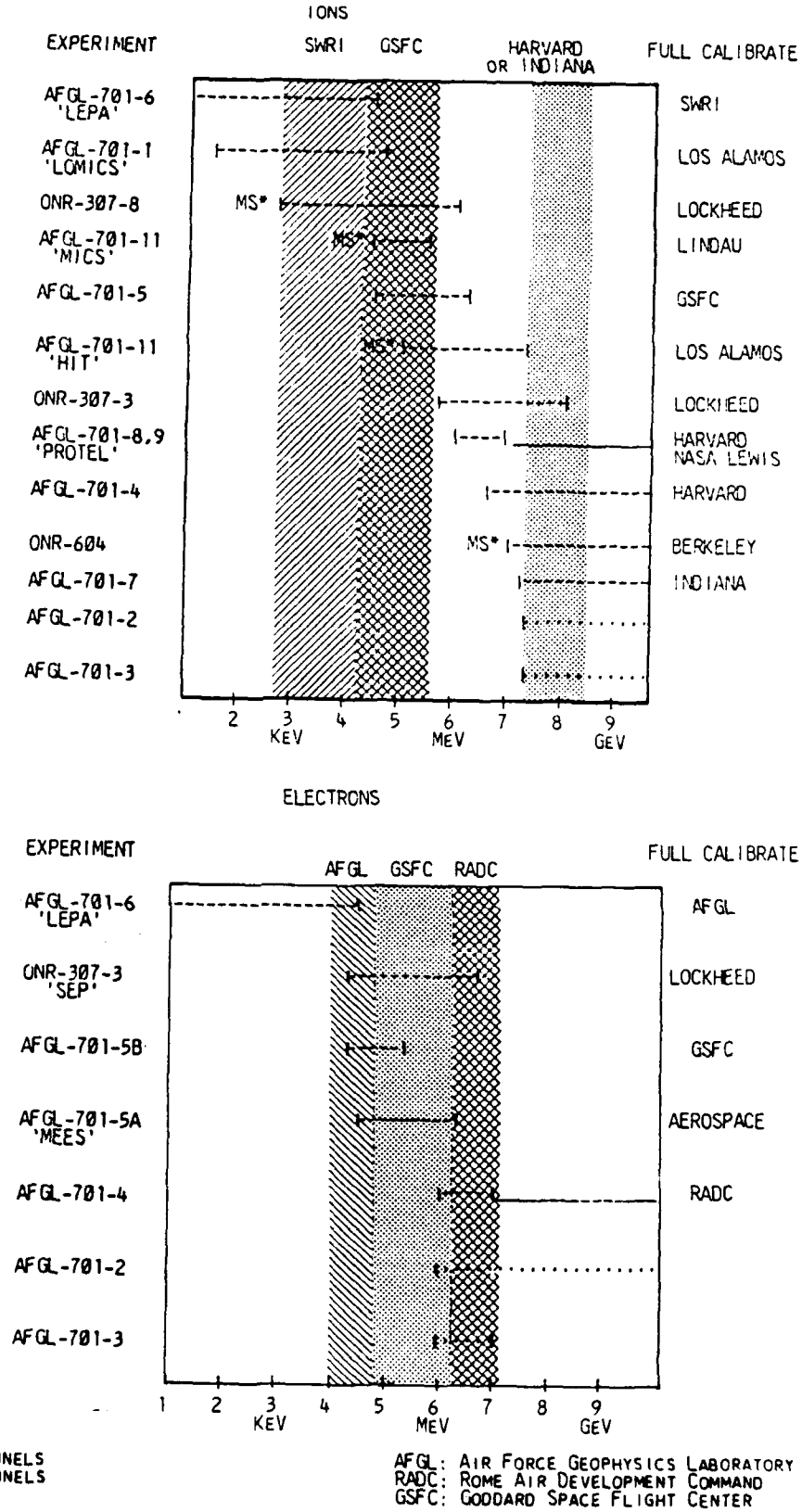

Figure 6 CRRES particle experiments and the energy ranges over which they operate. Calibration facilities are shown at right.

CRRES also contains a set of instruments that are only operated near perigee to study ionospheric irregularities (Low Altitude Satellite Studies of Ionospheric Irregularities - LASSII). The NRL-701 experiment consists of the Pulsed Plasma Probe, the Very Low Frequency Wave Analyzer, and the Quadrupole Ion Mass Spectrometer (QIMS). There was indication early in the mission that the QIMS door did not deploy and repeated attempts to open it failed. Late in 1990, it was determined that the door had opened, at least partially, and some data were being obtained. LASSII mode is to be used every other orbit for 35 minutes within 3000 km of perigee during part of the mission, every fourth orbit for 15 minutes within 1000 km of perigee for the remainder of the mission, and during low altitude dawn and dusk chemical releases. In the LASSII mode of operation the data from most of the radiation belt experiments are not included in the telemetry stream. Of the Lockheed instruments, SEP is the only one that receives data in the LASSII mode.

The CRRES orbit parameters are given in Table 5. The Atlas I booster performed poorer than expected and the achieved orbit apogee was 2200 km below the nominal value. Although this impacted the planning of the chemical release campaigns, it is expected to have little effect on the radiation belt experiments. The spacecraft is oriented with its spin axis pointing approximately toward the sun. This keeps the solar panels exposed to sunlight continuously except during eclipses. Figure 7 shows how the local time of perigee precesses with time. At launch apogee was at 10:00 A. M. and the precession is toward earlier local times. Figure 8 shows the approximate duration of eclipses. The longest eclipses were in late December and early January when apogee was near midnight. Eclipses will be negligible until the end of March, 1991 when eclipse durations exceeding one hour will again occur. Figures 7 and 8 were duplicated from a report produced by R. Hopkins of The Aerospace Corporation.

TABLE 5. CRRES ORBIT AND ATTITUDE

APOGEE ALTITUDE	33510± 60 km (6.3 Re radial distance)
PERIGEE ALTITUDE	340± 40 km
ECCENTRICITY	.712± .002
INCLINATION	18°± 0.2°
SPIN RATE	~2.0 RPM
ORIENTATION	Spin Axis Maintained Between 5° + 15° from Sun
ORBITAL PERIOD	9.85 hrs

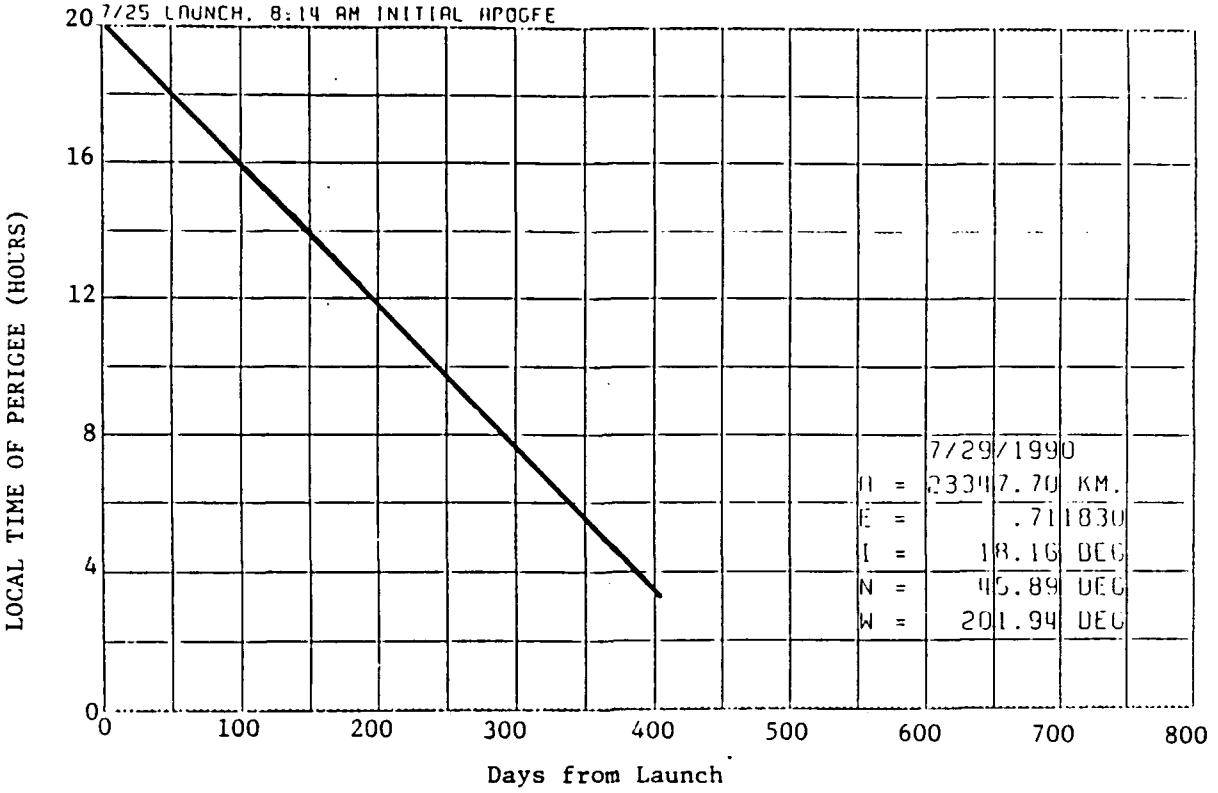

Figures 7. Precession of the local time of perigee.

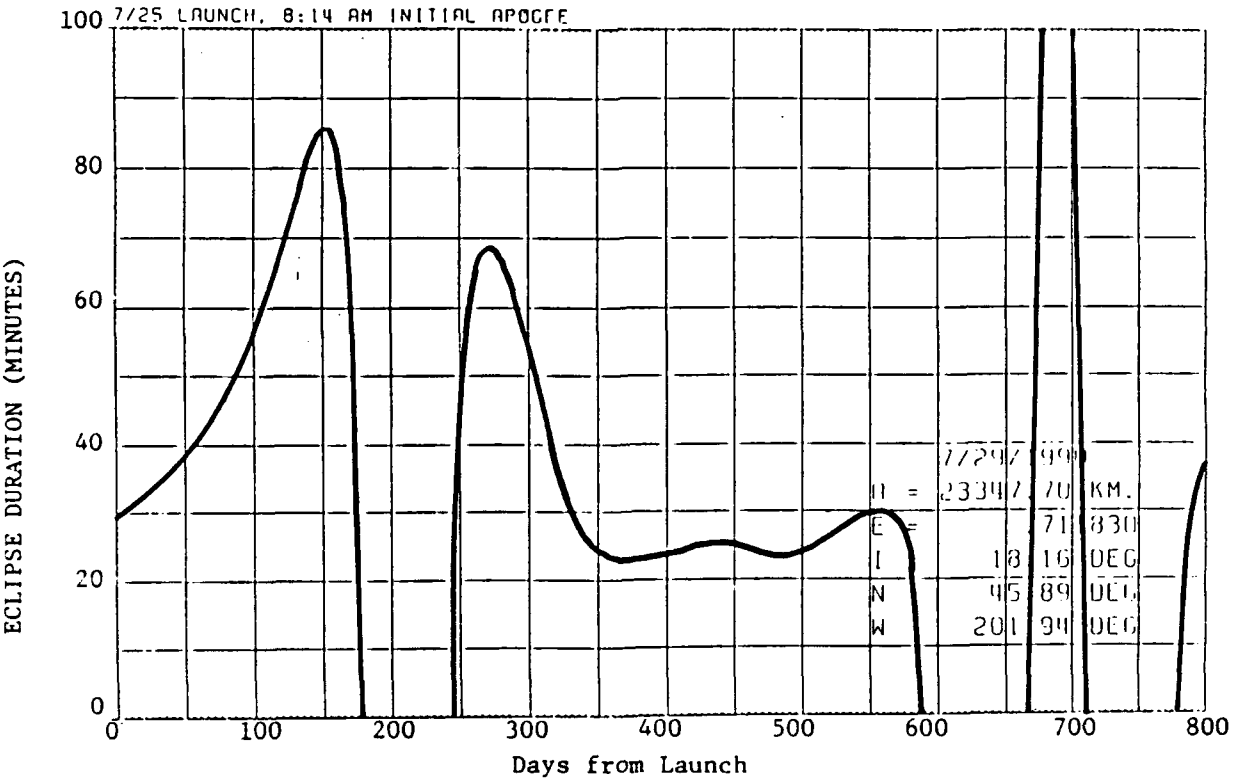

Figure 8. Eclipse durations during the first 800 days of CRRES mission.

The CRRES orbit, attitude and spin were selected so that the instruments would obtain good coverage of the pitch angle distribution of the particles. The GTO orbit and low inclination enables the spacecraft to sample all of the magnetic field lines as close to the geomagnetic equator as possible since this will define the environment of the entire radiation belts. The design lifetime of three years provides nearly continuous temporal coverage so that meaningful fluxes are measured over the highly dynamic variations experienced as a result of solar and geomagnetic storms and substorms.

Command and control of CRRES is done through the Consolidated Space Test Center (CSTC) at Onizuka Air Force Base in Sunnyvale, CA. Initialization of the instruments was performed primarily during real time contacts, although part was also done by way of commands stored in memory and time-tagged for later execution (CSM). Typically real-time contacts occurred three times per orbit as indicated in Figure 9. Contact number 1 was usually about ten minutes and was used for loading CSM commands. Contact number 2 occurred near apogee and was about 30 minutes long. Contact number 3, on the in-bound portion of the orbit, was a 60-minute contact used for telemetering the tape recorded data. After initialization, the contact near apogee was not performed on every orbit. Also, chemical release campaigns required a significant change in the schedule of real-time contacts.

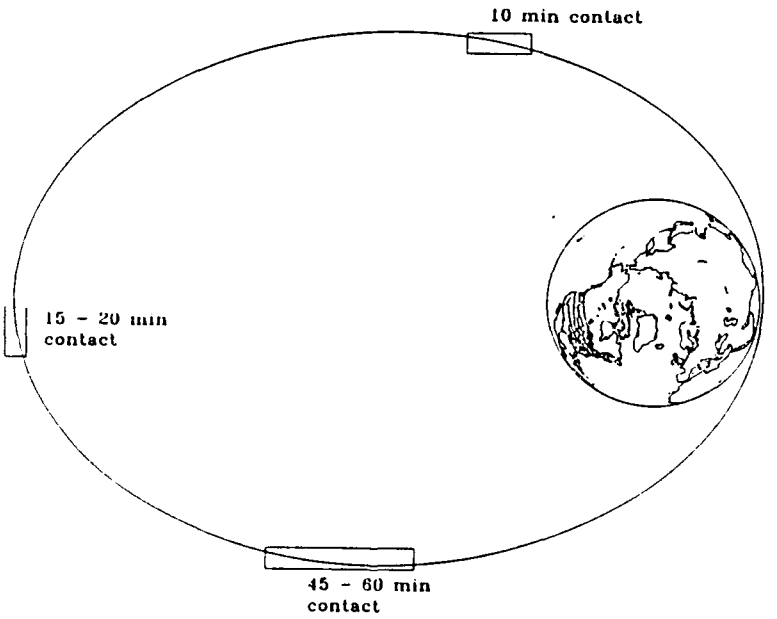

Figure 9. CRRES orbit shown to scale with locations of real time contacts.

For the purposes of data analysis, CRRES orbits are numbered with the start of the orbit defined as perigee. For the year 1990 an equation that gives the orbit number as a function of date and time is

$$\text{Orbit number} = 24(\text{Day number} + f - 208.88054)/\tau + 6$$

where f is UT expressed as fraction of a day and τ is the orbital period. The average orbital period for the first year of the mission is about 9.85 hours, but a more accurate determination can be obtained from the following:

$$\tau = 9.86 - .035 \times \text{Orbit elapsed time in days}$$

Note that CSTC numbers orbits differently with the start of the orbit at the ascending node, usually shortly after contact number 3.

A timeline of events during the first six months of the mission is given in Table 6. The satellite spin was increased to 20 rpm by the end of July to enable deployment of the magnetometer booms and a pair of wire booms for the Langmuir probe and electric field experiments. After boom deployment, the spin was decreased to the desired rate of approximately 2 rpm which was achieved near the end of August. Table 7 is a list of geomagnetically active periods during the first 6 months of the mission. Most of this information was compiled from plots of preliminary Ap indices provided by CSTC. A solar proton event occurred within a few days after launch and its effects were observed in instruments that were operating at that time. The period after orbit 76 following a sudden storm commencement has been selected for in-depth study by the CRRES science team. Several other active periods occurred in October and November, but activity has been low throughout December, January, and February.

TABLE 6. CRRES ON-ORBIT OPERATIONS

DATE	EVENT
25 July 1990	Launch
27 July	Instrument initialization begins
31 July	Spin-up to 20 rpm for boom deployment
1 August	Magnetometer and wire booms deployed
6 August	Wire booms extended to 50 M
7 August	Spin-down commences
21 August	Instrument initialization ends
7 September	Half of microelectronics package fail
10-14 September	Four pair of low altitude chemical re
14 December	Battery #2 fails; eclipse duty-cyclin of instruments begins
26 December	Longest eclipse: 90 min
13-20 January 1991	Nine high-altitude chemical releases
18 January	Eclipse duty-cycling ends

TABLE 7. GEOMAGNETICALLY ACTIVE PERIODS DURING CRRES OPERATIONS
(As of 1 MARCH 1991)

DATE		MAGNETIC INDEX Ap
29	July 1990	*
20	Aug	40
22	Aug	60
23	Aug	80
24	Aug	60
26	Aug	100
30	Aug	40
6	Oct	38
10	Oct	90
11	Oct	70
12	Oct	60
15	Oct	45
20	Oct	35
24	Oct	45
30	Oct	50
16	Nov	35
17	Nov	35
27	Nov	100
24	Jan 1991	30
2	Jan	75
9	Feb	30
23	Feb	30

*Ap not available - Solar Proton Event

Up to Dec 13, when battery number 2 failed, the spacecraft performance was satisfactory. The only anomalies were (1) failure of the magnetometer boom to deploy properly, leaving the magnetometer oriented at 15 degrees from its desired orientation, (2) random jumps in the vehicle time code word that may cause the ONR-307 instruments to lose synchronization, and (3) spurious commands received by several instruments. In early September, battery number 2 was inadvertently overheated during a planned overcharge test. In mid-December this battery failed completely requiring most of the instruments to be duty cycled during eclipses which were getting longer as apogee precessed into the midnight sector. The microelectronics package was kept on during the eclipses, along with two or three other instruments.

All of the chemical releases to date have been successful. Four canisters were released in September near perigee over the South Pacific. Six high altitude releases were performed between January 13 and 20, and two in February on the 12th and 17th. Ten more perigee releases are planned for the summer of 1991 over the Caribbean.

V. ONR-307 Initialization and On-orbit performance

The initialization of the ONR-307 instruments is summarized in Table 8. Because of their placement in the anti-sunward side of the spacecraft, the thermal control of the instruments has to be monitored carefully to ensure that they do not cool to critical temperatures. For this reason, power was turned on within a few days after launch although high voltage was not applied until some days later. The high-voltage turn-on for ONR-307-3 was particularly involved owing to the step-wise fashion in which the voltage was raised. Analog tapes from the ground stations were processed immediately at Lockheed to ensure that the instrument was working properly before the next step in voltage was applied. All the ONR-307 instruments were in normal operating modes by August 7.

TABLE 8. CRRES ONR 307 EVENT TIMELINE

DATE	GMT	ORBIT #	EVENT
25 July	1921		Launch
26 July	1310	2.3	-3 and 8-3 power on (phase 1)
28 July	2140	8.1	8-1 and 8-2 power on (phase 1)
29 July	0740	9.1	8-1 and 8-2 memory load and check (phase 2)
29 July	1050	9.2	-3 memory load and check (phase 2)
29 July	1805	10.1	8-3 memory load and check (phase 2)
30 July	0315	11.1	ONR 307 real time checkout (phase 3)
1 Aug	1510	17.1	ONR 307 memory load (phase 4)
2 Aug	1050	19.1	8-1 high voltage on (phase 5)
2 Aug	1615	19.4	-3 CSM load, start HV advance (phase 5)
2 Aug	2140	20.1	8-2 high voltage on (phase 5)
3 Aug	1720	22.1	8-3 high voltage on (phase 5)
3 Aug	1840	22.2	-3 HV advance to level 1 (phase 5)
4 Aug	1200	24.1	8-1,2,3 configure for normal operations (phase 6)
6 Aug	0400	28.1	-3 HV advance to level 2 (phase 5)
7 Aug	0950	31.1	Start CRRES spin down maneuvers
7 Aug	1155	31.2	-3 HV advance to level 3 (phase 5)
7 Aug	1850	32.1	-3 partial memory load (phase 6, part 1)
20 Aug			Spin down complete
26 Aug	1710	78.1	-3 calibration, 8-1,2 reconfiguration
5 Sept	2025	103.1	-3 complete memory load (phase 6, part 2)
Sept			ONR 307 calibrations performed every 4 orbits
Oct			ONR 307 calibrations performed every 17 orbits (orbits 169, 185, 202, 219, 236, 253)

The ONR-307 instruments are working perfectly. The only loss of data occurs as a result of the loss of synchronization caused by the dropouts in the vehicle clock. When this happens all ONR-307 instruments lose synchronization temporarily. ONR-307-8-1,2 and 3 recover to their normal operating modes within a couple of minutes. ONR-307-3 recovers in a backup mode in which it only measures high energy electron fluxes. The instrument must be

commanded back to its normal operating mode during the next real-time contact. Table 9 is a list of times when this loss of data has occurred. Presumably each of these events corresponds to a time when the vehicle time code word jumps, but not every vehicle time code word jump causes ONR-307-3 to switch to its backup mode.

The ONR-307 instruments operated continuously from launch to December 22. On December 22, because of the loss of battery 2, eclipse duty-cycling began. A careful study of the possible effects of duty-cycling on the instruments' thermal control was performed prior to the first time they were turned off. After the first turn-off the temperatures were monitored before continuing this duty-cycling for subsequent eclipses. Although the temperatures dropped about ten degrees they were still within safe limits. However, owing to the drop in overall spacecraft temperature as eclipses became longer, the ONR-307 instruments did not recover entirely to their previous temperatures after being turned back on. Only after December 26, when eclipses began to shorten, did the spacecraft and instrument temperatures rise steadily. Duty cycling for eclipses ended on January 18.

TABLE 9. TIMES OF ONR 307-3 LOSS OF SYNCH
(As of 1 March 1990)

FIRST REAL-TIME CONTACT AFTER LOSS OF SYNCH			RESTORED TO RUN MODE
DATE	TIME	CSTC REV #	CSTC REV #
15 Aug	0650 (approx)	50.2	54.3
24 Aug	1040 (approx)	72.3	74.1
25 Aug	0424 (approx)	74.2	74.2
25 Aug	1020 (approx)	75.1	75.1
26 Aug	0524 (approx)	77.1	77.1
10 Sep	1940 (approx)	115.1	115.1
26 Sep	1554 (approx)	153.3	154.1
28 Sep	1650	158.3	158.3
1 Oct	2335	166.4	166.4
13 Oct	1540 (approx)	195.1	195.1
15 Oct	2250	200.3	200.3
17 Oct	0100	203.2	203.2
23 Oct	1030	219.1	219.1
26 Oct	0500	225.3	225.3
24 Nov	2200	298.1	298.1
30 Nov	0819	311.2	311.2
26 Dec	2044	376.1	376.1
14 Jan	0121	420.2	420.2
27 Jan	2038	454.1	454.1

VI. Preliminary Results from the ONR-307 Experiment

The first step in analysis of CRRES data involves processing agency tapes provided by Geophysics Laboratory, Hanscom Air Force Base. The agency tapes for Lockheed contain data from each of the ONR-307 instruments along with ephemeris data and magnetometer data. The data from these tapes are extracted and separated into five separate files, one for each instrument, one for ephemeris data and one for magnetometer data. Data from approximately 12 orbits can be kept on-line at any one time. Data from other orbits are presently being backed up to tape, but eventually will be stored on optical disks to be more easily accessible.

Analysis of ONR-307 data has had several major thrusts during the initial portion of the CRRES mission. Most important is the validation of the data through intercomparison among instruments. Efforts are already underway in this area. The ONR-307-3 measurements of electron fluxes have been compared with the Aerospace MEEPS data. Good agreement is found at the energy of overlap. IMS-LO data are to be compared with IMS-HI data at energies of around 18 keV and with the proton measurements made by the AFGL LEPA instrument. The IMS-HI proton flux measurements can also be compared with SEP measurements at energies of a few MeV.

Another area of concentration during this preliminary data analysis phase is the development of software for extracting and displaying data. In general, the data from each instrument are able to be displayed either in a quick look fashion, usually one orbit per page, or at high time resolution whereby spectra and pitch angle distributions are shown over the shortest time interval possible. These routines have been developed using a test-bed data base consisting of ONR-307 measurements obtained during orbits 75 to 82. A moderate magnetic storm occurred during this time and the event has been selected by the CRRES science team for detailed study. The event began with a sudden storm commencement at 0552 UT on day 238. Figures 10 through 22 show some of the data obtained by the ONR-307 instruments during this storm and demonstrate the types of display routines that have been developed.

Figure 10 shows data from the SEP instrument obtained during orbit 75, prior to the sudden commencement. Data from each of the three sensors are shown in two panels with the lower panel being the low energy electron fluxes and the upper panel being the high energy electron fluxes. The spin-averaged flux in each of the 24 energy channels is shown in a gray shade format. The plots begin and end with the perigee portion of the orbit and the center of the plot is apogee. The two enhancements in flux near perigee represent particles encountered in the radiation belts. The in-bound and out-bound portions of the orbit are fairly similar indicating little change in fluxes during the time between the two

passages. This behavior can be contrasted with that shown in Figure 11 which shows data from orbit 77 after the storm commencement. There is a general depression in flux levels over all parts of the orbit with a more dramatic decrease between 1300 and 1600 UT. This is presumably due to the effects on the energetic electron distributions from the storm commencement and accompanying change to the magnetospheric fields. Figure 12 is a pitch angle spectrogram for orbit 76. Here the low and high energy electron channels have been integrated in energy with the integrated flux given by the line plots. The pitch angle distributions in these two energy bands (ELEC1 and ELEC2) are shown by the gray shade. Proton pitch angle distributions are shown on the bottom. In Figure 13 the electron flux data in several energy channels are plotted as a function of universal time during orbit 79. These plots allow a more quantitative visualization of the measured fluxes. Figure 14 is a similar plot except that the fluxes are divided into one of several four-degree wide pitch angle bins. Note that pitch angles as close as 2 degrees from the loss cone are sampled during the orbit. Figure 15 is a pitch angle spectrogram and Figure 16 is a spin-averaged electron spectrum.

Storm-time data from the IMS-LO instrument are shown in Figure 17. Data from the two IMS-LO instruments are shown at three different energies. The horizontal bands of enhanced fluxes represent H^+, O^+ and He^+ fluxes. A sudden change in particle fluxes is seen at 0800 UT several hours after the storm commencement. The change in fluxes of O^+ at this time is shown in more detail in Figure 18 where pitch angle distributions at various energies are shown before (upper panel) and after (lower panel) the sudden commencement. The bottom panel shows that the enhancement is observed primarily in ions moving along the magnetic field as might be expected from the particles being of ionospheric origin. Figure 19 shows electron data from the IMS-LO instrument. The upper panel shows the spin-averaged electron spectra in gray-shade format. The bottom eight panels show pitch angle distributions in four energy ranges for each of the two IMS-LO sensors.

Figure 20 shows data from the IMS-HI instrument obtained during orbit 77. The histograms give the count rates in the 64 channels into which each of the events in the seven detectors is pulse-height analyzed. Only data from three of the seven detectors are shown. The capabilities of the instrument to distinguish many different types of ions over a broad energy range are demonstrated by the well-defined peaks in the distributions. Data from an entire orbit are shown in gray-shade spectrogram format in Figure 21. Each of the horizontal bands represents an ion with energy in a specific range. Figure 22 is a line plot of the count rates for H^+ ions in the seven detectors showing the

highest time resolution possible. The spin modulation shows that the pitch angle distribution of individual ions can be measured.

The data from the ONR-307 instruments during the August 22 magnetic storm will eventually be combined with data from other CRRES instruments as well as information about the interplanetary magnetic field from the IMP-8 spacecraft. Solar wind plasma density measurements are consistent with a compressed magnetopause boundary owing to high solar wind velocity and density following the storm commencement. Examination of magnetometer data indicates large perturbations in the magnetic field during orbit 77 at the time that the large decrease in energetic particle flux measured by SEP is observed. Other interesting aspects of this event are oscillations in the IMS-HI data correlated with magnetic perturbations prior to the storm commencement. Also, SEP measured a series of dispersive-type injection events near apogee in orbit 79.

We are also studying SEP data for particle events that would indicate precipitation at the trapping boundary. These precipitation events have been observed from low-altitude satellites, but the source region for these populations has not been studied. In addition, IMS-LO has been reconfigured to observe barium or lithium in association with the high altitude chemical releases.

VII. Future Plans

Over the next year we will continue efforts in the areas outlined above. As new data become available, summary plots will be examined to identify other times of interest. These times include events associated with relativistic particle precipitation, events associated with substorms, and variations associated with changes in radiation belt dynamics as a result of magnetic storms. As our display software becomes more well-developed we anticipate that our software efforts will eventually concentrate on modeling the observed fluxes. Furthermore, our future efforts will incorporate more data from other CRRES instruments to achieve a more comprehensive determination of the radiation belt and plasma sheet particle populations.

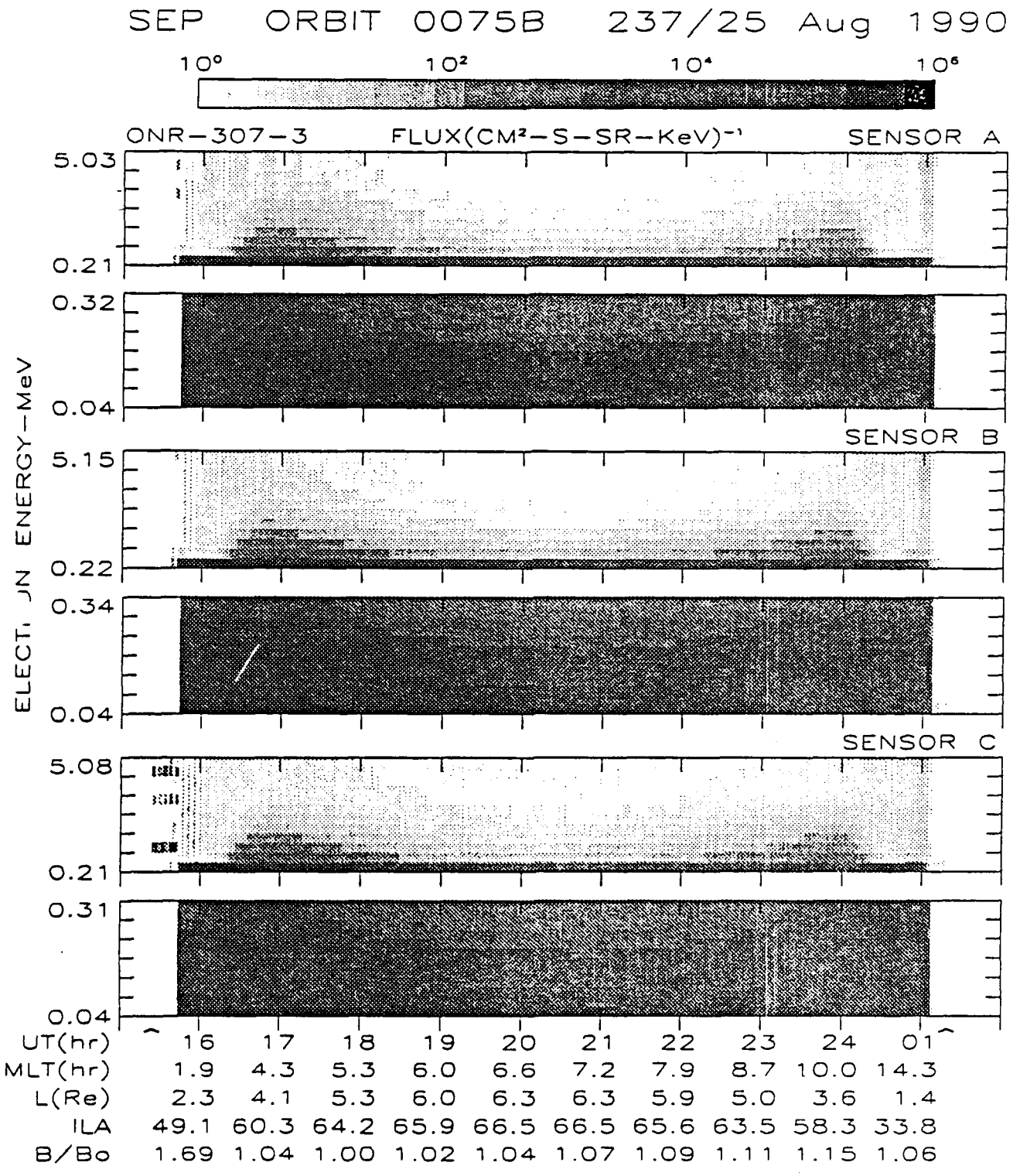

Figure 10. SEP data for orbit 75 showing low and high energy electron fluxes measured by the three detectors.

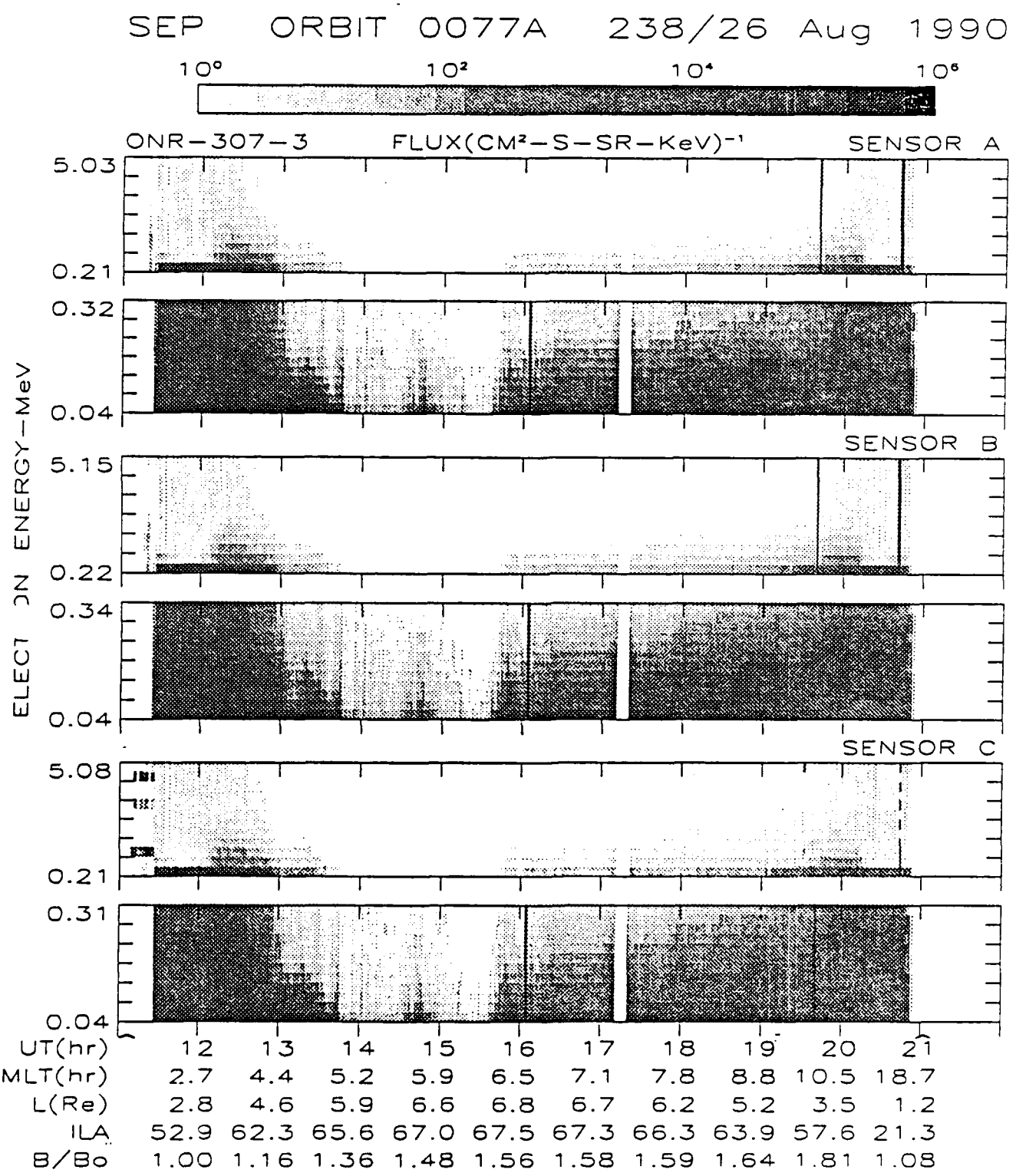

Figure 11. SEP data for orbit 77 showing the large dropout in fluxes between 13 and 16 UT.

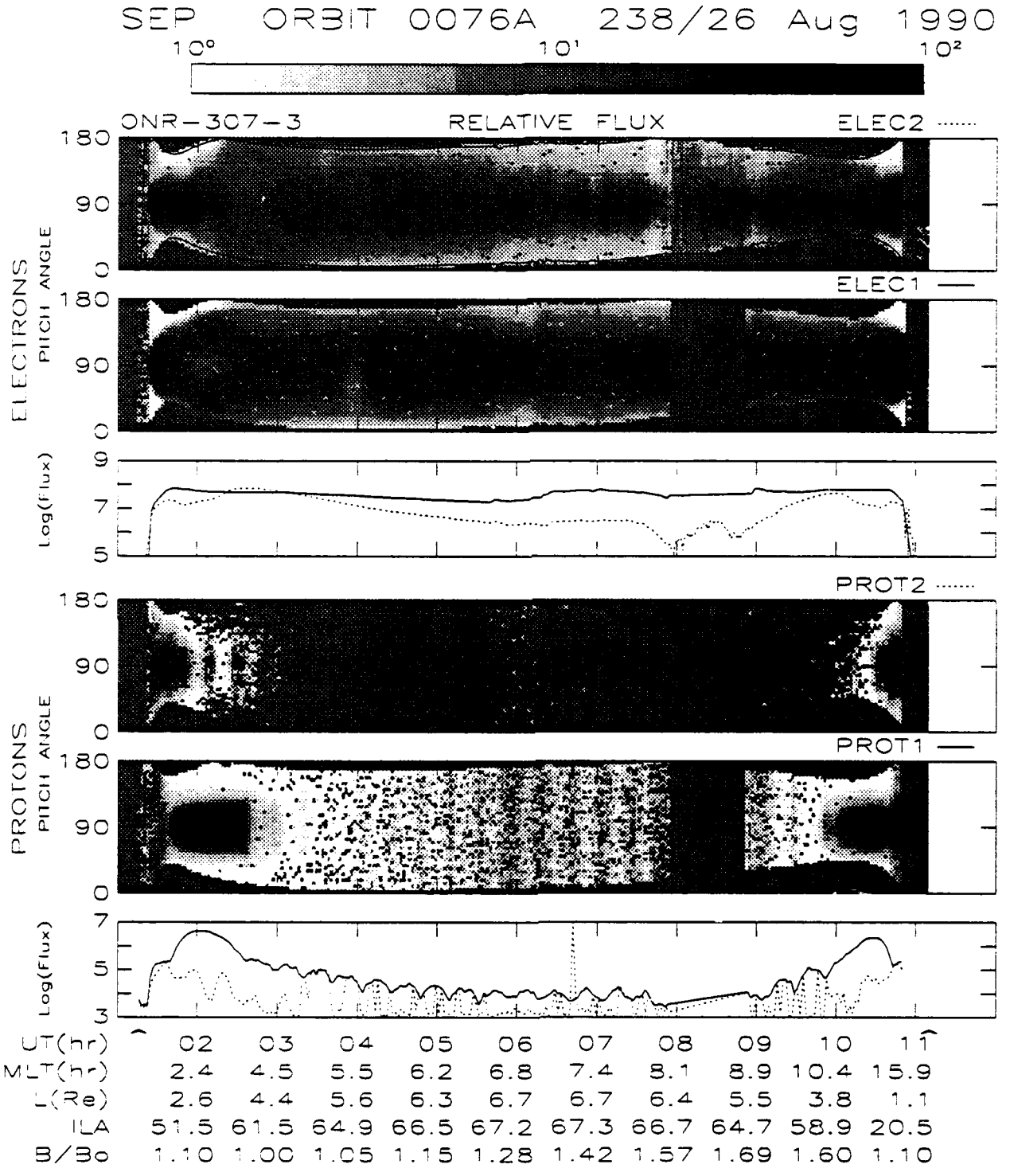

Figure 12. Pitch angle spectrograms derived from high and low energy electron and proton data obtained by SEP during orbit 76.

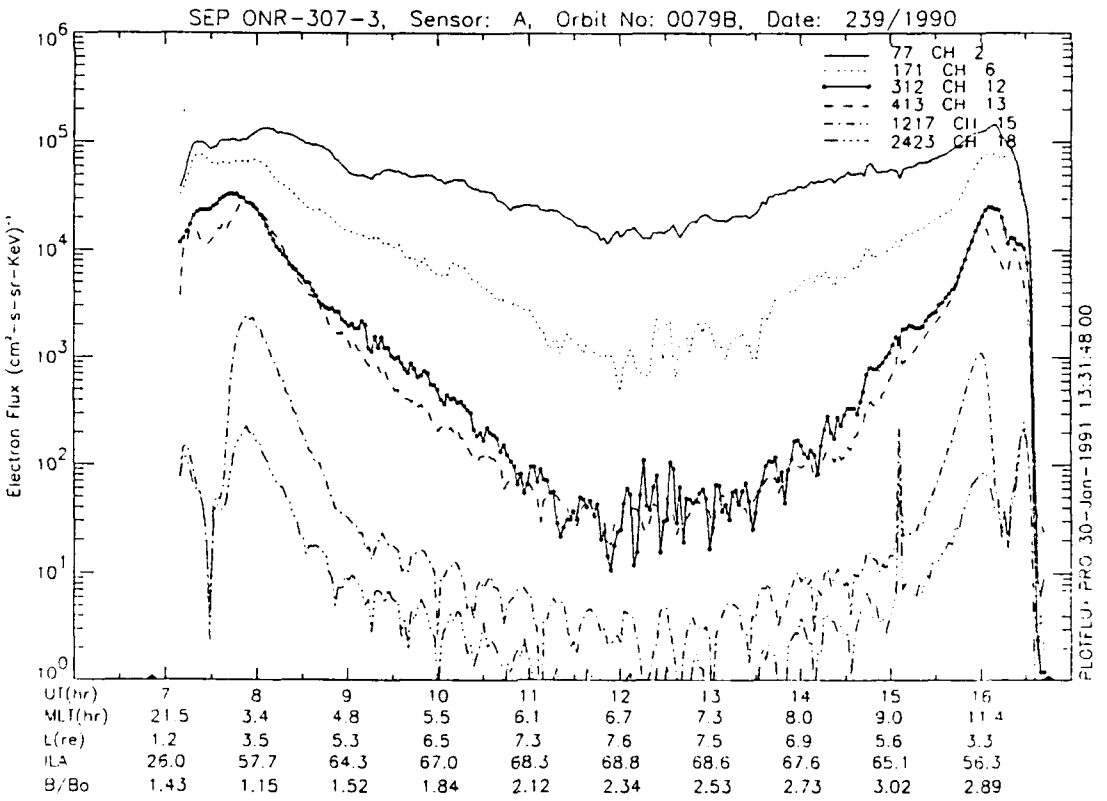

Figure 13. Line plots of electron fluxes in six different energy channels measured during orbit 79.

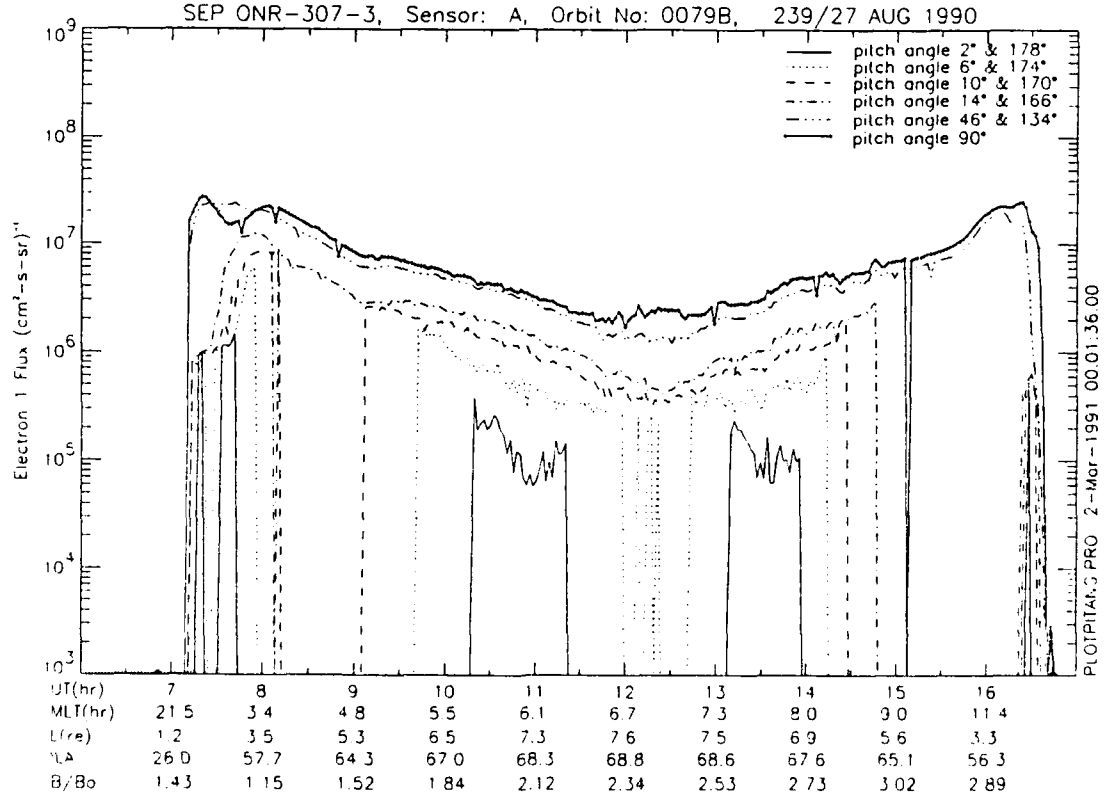

Figure 14. Line plots of electron fluxes in six different pitch angle bins measured during orbit 79.

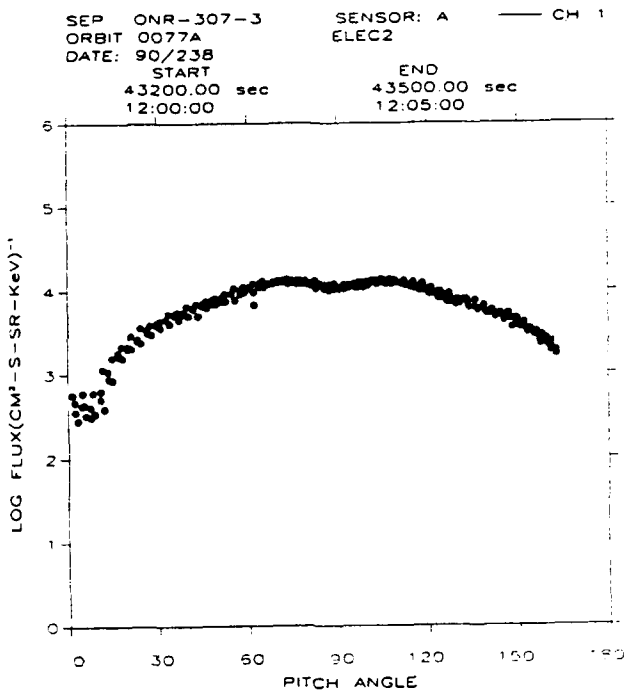

Figure 15. Pitch angle distribution of 200-600 keV electrons measured by SEP during orbit 77.

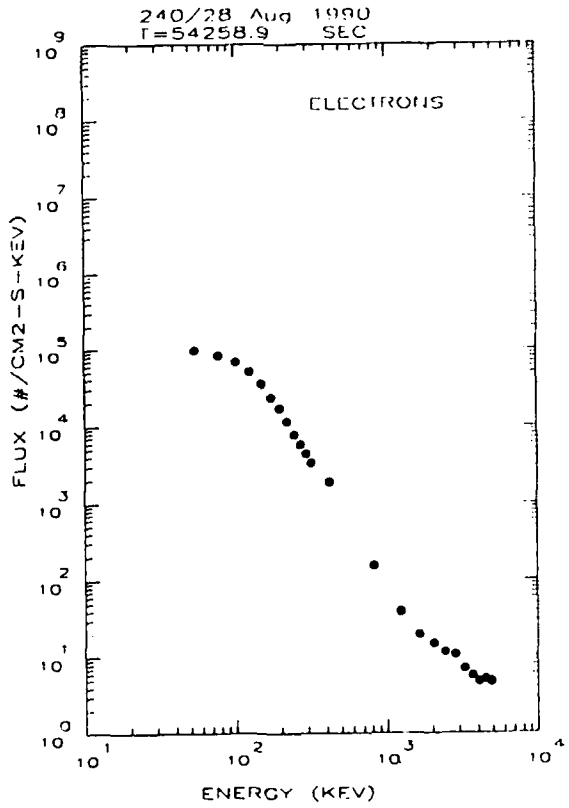

Figure 16. Electron energy distribution measured by SEP during orbit 82.

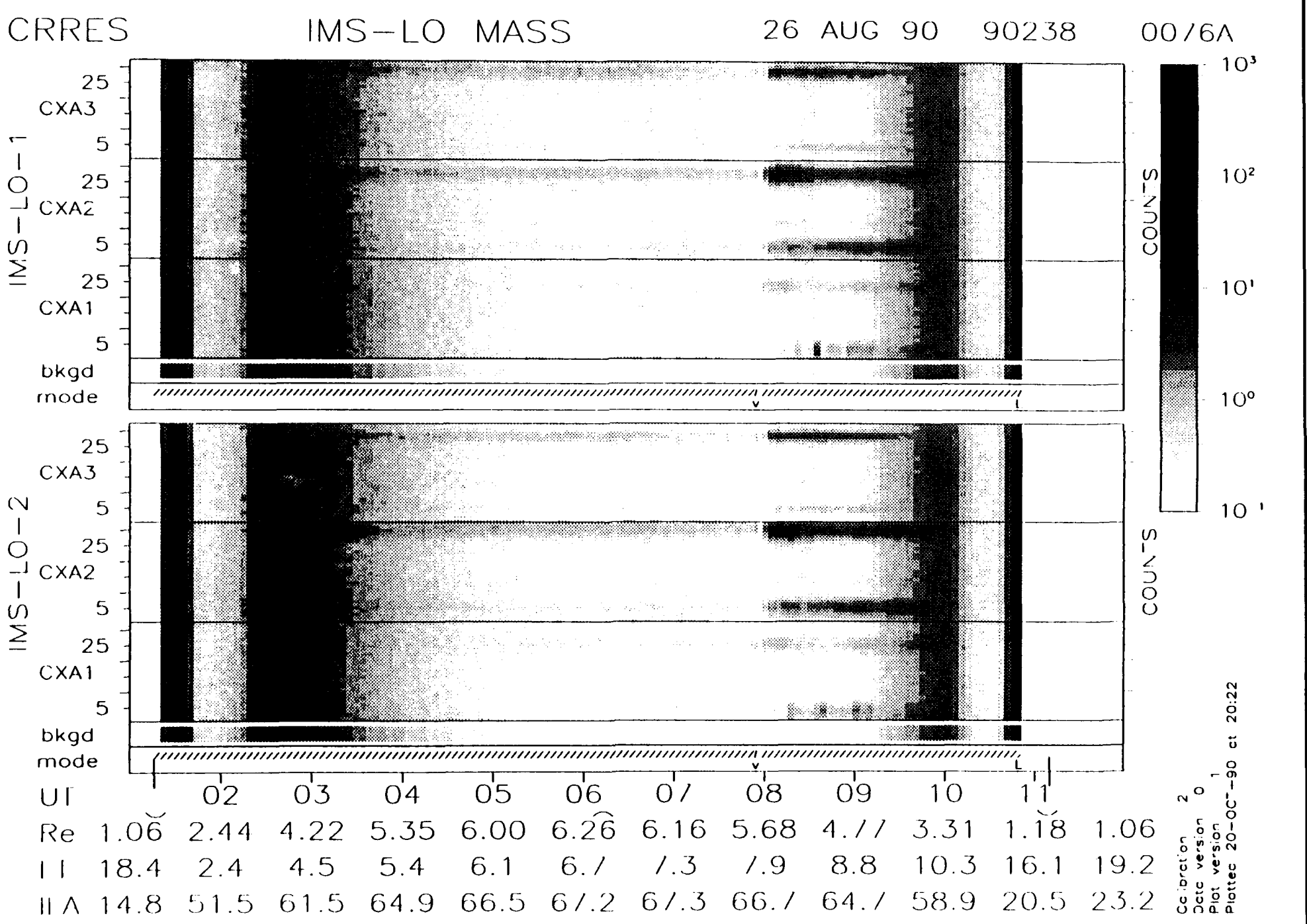

Figure 17. Mass spectorgrams showing fluxes measured by the two IMS-LO detectors at three different energies.

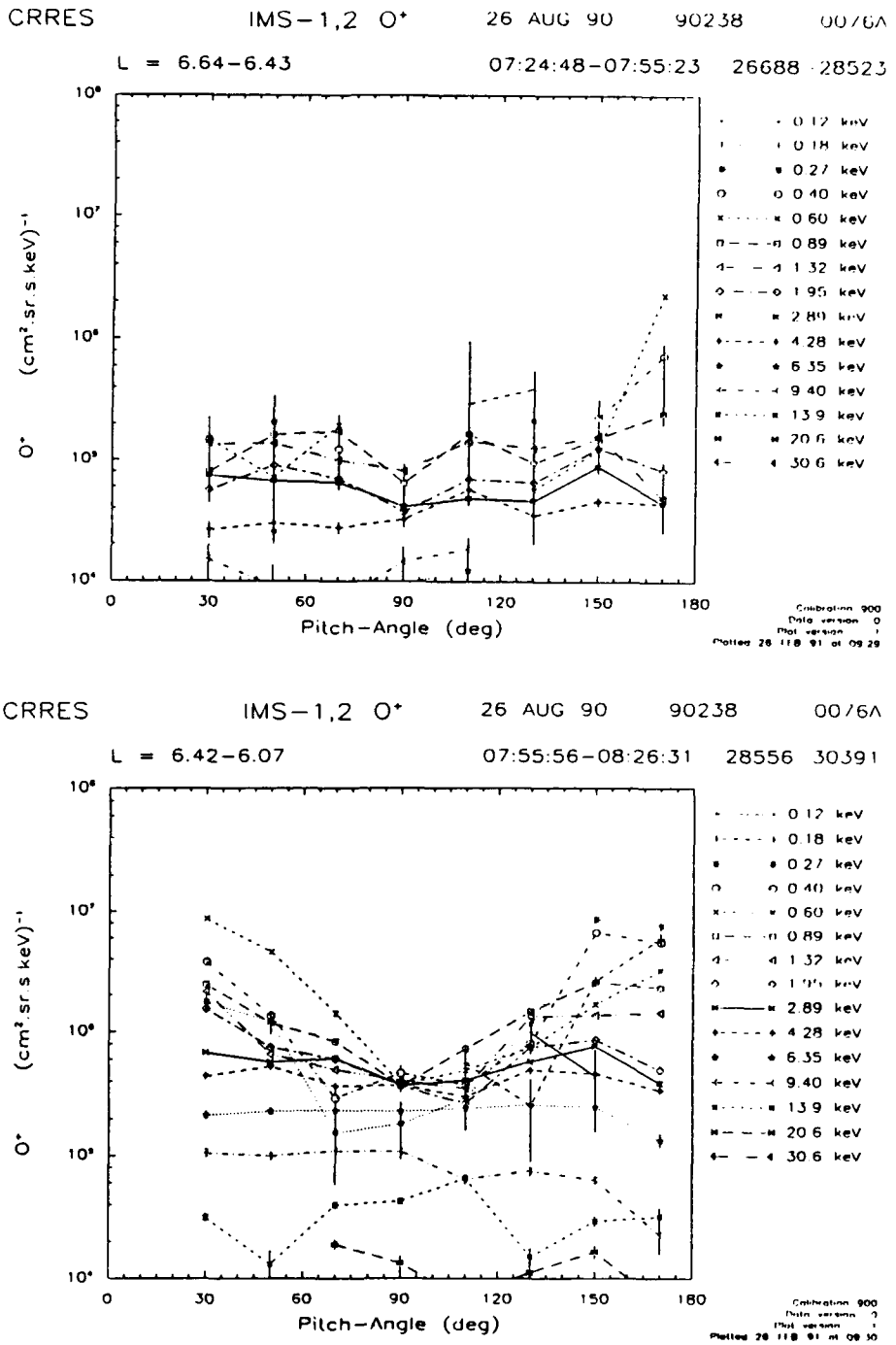

Figure 18. Pitch angle distributions of O^+ at different energies measured near L = 6 by IMS - LO before (upper panel) and after (lower panel) a magnetic storm.

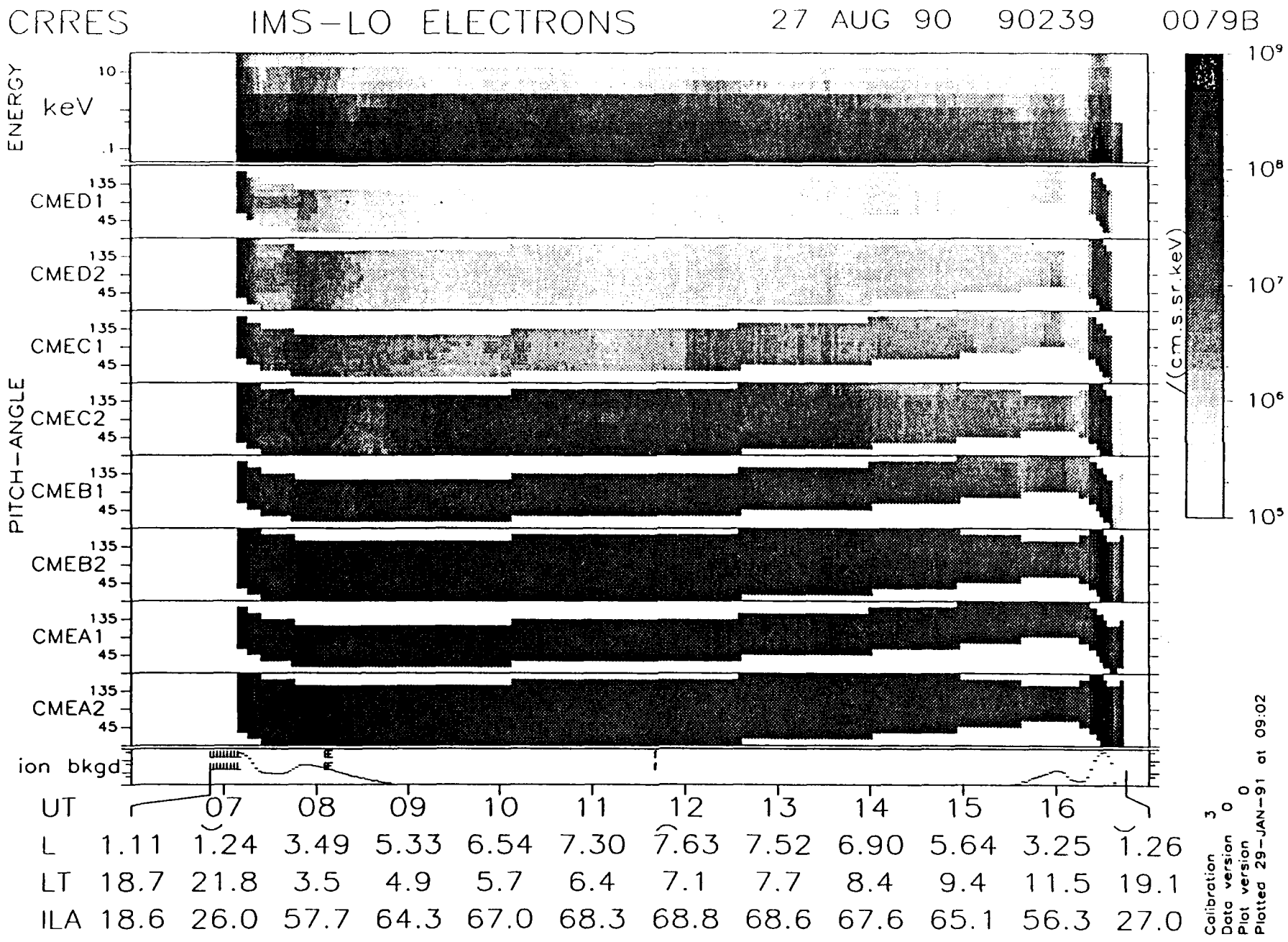

Figure 19. Energy and Pitch angle spectrograms of electron fluxes measured by IMS - LO during orbit 79.

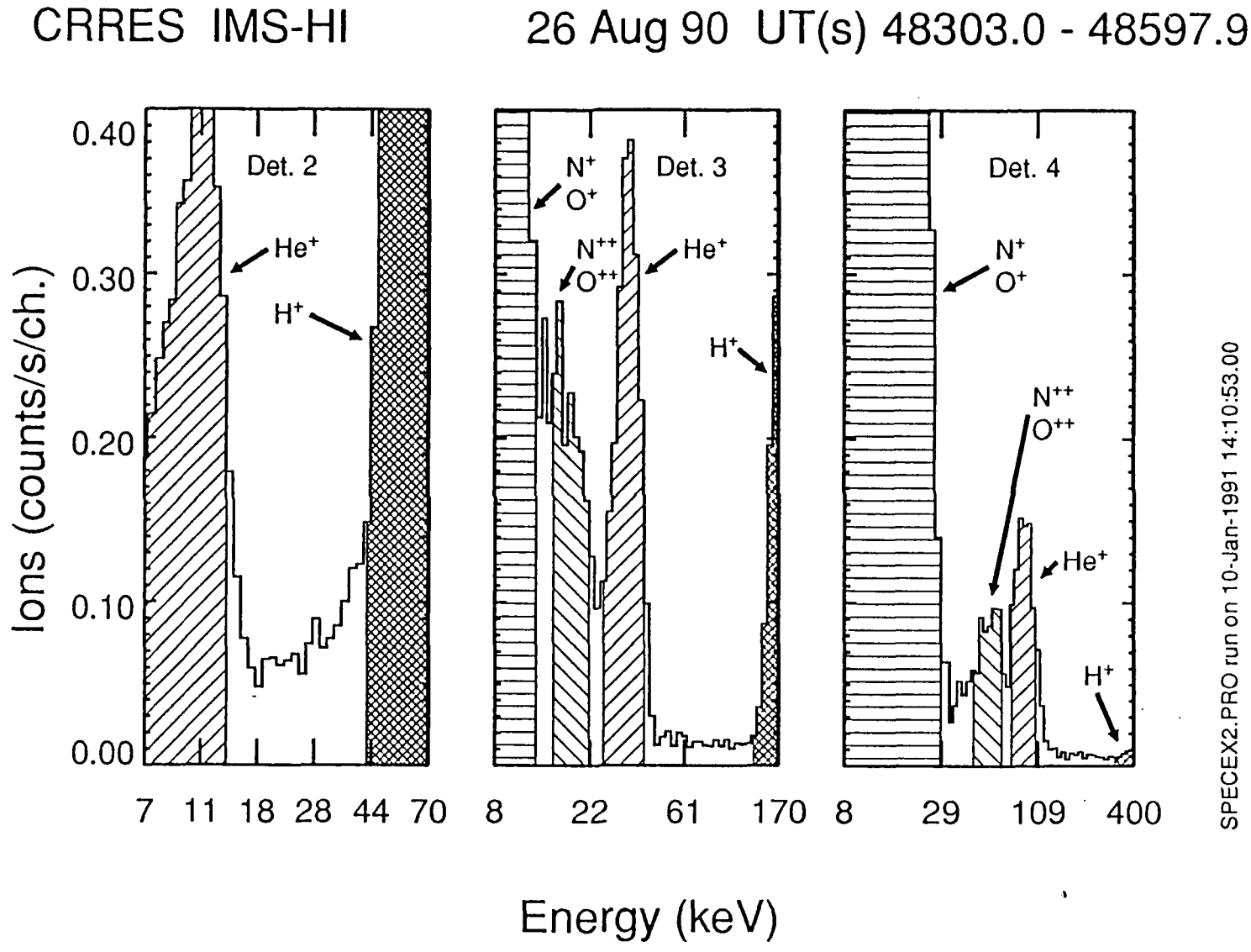

Figure 20. Mass spectral distributions measured in three of the seven IMS-HI detectors.

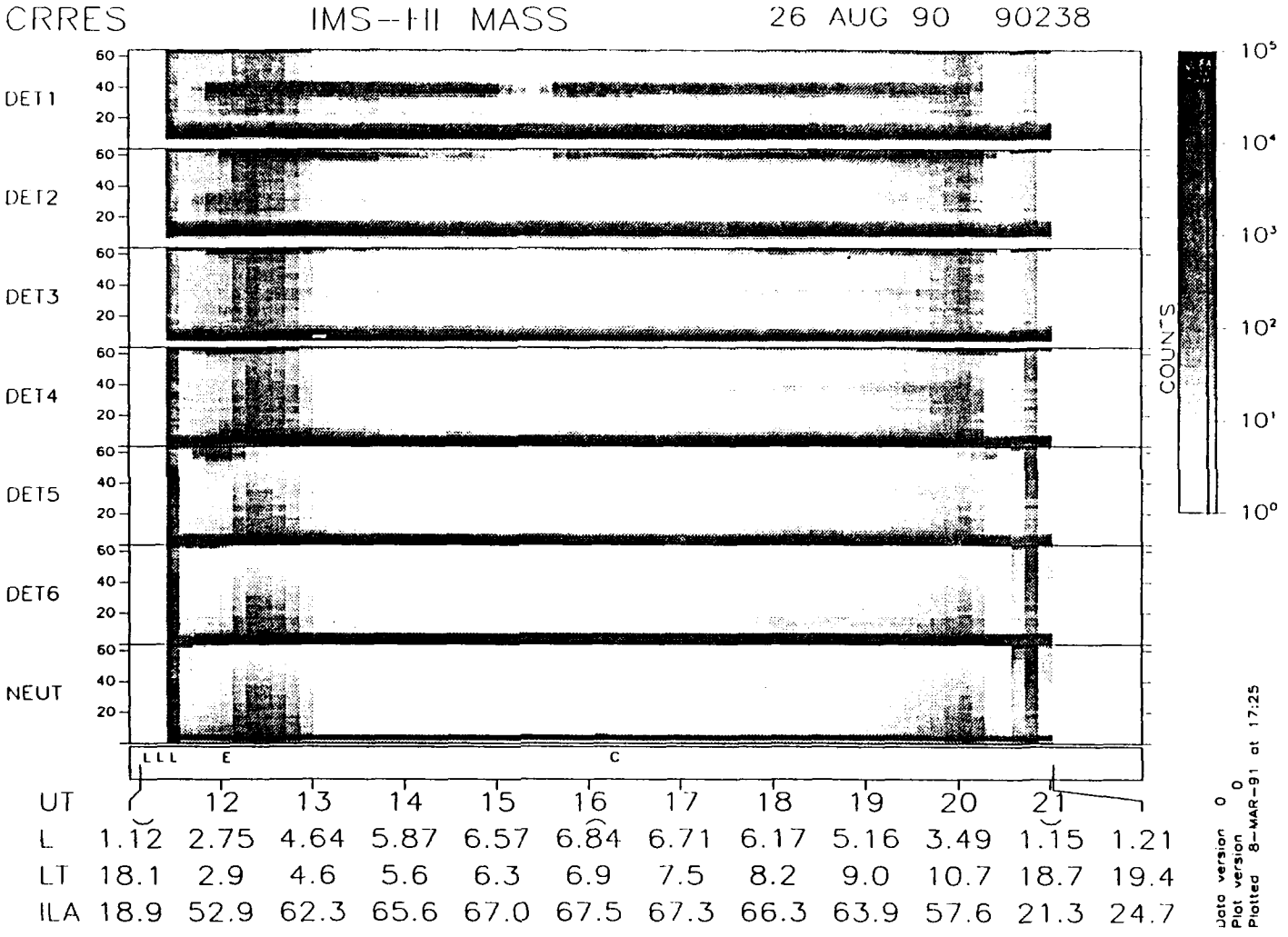

Figure 21. Gray-shade spectrogram of IMS-HI data obtained during orbit 77.

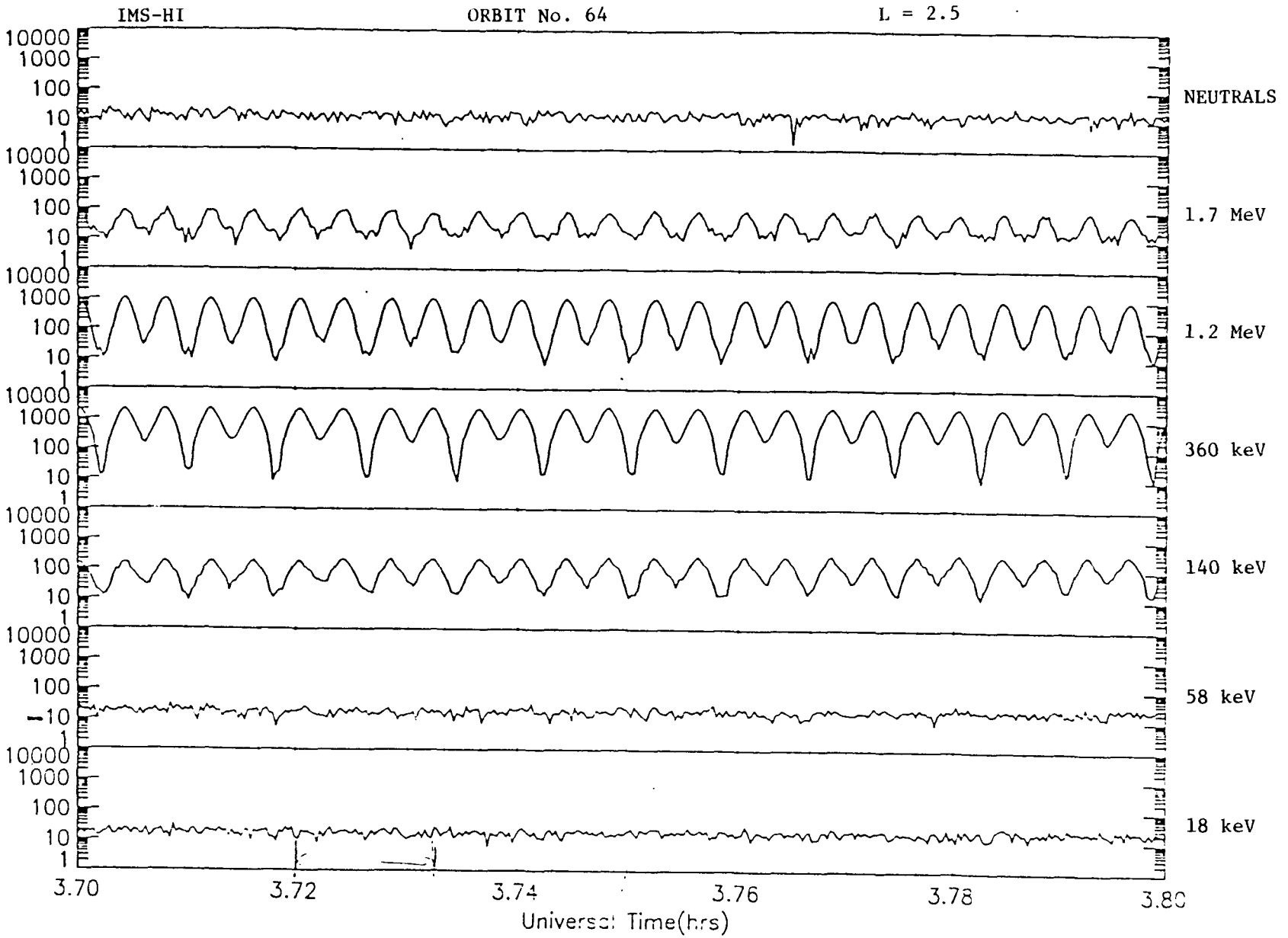

Figure 22. H^+ fluxes at six different energies measured in six minutes during orbit 64.

APPENDIX 1

THE ONR-307-3 SPECTROMETER FOR ELECTRONS AND PROTONS (SEP) ON THE CRRES MISSION

The ONR-307-3 Spectrometer for Electrons and Protons (SEP) on the CRRES Mission

R.W. Nightingale, R.R. Vondrak, E.E. Gaines, W.L. Imhof,
S.J. Battel, D.A. Simpson and, J.B. Reagan
Lockheed Palo Alto Research Laboratory
Palo Alto, CA 94304

ABSTRACT

The SEP experiment measures continuously the energy and full angular distribution of the energetic electrons and protons in the CRRES geosynchronous transfer orbit from ~350 km to ~33,500 km at an inclination of ~18°. The experiment consists of three identical particle telescopes composed of surface-barrier silicon detectors with active anticoincidence shielding and narrow (3° FWHM) collimation to provide fine pitch-angle resolution. The energy spectra for the energetic electrons can be measured in 24 contiguous channels from 20 to 5100 keV, while the protons can be observed in 48 contiguous channels from 300 keV to 105 MeV. The three particle telescopes are mounted at optimum angles to the CRRES spin axis to provide nearly complete pitch-angle coverage on each spacecraft spin. These data will be used to construct predictive models of the dynamical behavior of the earth's radiation belts.

I. Introduction

Important components of the magnetospheric plasma to be explored by the CRRES satellite are the energetic electrons and protons that populate Earth's radiation belts. The fluxes of these particles depend critically on the production and loss mechanisms in the radiation belts and exhibit dynamic behavior in response to solar and geomagnetic activity. The understanding of these processes requires detailed measurements of the particle

distribution functions including the pitch angle. Previously such measurements were made by the SC-3 instrument on SCATHA, but the unique CRRES orbit offers exciting new possibilities for developing improved models of the electron and proton radiation belts. For example, the particle distributions measured along the spacecraft trajectory can be used to map the two-dimensional radiation belt morphology in the orbit plane.

The ONR 307-3 Spectrometer for Electrons and Protons (SEP) is one component of the ONR 307 Energetic Particles and Ion Composition (EPIC) experiment. The other EPIC instruments are the ONR 307-8-1,2 Low Energy Ion Mass Spectrometer and the ONR 307-8-3 Medium Energy Ion Mass Spectrometer which are described separately in this issue by Collin et al.(1991) and Voss et al. (1991), respectively.

The overall objective of the SEP experiment is to obtain necessary data to construct predictive models, suitable for engineering purposes, of the energetic particle and plasma environment in those regions of space of primary interest to the Department of Defense satellite operations. The CRRES orbit provides a unique opportunity to study the entire radiation belt region from $1.05 < L < 6.3$ near the geomagnetic equator during this solar maximum epoch. The specific science objectives of this experiment are:

To measure the intensity, energy spectrum, and pitch-angle distribution of energetic electrons and protons continuously as a function of time. These measurements will characterize the dynamical behavior of the radiation belts.

To compute accurately the total omnidirectional flux and

energy spectrum at the satellite position.

To understand the physics of the sources, energization, transport, lifetimes, and losses of energetic particles in the earth's radiation belts.

To understand the details of wave-particle interactions (WPI), both natural and man-made, that are a principal loss mechanism for radiation belt particles. These WPI produce particle precipitation into the ionosphere that can disrupt radiowave communications of vital interest to the U.S. Navy.

To utilize this experimental data base to greatly improve the accuracy of the trapped radiation belt models and to characterize model particle precipitation.

II. Experiment Description and Operations

The SEP instrument is based heavily on the successful SC-3 spectrometer flown on the SCATHA mission. It consists of three such solid-state particle spectrometers to provide good coverage of the pitch-angle distribution. The SC-3 instrument was described in detail by Reagan et al. [1981] and in the SCATHA program description by Stevens and Vampola [1978]. A cross-sectional view of one of the telescopes is shown in Figure 1. Each spectrometer has four detector elements labeled A, D, E and E'. Various logic combinations of the four detector elements in each spectrometer are used to determine the particle types and energy ranges which are measured sequentially. The operational modes of each telescope are individually commandable.

The D-detector, which is 200-μm thick intrinsic silicon, is used to measure both the rate of energy loss of the higher-energy

particles and to directly stop and measure the lower-energy particles. The E-detector, which consists of a stack of five 2-mm thick detectors in parallel, is located behind the D-detector to stop the higher-energy particles and to measure their total energy loss. The E'-detector, which is 1000-μm thick, is located behind the E-detector and is used as an active collimator. Behind the E'-detector is a tungsten absorber that sets the upper energy limit for analysis. All of these detectors are silicon surface-barrier type and are stacked together in a telescope configuration. The entire stack is surrounded by the anticoincidence A-detector, which consists of a plastic scintillator viewed by a photomultiplier tube. The purpose of the anticoincidence detector is to sense and reject energetic particles and bremsstrahlung that penetrate either the outer shielding walls of aluminum and tungsten or the silicon detector stack and absorber. The detector stack is located behind a long, narrow collimator that defines the 3° angular field of view (FWHM). The instrument geometric factor is approximately 3×10^{-3} cm^2 - sr [Reagan et al., 1981].

The aluminum shielding is sufficiently thick to stop electrons effectively with energy up to 5 MeV. Low-energy bremsstrahlung photons with energy up to about 150 keV, which are created in the low-atomic-number aluminum, are effectively attenuated by the tungsten shield located inside the aluminum and around the scintillator. Bremsstrahlung photons above about 150 keV, are not effectively attenuated by the tungsten nor detected in the plastic scintillator. A fraction of these photons can

interact in the E detector. Laboratory measurements with intense SR-Y-90 sources normally incident on the shielding of the SCATHA SC-3 instrument showed that the resulting bremsstrahlung count rate was only 3.4×10^{-4} , 5.1×10^{-4} , and 6.4×10^{-5} of the electron count rate at 250, 500 and 1000 keV, respectively. However, intense, energetic electron spectra observed on SCATHA showed some bremsstrahlung contamination in 390-keV-wide channels centered at 448, 830 and 1214 keV, but most predominately at the 448 keV channel [Davidson et al., 1988]. The bremsstrahlung detection efficiency in the D-detector was observed to be completely insignificant because of the small volume of this sensor. This observation was verified by the lack of bremsstrahlung observed in the D-detector in SCATHA SC-3 results.

Each of the three identical SEP particle telescopes has a high-resolution, 3° (FWHM) field of view provided by a long collimator (20 cm) containing 10 baffles that define this response. The collimators are identical to that used on SC-3. The three SEP telescopes are stacked at 80°, 60°,and 40° to the CRRES spin axis. High-temporal resolution measurements over 12 energy channels are obtained every 0.25 seconds, with a dead time of 2 ms, by the $80^{\circ}$and 60° telescopes. The 40° telescope accumulates for 0.5 seconds, due to telemetry restrictions, with a dead time of 4 ms. A pitch-angle distribution from 0° to 180° over 12 channels is completed every 15 seconds at the CRRES final spin rate of 2 rpm. The fine angular resolution together with this optimum arrangement of the three telescopes provides nearly complete measurements of the particle distribution function for

all orientations of the spin axis with respect to the magnetic field direction.

The three SEP spectrometer heads are packaged into one unit as shown in Figure 2. A separate instrument analyzer electronics package is mounted near the sensors; both units are mounted on the bottom of the spacecraft and are separated to achieve a lower temperature in the silicon detectors for improved low-energy electron detection. [Voss et al., 1982a, 1982b].

A functional block diagram of the SEP instrument is shown in Figure 3. Each sensor (A - 80°, B - 60°, C - 40°, respectively) operates from its own 256, 8-bit word CMOS memory, which is individually addressable and loadable via a 16-bit serial-digital command. Four of these words completely define one operating mode (32-bit control register) for an individual sensor. A mode is defined by specifying the logic conditions (coincidence/anticoincidence), gain, and energy thresholds required between the four detector elements to uniquely establish a particle type and energy range for analysis. A choice of two amplifier gain settings for the D- and E-detectors is available. The lower- and upper-energy thresholds selected for analysis by the 12-channel pulse-height analyzer are determined to 8-bit and 6-bit resolution, respectively. Either the D- or E-detector is selectable at any time through the multiplexer for analysis by the pulse-height analyzer (PHA). The energy threshold of the sensor not selected for analysis can be set to 8-bit resolution.

The operating modes can be structured to emphasize one particle type (i.e., electrons) or all particle types in a

sequential fashion to concentrate on special events, such as solar particle events, or to dwell on a narrow energy region of interest with any particle type. The commandable options are extensive, but an optimum operating configuration will be loaded initially and adjusted as conditions dictate. The ability to select a hard-wired backup mode is also available should a major failure occur in the memory operation. The hardwired backup mode measures the higher-energy electrons (215-5100 keV) and is independent of the memory. The instrument operates in this condition automatically at turn-on and whenever the memory is being loaded or disabled.

The operating modes will be selected as required to optimize data collection in the inner and outer radiation belts. The basic programmable mode parameters are the energy range and energy channel widths for the electrons and for the protons. Typical modes that may be used during the CRRES mission are shown in Table 1. During the first several months of operation, ELEC1, ELEC2, PROT1 and PROT2 have been used. These four modes are sequentially cycled by all three telescopes in unison, when possible, with a dwell of 32 seconds in each mode. Modifications to this sequence will be made after examination of the data, in response to changes in geophysical conditions, and for special studies. During a solar particle event, for example, all seven modes will be cycled at a 32 second dwell.

III. Calibration

The SEP sensor heads were calibrated using electron and proton beams from accelerators at the Goddard Space Flight Center

(GSFC) in Greenbelt, MD, and at Harvard University in Cambridge, MA. Two accelerators were utilized at GSFC, a low-energy electron machine for energies up to 150 keV and a Van de Graaff accelerator with a maximum energy of 1.5 MeV for both electrons and protons. The sensors were in vacuum at room temperature for these runs. The beam rate of the low-energy accelerator was stable to about 25% at a few thousand counts per second for electrons between 25 and 150 keV. The Van de Graaff accelerator extended the electron measurements to 1500 keV in ten steps and started the proton range from 500 to 1500 keV in five energy steps.

High-energy proton calibrations were done in air at the Harvard Cyclotron Laboratory for eight energy steps between 35 and 100 MeV. The 159 MeV proton beam is reduced in energy by absorbers which produce a beam energy spread of less than 6% at 90 MeV and above, while the spread is about 40% at the lowest energies. The measured energy deposition from higher-energy protons penetrating the detectors is within 1 MeV of calculated values. The resulting energy ranges of the initial setting for each mode of each sensor are shown in Table 1. The mode ranges are electronically divided into 12 channels, each approximately having the channel width shown in the table. The energy ranges in Table 1 show some overlap between modes. The particle collimation, the D-detector absorption, and the sensor coincidence circuitry combine to significantly reduce the overlap. Further minor adjustments will be made in the energy-range programming after examination of the data.

IV. Results

SEP has been working well since turn-on and commenced normal operations on August 7, 1990, after a succesful instrument activation period. Preliminary results for orbit 68, which occurred on August 22, day 234 of 1990, are shown in Figure 4. Spectrograms of the spin-averaged count rates over 32 s for both electrons and protons from sensor A are displayed as a function of energy and time to present an overview of the changing particle populations. The upper two panels contain electron intensities for energies from 42 to 5030 keV. The lower-energy electrons (ELEC1) in the upper panel demonstrate smooth, slowly varying count rates except at the lower altitudes, where the spectrum begins to harden. The higher-energy electrons (ELEC2) in the second panel show variations associated with the inner and outer radiation belts. The lower two panels present the proton count rates with energies from 0.88 to 38.7 MeV (PROT1 and PROT2). While the 1 MeV protons are observed throughout the orbit, the 10 to 20 MeV protons seen in the bottom panel are primarily in the inner proton belt at low altitudes.

To determine the differential particle flux from the SEP count rate, the net count rate is calculated by subtracting any known background count rate, such as that from the weak radioactive calibration sources located in each spectrometer head. Then the net count rate is divided by the product of the live time percentage (which falls below 100% at high count rates), the spectrometer geometric factor, the energy width of the channel for the particular mode, and the sensor particle detection efficiency

for the channel (which is about 70 percent). Pitch-angle distributions for each sensor can be calculated using the sensor look directions and the magnetic field direction in the same frame of reference.

V. Conclusion

A full description of the particle distribution in time, energy, pitch angle and magnetic L-shell parameter, utilizing data from all three sensors, will allow the computation of the particle distribution functions in phase space for the energetic electrons and protons. These distributions can then be used for developing models of the dynamic behavior of the radiation belt populations. Preliminary work towards this goal has been completed utilizing SCATHA outer-belt electron distributions together with a general solution to a simple form of the simultaneous bimodal (radial and pitch-angle) diffusion equation [Chiu et al., 1988; 1990]. The CRRES SEP data set should facilitate the dynamic modeling of the radiation belts.

Acknowledgements

The authors wish to thank J.C. Bakke, L.A. Hooker, and V.F. Waltz for their efforts in the design, development, and fabrication of this instrument. We also deeply appreciate the assistance of our coinvestigators, H.D. Voss, J.M. Quinn and R.M. Robinson. This work was primarily supported by the Office of Naval Research under contract N00014-83-C-0476 and in part by the Lockheed Independent Research Program. Special appreciation goes

to the Ball Aerospace Systems Division who built the successful CRRES satellite; to the USAF Space Test Program and the NASA Marshall Space Flight Center, who share in the management of the project; to General Dynamics for the successful launch of Atlas-Centaur rocket; and to the USAF Consolidated Space Test Center, which operates the satellite, for their important contributions to the success of the ONR-307-3 experiment.

Chiu, Y.T., M.A. Rinaldi, and R.W. Nightingale, Toward dynamic modeling of the outer electron radiation belt, J. Geophys. Res., 95, 12069, 1990.

Chiu, Y.T., R.W. Nightingale, and M.A. Rinaldi, Simultaneuos radial and pitch angle diffusion in the outer electron radiation belt, J. Geophys., Res. 93, 2619, 1988.

Collin, H.L., J.M. Quinn, G.R. Smith, E. Hertzberg, S. Roselle, and S.J. Battel, The low energy ion mass spectrometer, this issue, 1991.

Davidson, G.T., P.C. Filbert, R.W. Nightingale, W.L. Imhof, and J.B. Reagan, Observations of intense trapped electron fluxes at synchronous altitudes, J. Geophys. Res., 93, 77, 1988.

Reagan, J.B., R.W. Nightingale, E.E. Gaines, W.L. Imhof, and E.G. Stassinopoulos, Outer zone energetic electron spectral measurements, J. of Spacecraft and Rockets, 18, 83-88, 1981.

Stevens, J.R. and A.L. Vampola, Description of the space test program P78-2 spacecraft and payloads, Space and Missile Systems Organization, Air Force Systems Command, Report No. TR-78-24, 1978.

Voss, H.D., A.G. Ghielmetti, S.J. Battel, K.L. Appert and R.R. Vondrak, The Medium Energy Ion Mass Spectrometer (IMS-HI) (ONR-307-8-3), this issue, 1991.

Voss, H.D., J.B. Reagan, W.L. Imhof, D.O. Murray, D.A. Simpson, D.P. Cauffman, and J.C. Bakke, Low temperature characteristics of solid state detectors for energetic X-ray, ion and electron spectrometers, IEEE Trans. Nucl. Sci., NS-29, 164, 1982a.

Voss, H.D., J.C. Bakke, and S.N. Roselle, A spacecraft multichannel analyzer for a multidetector solid state detector array, IEEE Trans. Nucl. Sci., NS-29, 173, 1982b.

Figure 1: A cross-sectional view of one of the SEP telescopes.

Figure 2: The SEP sensor package showing the look directions of each of the 3° FWHM telescopes.

Figure 3: A functional block diagram of the SEP analyzer package.

Figure 4: Spectrograms of the spin-averaged SEP count rates for electrons (upper two panels) and protons (lower two panels) during CRRES orbit 68 on August 22, 1990.

Table 1. SEP Initial Energy Range and Channel Widths

	SENSOR A		SENSOR B		SENSOR C	
MODE	ENERGY RANGE (MeV)	WIDTHS (MeV)	ENERGY RANGE (MeV)	WIDTHS (MeV)	ENERGY RANGE (MeV)	WIDTHS (MeV)
ELEC1	.042-.324	.0235	.042-.336	.0245	.041-.313	.0227
ELEC2	.212-5.03	.402	.218-5.15	.410	.209-5.08	.406
PROT1	.875-6.60	.478	.916-6.70	.482	.920-6.80	.490
PROT2	2.5-38.7	3.01	2.2-33.7	2.62	2.0-30.4	2.37
PROT3	35.8-80.2	3.7	31.2-69.9	3.22	28.2-63.1	2.91
PROT4	45-94	4.08	45-105	5.00	45-110	5.42
ALPHAS	6.8-24	1.43	6.90-24.3	1.45	7.00-24.6	1.47

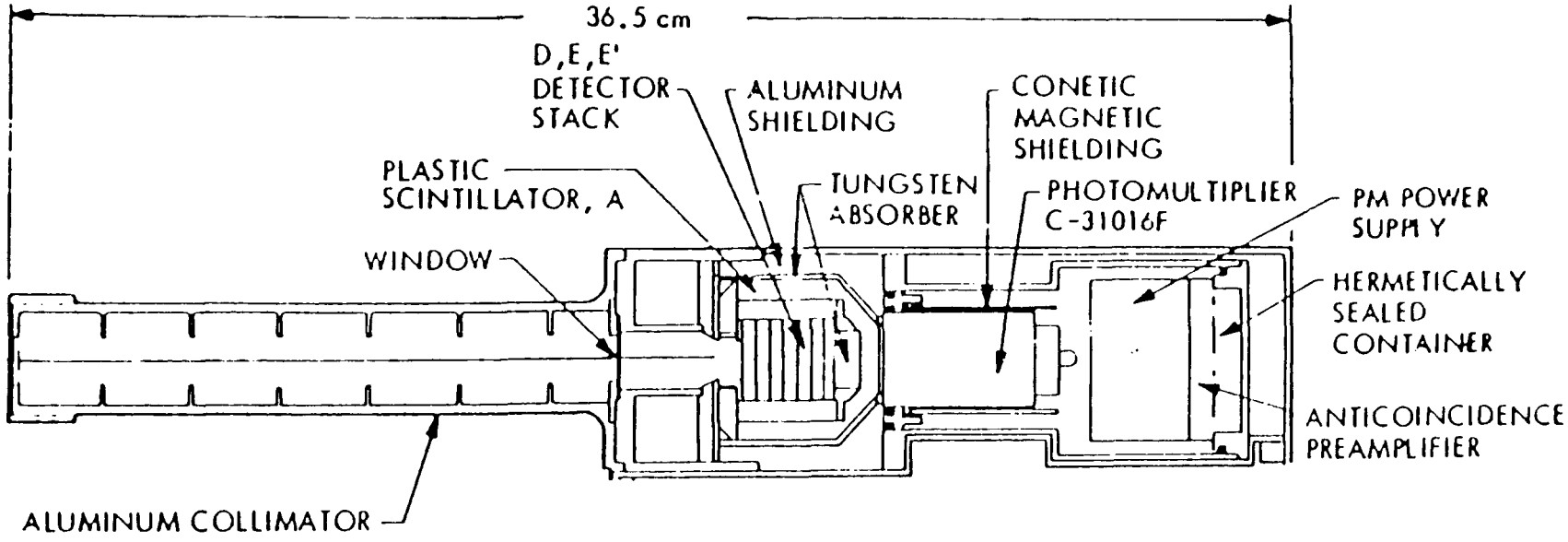
36.5 cm
D,E,E'
DETECTOR
STACK
ALUMINUM
SHIELDING
CONETIC
MAGNETIC
SHIELDING
PLASTIC
SCINTILLATOR, A
TUNGSTEN
ABSORBER
PHOTOMULTIPLIER
C-31016F
PM POWER
SUPPLY
WINDOW
HERMETICALLY
SEALED
CONTAINER
ANTICOINCIDENCE
PREAMPLIFIER
ALUMINUM COLLIMATOR

Figure 1

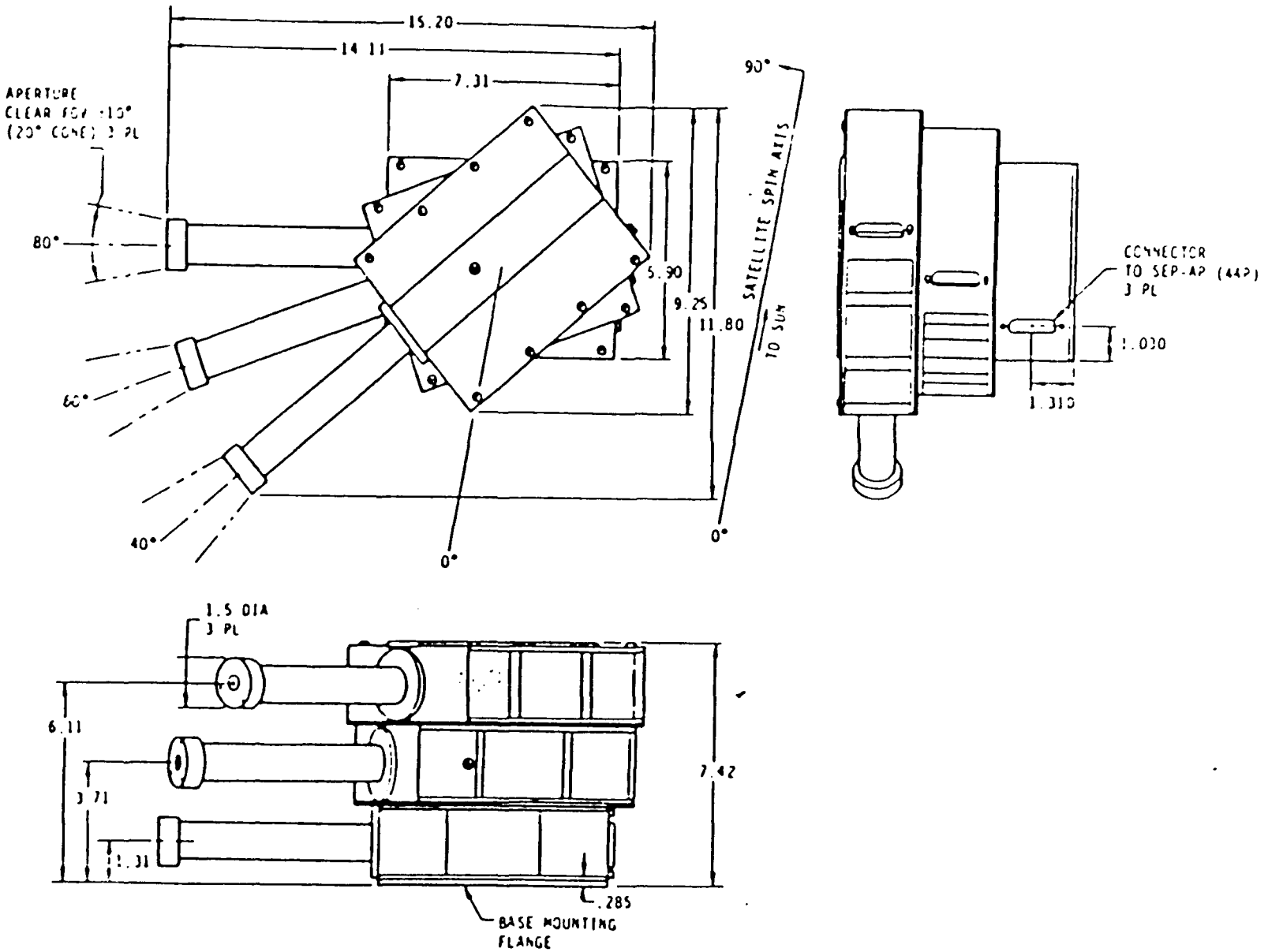
15.20
14.11
7.31
APERTURE
CLEAR FOV ±15°
(20° CONE) 3 PL
80°
60°
40°
0°
5.90
9.25
11.80
90°
SATELLITE SPIN AXIS
10 SUN
0°
CONNECTOR
TO SEP-AP (44P)
3 PL
1.030
1.310
1.5 DIA
3 PL
6.11
3.71
1.31
7.42
.285
BASE MOUNTING
FLANGE

Figure 2

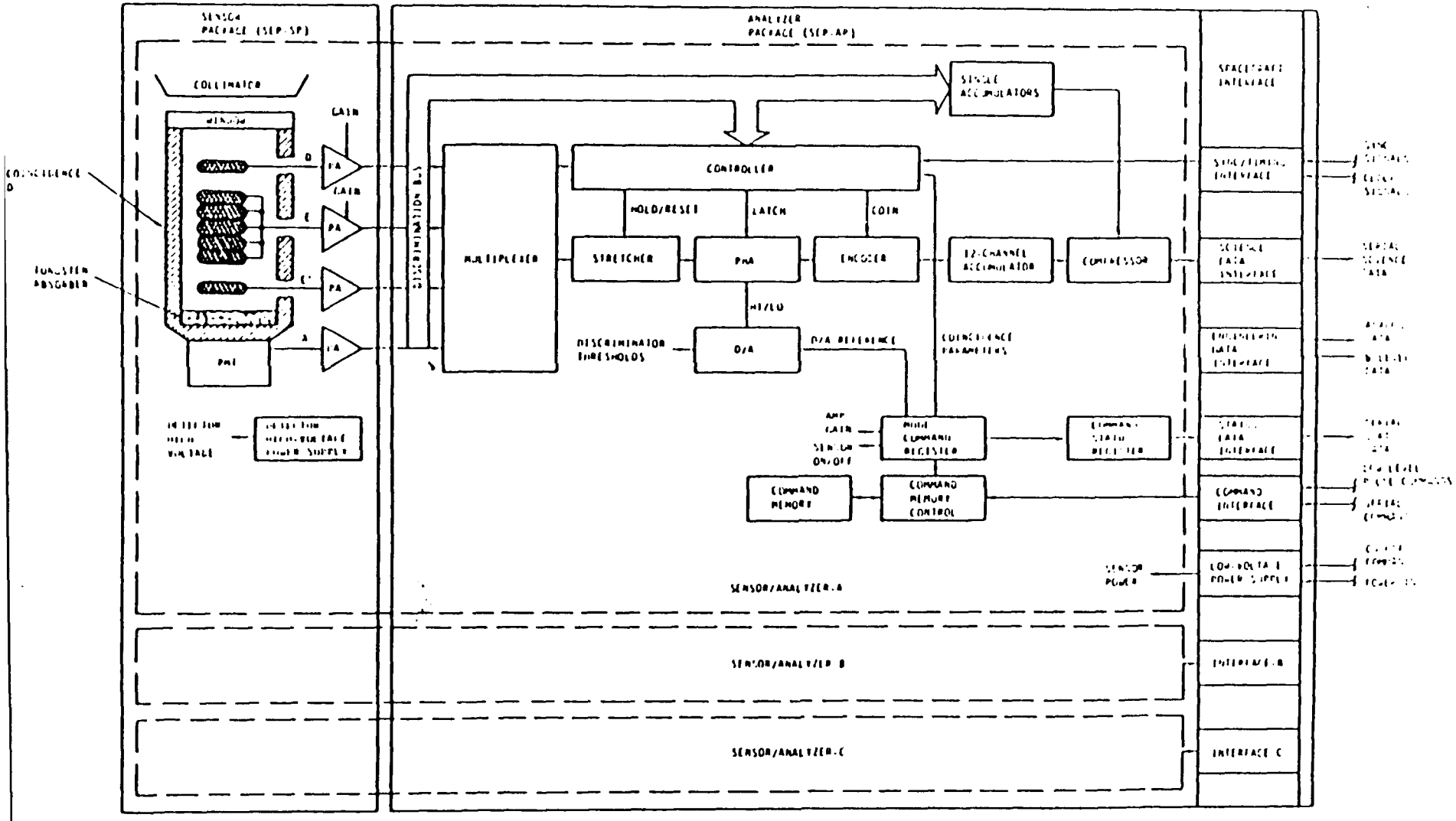
SENSOR PACKAGE (SEP-SP)
ANALYZER PACKAGE (SEP-AP)
COLLIMATOR
GAIN
PA
TUNGSTEN ABSORBER
PMT
MULTIPLEXER
CONTROLLER
HOLD/RESET
LATCH
COIN
STRETCHER
PHA
ENCODER
SINGLE ACCUMULATORS
12-CHANNEL ACCUMULATOR
COMPRESSOR
HI/LO
D/A
DISCRIMINATOR THRESHOLDS
D/A REFERENCE
COINCIDENCE PARAMETERS
APP GAIN
SENSOR ON/OFF
MODE COMMAND REGISTER
COMMAND MEMORY
COMMAND MEMORY CONTROL
SPACECRAFT INTERFACE
SCIENCE DATA INTERFACE
COMMAND INTERFACE
SENSOR POWER
SENSOR/ANALYZER-A
SENSOR/ANALYZER-B
SENSOR/ANALYZER-C
INTERFACE B
INTERFACE C

Figure 3

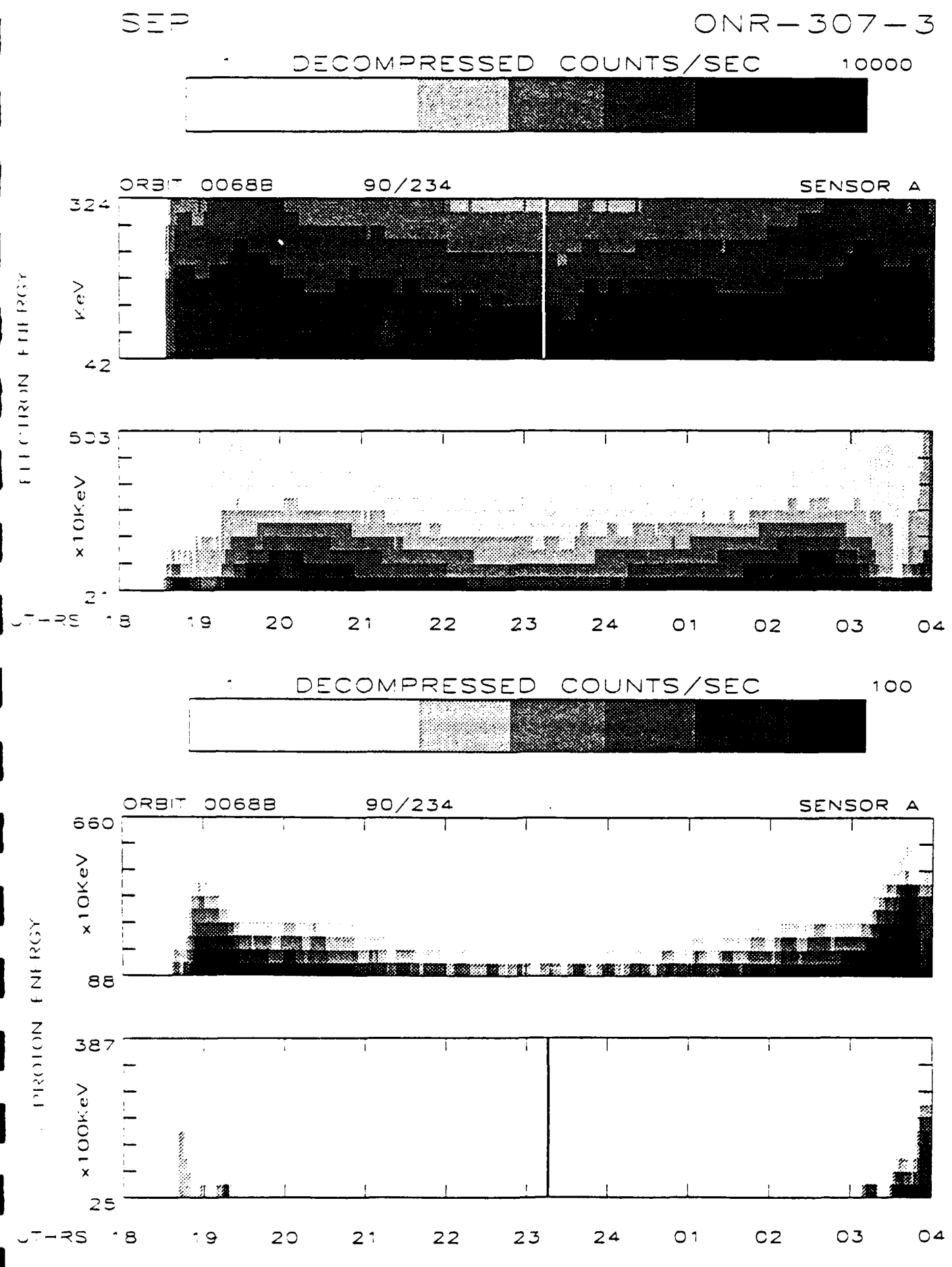
SEP
ONR-307-3
DECOMPRESSED COUNTS/SEC
10000
ORBIT 00688
90/234
SENSOR A
324
KeV
42
503
x10KeV
18
19
20
21
22
23
24
01
02
03
04
DECOMPRESSED COUNTS/SEC
100
ORBIT 00688
90/234
SENSOR A
660
x10KeV
88
387
x100KeV
25
18
19
20
21
22
23
24
01
02
03
04

Figure 4

APPENDIX 2

THE LOW ENERGY ION MASS SPECTROMETER (ONR-307-8-1,2)

The Low Energy Ion Mass Spectrometer (ONR-307-8-1,2)

H. L. COLLIN, J. M. QUINN, G. R. SMITH, E. HERTZBERG,

S. ROSELLE, AND S. J. BATTEL

Abstract -- The Low Energy Ion Mass Spectrometer on the CRRES satellite is designed to measure the energy and pitch-angle distributions and composition of ring current ions in the range of 0.1 - 35 keV and 1 - 32 AMU/e or optionally higher masses in a lower energy range. The background electron flux monitors measure electrons between 0.067 - 20 keV in eight broad energy bands.

I. SCIENTIFIC OBJECTIVES

The Low Energy Ion Mass Spectrometer (IMS-LO) on CRRES is designed to measure the composition of plasmas which are the sources of radiation belt particles, and to provide data on the origin and acceleration processes of these plasmas. In order to achieve these objectives, the instrument measures energy and mass spectra covering the ranges of E/q = 0.11 - 35 keV/e and M/q from 1 - 32 AMU/e with good coverage of pitch angles throughout the CRRES orbit.

The determination of the behavior of different ion species in the energy range covered by the IMS-LO instrument is critical to the development of detailed dynamic ring current models. These modelling efforts will require detailed knowledge of the particle source contributions, transport phenomena, energization processes and, finally, scattering and loss mechanisms. Ion composition data are essential for the determination of total ion energy density (ring current) and they provide a necessary link in modelling the life of ring current ions.

These data will be used to investigate plasma interaction processes including: 1) the plasma and field conditions that produce the acceleration of ions, precipitation of energetic particles from the trapped populations, and VLF wave generation and amplification; 2) the local time and invariant latitude distributions of ionospheric ion source regions; and 3) the large-scale and small-scale transport and energization processes for the hot plasmas.

II. MEASUREMENT TECHNIQUES

The IMS-LO-1,2 instruments on CRRES rely upon essentially the same design that was successfully implemented with previous Lockheed instruments on SCATHA (launched January 1979) and S3-3 (launched July 1976). Improvements have been made with each version of the instrument in range of coverage, resolution, and operating flexibility.

IMS-LO-1 and IMS-LO-2 are identical instruments which are mounted at 45° and 75° to the spacecraft spin axis in order to maximize coverage of fluxes near the magnetic field line direction. Each instrument performs ion composition measurements in the energy per charge range 0.11-35 keV/e and the mass per charge range 1 - 32 AMU/e. The energy range, which is covered by 45 energy steps, is broken into three contiguous parts (j = 0,2), each consisting of 15 energy steps (i = 0,14). The mean energy per charge (E_{ij}) of ions on the i^{th} step of the j^{th} part is given by

$$E_{ij}\,(\text{keV}) = 0.109 \times (1.14008)^{(i+15j)}$$

The three parts of the energy coverage are sampled in parallel by three separate analyzer and sensor units ("heads"). At the completion of each 15 step sequence, the background counting rate is measured for each sensor head. The mass range (1 - 32 AMU/e) is covered by 32 steps. Alternatively, the spectrometer can be commanded to sample the high mass range above 8 AMU/e. In addition to ion measurements, each of

the two instruments monitors the background electron flux at four fixed energies. The electron channels are described in a separate section below.

A. Ion Optics

Each of the IMS-LO mass spectrometers consists of three analyzer heads which measure ions in a different portion of the E/q range from 0.11-35 keV/e. One of the analyzer heads is illustrated in Figure 1. The analyzer consists of four sections, a collimator, a velocity filter, an energy analyzer and a channel electron multiplier detector.

Ions enter the instrument through the collimator which provides an acceptance cone of approximately 5° full width. Following collimation, the ions enter the crossed electric and magnetic field velocity filter (Wien Filter), which acts as the mass analyzer (MA). Its magnetic field is fixed while the crossed electric field is varied according to the value of E/q and M/q being sampled. The fields are oriented so that the electric and magnetic forces on an ion are in opposition, and the electric field is chosen so that there is no net force on an ion of the desired mass and energy, allowing it to pass through the MA in a straight trajectory. The MA magnetic fields in the three heads are nominally 445, 1211, and 3304 Gauss. The electric field plates of the MA are driven symmetrically and the voltages for a given mass selection scale as the square root of the ion energy which is determined by the voltage applied to the electrostatic analyzer. The maximum MA plate potentials in the three heads, corresponding to the minimum ion mass and the maximum energy per charge sampled within each head, are nominally, ±35, ±253, and ±1850 V for the normal mass range and a factor of four lower for the heavy ion mode. All three heads are driven by a common high voltage power supply and a divider network which provides the different ranges required.

Following the velocity filter, ions are bent 180° in a hemispherical sector electrostatic analyzer (EA) which is angle focusing and energy dispersive. As with the MA,

the EA plates in all three heads are driven by a common power supply and a divider network. The ratio between consecutive values of the logarithmically spaced energy steps is approximately 1.14, and there are 15 energy steps assigned to each head. Thus the energy per charge being simultaneously sampled by the three heads are spaced by a factor of approximately 7, with the first head covering from 0.11-0.68 keV/e, the second from 0.78-4.9 keV/e, and the third from 5.6-35 keV/e. The EA plate separation in the high energy head is reduced from that of the other two heads in order to achieve the desired energy range without the need for excessively high voltages. After exiting the EA, ions are post-accelerated and enter the channel electron multiplier detector.

The stepping of the EA and MA is coordinated under digital control in a number of modes as described in the following section. Each sample of a particular mass-energy value takes 64 ms. There is a 12 ms deadtime at the beginning of each sampling period to ensure complete settling of the analyzer power supplies, even in the worst-case transitions.

In addition to the energy steps described above, there is an additional setting in which each of the three heads measures background counts. The background measurement is performed by disabling the MA power supply and setting the EA power supply to step 4. As the MA power supply decays toward zero, the analyzers pass continually higher masses. Following the 12 ms deadtime, the background channel is sampling mass per charge values well above those of ambient ions and measures the instrument background response only.

B. Electron Detectors

Each of the IMS-LO instruments contains a set of four broadband, fixed-energy electron detectors, Figure 3, which are used to monitor electron fluxes between 50 eV and 25 keV. Electrons entering one of these instruments are collimated to a 5° acceptance cone and pass through an aperture which sets the geometric factor. The electrons are

then bent 180° in a magnetic analyzer and pass through an exit aperture which sets $\Delta E/E$ before entering the channeltron sensor. The $\Delta E/E$ for each detector is 50% and the central energies of the electron channels on IMS-LO-1 and IMS-LO-2 are interleaved, providing a total of eight channels with central energies from 0.067 to 20 keV. The electron detectors accumulate for 512 ms, providing samples approximately every 6° of spacecraft spin.

III. OPERATING MODES AND CONTROL

There are two basic submodes of operation of the mass spectrometers; SWEEP and LOCK. Each of these submodes takes 32.768 seconds to complete, approximately one spacecraft rotation.

The LOCK submode maximizes resolution in time and pitch-angle by concentrating on selected masses. The instrument is locked on the selected mass per charge while stepping in energy. Each energy step and background are sampled for 64ms and the three sensor heads together acquire a 45 point energy spectrum in 1.024 seconds, approximately 12° of spacecraft rotation. In the LOCK submode 32 consecutive energy spectra are acquired at the selected mass before the instrument moves into the next submode.

The SWEEP submode examines the mass spectrum in more detail but with reduced resolution in time and pitch-angle. In this submode the instrument acquires a mass spectrum at each energy step by sweeping through all 32 mass steps while the energy is held steady. Each mass step is sampled for 64ms and a full mass spectrum is acquired in 2.084 seconds. The complete mass-energy spectrum, 32 mass steps at each of 45 energy steps together with 32 background measurements, is acquired in 32.768 seconds.

Eight submodes are combined to form the three basic modes of operation; LOCK-ONLY, SWEEP-ONLY, and SWEEP-LOCK. As the names imply, LOCK-ONLY consists of LOCK submodes only, SWEEP-ONLY is composed of SWEEP submodes, and SWEEP-LOCK alternates between SWEEP and LOCK. In either the LOCK-ONLY or SWEEP-LOCK modes, the mass steps used in

the LOCK submode are taken sequentially from four values which are held in the instrument memory. These values may select any four of the 32 M/q steps corresponding to any four ion species; for instance, H^+, He^+, He^{++}, O^+; or H^+, O^+, H^+, O^+; or O^+, O^+, O^+, O^+. IMS-LO-1 and IMS-LO-2 are commanded independently so that it is possible to have the two instruments operating in different modes simultaneously. The operating mode and LOCK mode mass steps can be selected by command.

In addition to the normal range of mass coverage, the instrument can be commanded into a Heavy Ion Mode. In this mode, the MA and EA voltages are reduced by a factor of four, scaling the M/q coverage upward and the energy downward to give an operating range of 8 - 256 AMU/e and 0.014 - 4.5 keV.

The discriminator threshold for each detector is set by command to one of four values. A special calibration cycle will be commanded periodically which locks on a selected mass step and sequentially steps through the thresholds in order to monitor the channel electron multiplier gain. In addition, the calibration command may optionally enable pulses at a known rate to monitor performance of the signal processing electronics. The channel electron multiplier bias is command selectable to one of four values to compensate for possible channel multiplier gain degradation over the life of the mission.

IV. CALIBRATION

A good understanding of the characteristics of the mass spectrometers' response to ambient ions is necessary in order to correctly interpret the data it obtains, to optimize its operating modes and to determine the correct ratios for the EA and MA voltage divider networks.

Three approaches were used which provided complimentary information on the spectrometers' characteristics. During the design phase, detailed ray tracing studies

provided a baseline description of the variation of the mass spectrometers' response to ions' energy, mass and approach direction.

The flight instruments were individually calibrated in the Lockheed Palo Alto Research Laboratory mass spectrometer calibration facility in which they were exposed to monoenergetic beams of selected ion species. The detailed energy-mass response of each spectrometer head was investigated at a number of representative energies. At each energy an ion beam of H^+ or Ne^+ at the selected energy was directed at the instrument and the EA and MA voltages varied in small increments to provide a dense mesh of measurements to characterize the response function.

Since the full response is dependent on approach angle and incidence position, as well as energy and mass, it was not practical to perform the huge number of individual measurements that would be needed with a monoenergetic beam in order to fully characterize all of the spectrometers' 45 energy steps. Instead ambient ring current ions were utilized as a multi-ion isotropic extended energy source which could be relied upon to fill the field of view of the spectrometer. With the instruments in SWEEP mode mass spectra were acquired at all energy steps. These measurements provided relative response functions for common mass species at all energy steps. Figure 2 shows peak shapes obtained in this way. The open circles with error bars are on-orbit data, while the dashed line represents inferred peak shapes. Separation of the species is seen to be quite good.

The acceptance angle is approximately conical with a full width at 50% sensitivity of 5°. The instrument geometric factors are $4 \times 10^4 cm^2$ ster for the two low energy heads and $2 \times 10^4 cm^2$ ster for the high energy head. The energy passband is approximately 10%.

V. DATA REDUCTION

The IMS-LO instruments completed their initialization sequence and began normal operations on August 4th 1990. They are operating well and returning good quality data. Figure 4 displays an example of a summary plot of data from one of the spectrometers. The summary plots provide an exellent overview of a whole orbit and display mass and energy spectra and pitch-angle distributions as a function of time. For these plots the data have been averaged over 262s intervals. The upper group of three panels show mass spectra from CXA1,2,3 each of which contain horizontal bands near the bottom and top. These correspond to H^+ and O^+ respectively. In the higher energy heads, CXA2,3, two faint intermittent bands corresponding to He^+ and He^{++} can also be distinguished. The next group of four panels show energy spectra of H^+, O^+, He^+, and He^{++}. For these plots the flux has been sorted into 15 logarithmically spaced energy bins. The lower two groups of three panels display the pitch-angle distributions of H^+ and O^+ in each of the three energy bands corresponding to the CXA heads for each of which the flux has been sorted into 15° pitch-angle bins.

ACKNOWLEDGMENTS.

The authors wish to express their appreciation to D. A. Simpson, A. L. Magoncelli, J. C. Bakke, L. A. Hooker, V. F. Waltz and T. C. Sanders for their efforts in the design, development and fabrication of this instrument. We are also deeply indebted to our co-investigators, R. G. Johnson, R. D. Sharp, R. R. Vondrak, and especially, E. G. Shelley for making this instrument (and its predecessors) possible.

Fig. 1. Schematic illustration of the ion mass and energy analysis optics for the Low Energy Ion Mass Spectrometer.

Fig. 2. Mass peak shapes at a representative energy step, from on orbit data. Points are actual data, lines are inferred peak shapes

Fig. 3. Schematic illustration of a single magnetic electron analyser.

Fig. 4. Example of summary plots of data from one ion mass spectrometer for a complete orbit.

This effort was supported by the Office of Naval Research under contract N00014-83-C-0476 and by the Lockheed Independent Research Program.

H. L. Collin, J. M. Quinn, G. R. Smith, E. Hertzberg, S. Roselle, are with Lockheed Palo Alto Research Laboratory Palo Alto, CA 94304.

S. J. Battel is with the University of Arizona,

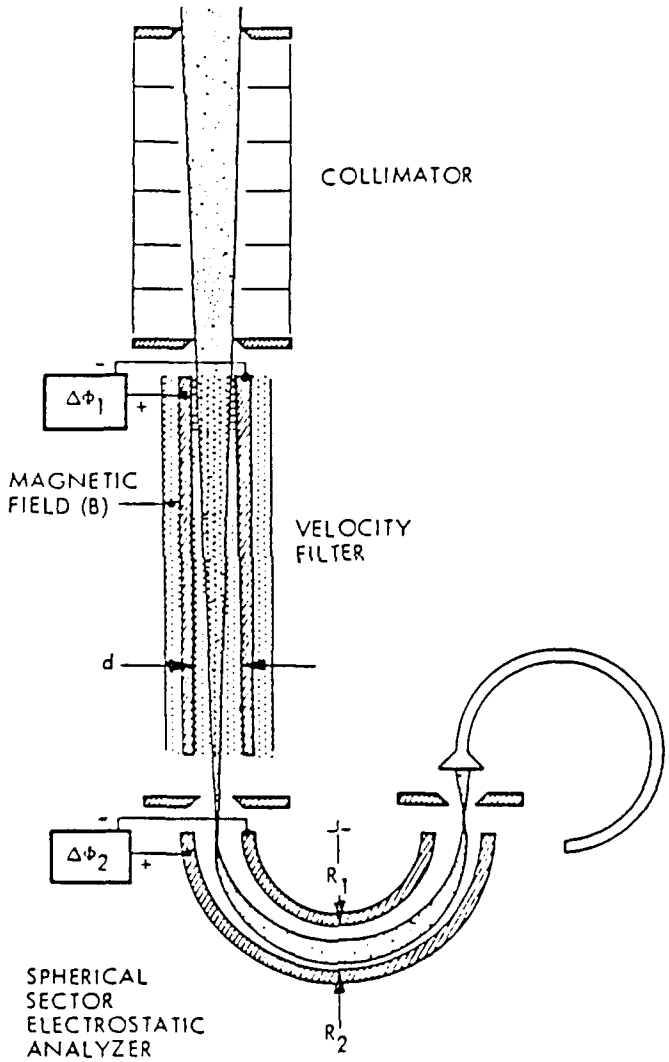

Fig. 1. Schematic illustration of the ion mass and energy analysis optics for the Low Energy Ion Mass Spectrometer.

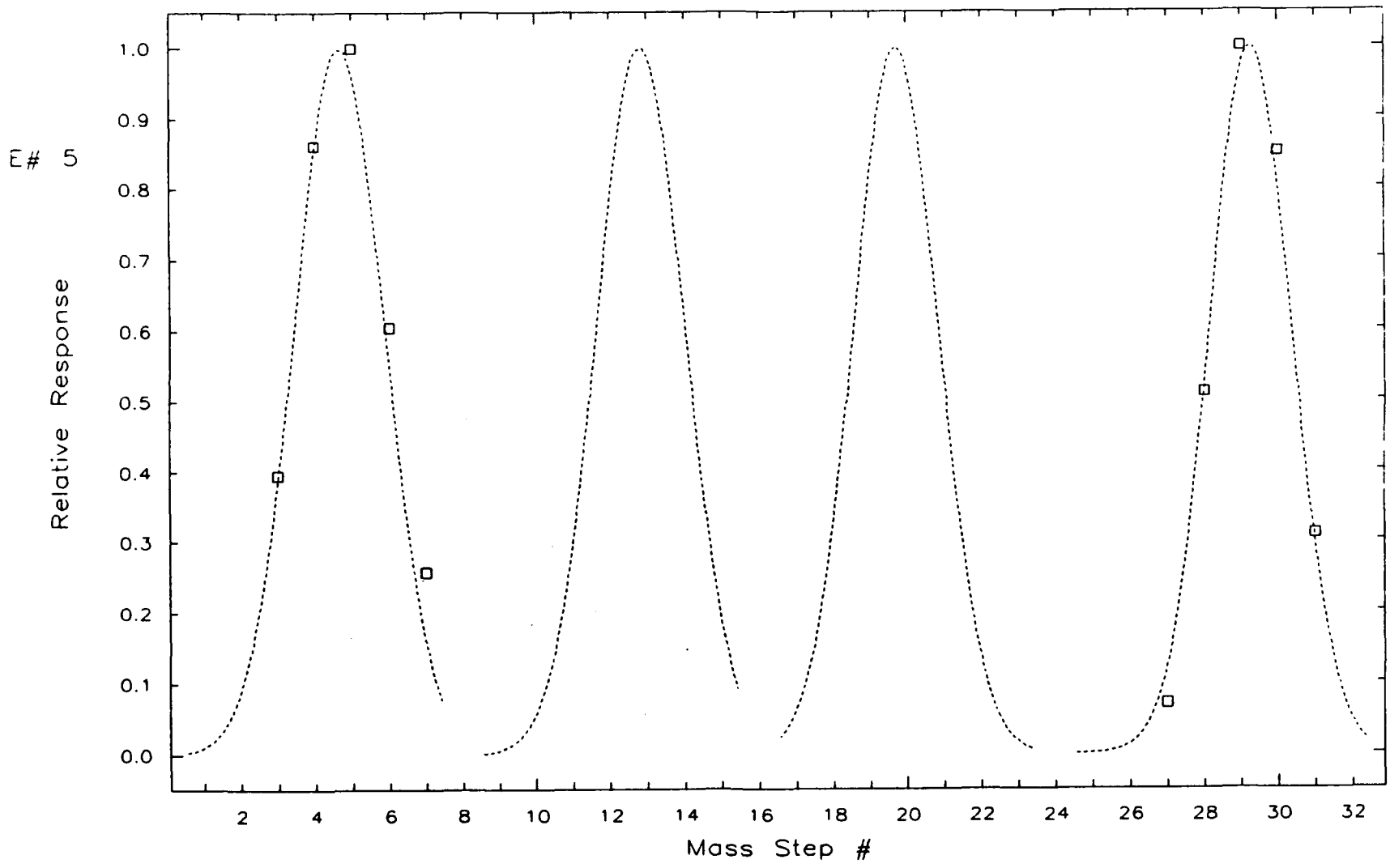
CXA3 IMS1
20-OCT-90 at 16:55
E# 5
Relative Response
1.0
0.9
0.8
0.7
0.6
0.5
0.4
0.3
0.2
0.1
0.0
2
4
6
8
10
12
14
16
18
20
22
24
26
28
30
32
Mass Step #

Figure 2

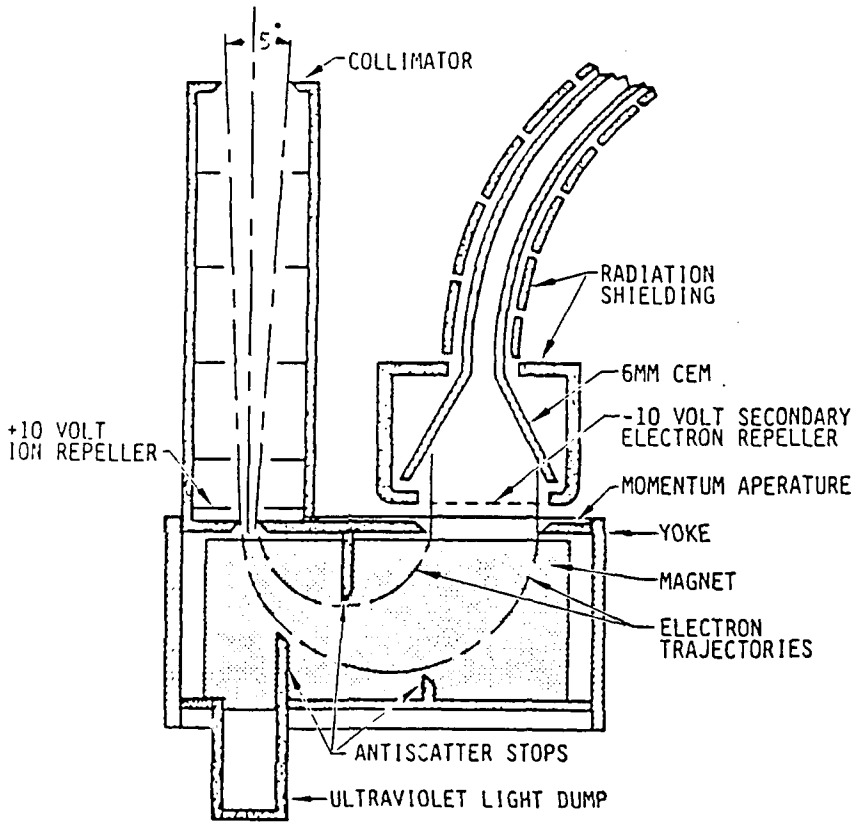

Fig. 3. Schematic illustration of a single magnetic electron analyser.

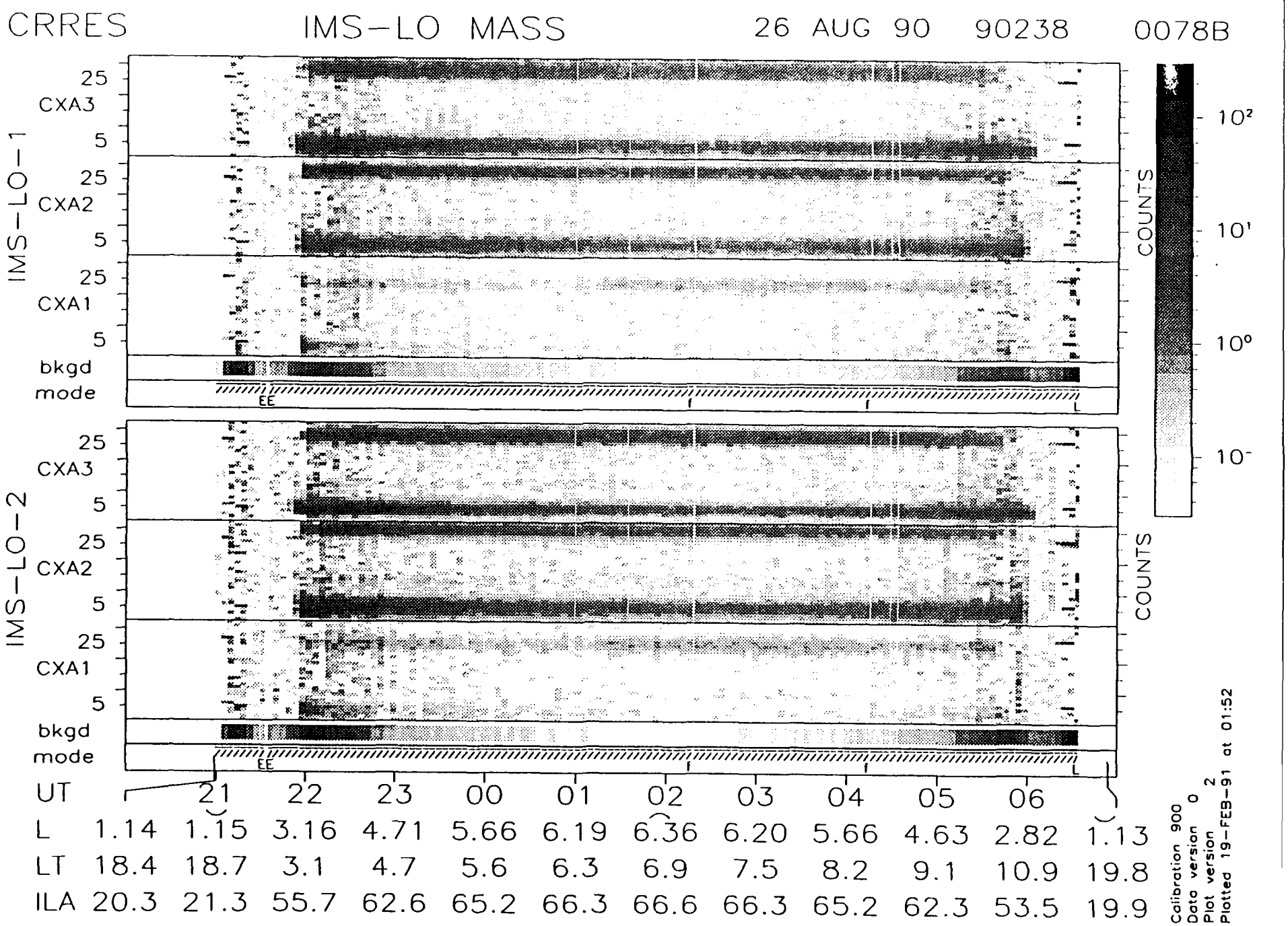
CRRES
IMS–LO MASS
26 AUG 90 90238 0078B
IMS–LO–1
IMS–LO–2
CXA3
CXA2
CXA1
bkgd
mode
EE
COUNTS
10^2
10^1
10^0
10^-
UT 21 22 23 00 01 02 03 04 05 06
L 1.14 1.15 3.16 4.71 5.66 6.19 6.36 6.20 5.66 4.63 2.82 1.13
LT 18.4 18.7 3.1 4.7 5.6 6.3 6.9 7.5 8.2 9.1 10.9 19.8
ILA 20.3 21.3 55.7 62.6 65.2 66.3 66.6 66.3 65.2 62.3 53.5 19.9
Calibration 900
Data version 0
Plot version 2
Plotted 19-FEB-91 at 01:52

Figure 4a

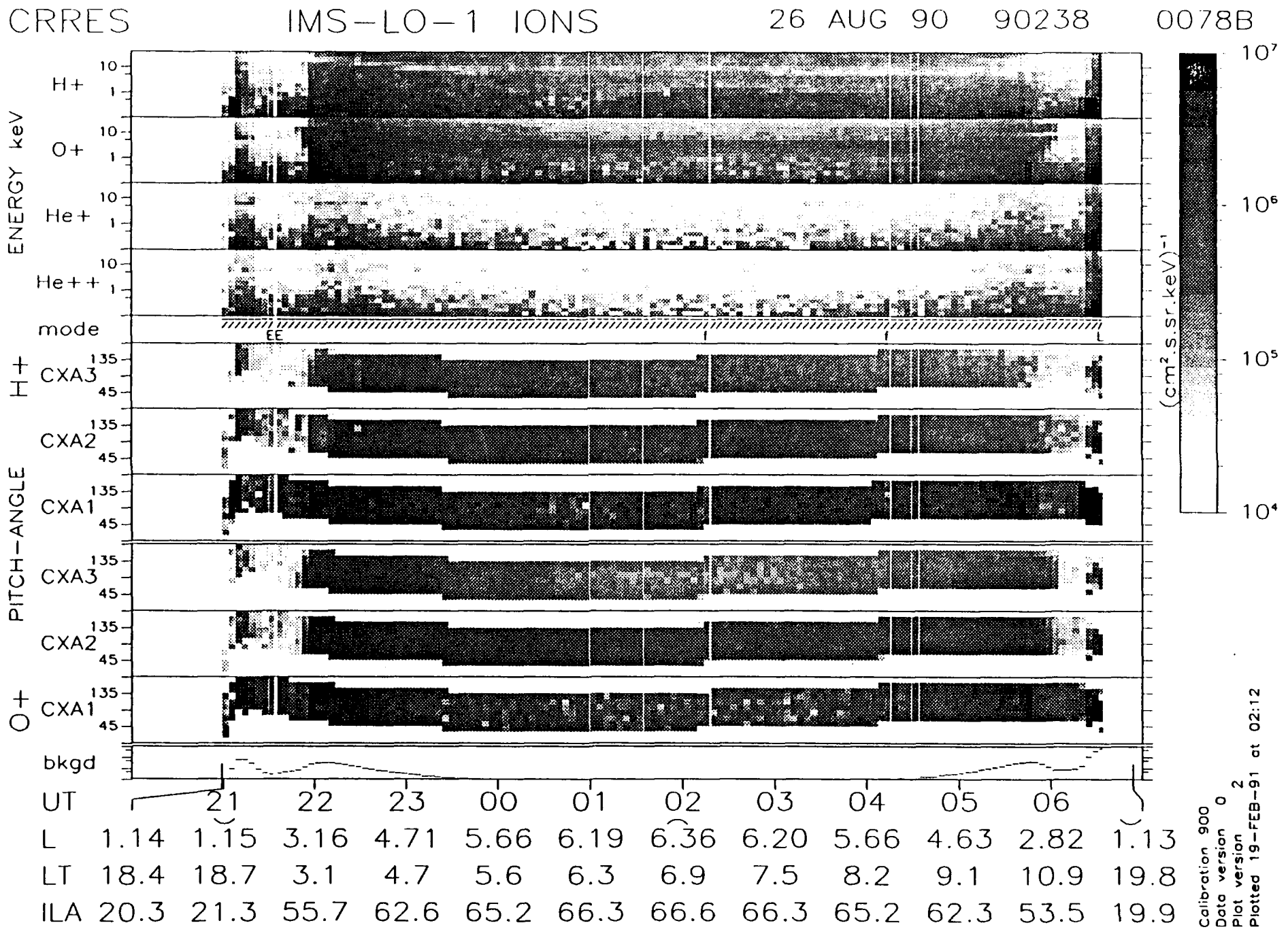
CRRES IMS-LO-1 IONS 26 AUG 90 90238 0078B
ENERGY keV
H+
O+
He+
He++
mode
EE
I
I
L
PITCH-ANGLE
H+
O+
CXA3
CXA2
CXA1
135
45
bkgd
(cm².s.sr.keV)⁻¹
10⁷
10⁶
10⁵
10⁴
UT 21 22 23 00 01 02 03 04 05 06
L 1.14 1.15 3.16 4.71 5.66 6.19 6.36 6.20 5.66 4.63 2.82 1.13
LT 18.4 18.7 3.1 4.7 5.6 6.3 6.9 7.5 8.2 9.1 10.9 19.8
ILA 20.3 21.3 55.7 62.6 65.2 66.3 66.6 66.3 65.2 62.3 53.5 19.9
Calibration 900
Data version 0
Plot version 2
Plotted 19-FEB-91 at 02:12

Figure 4b

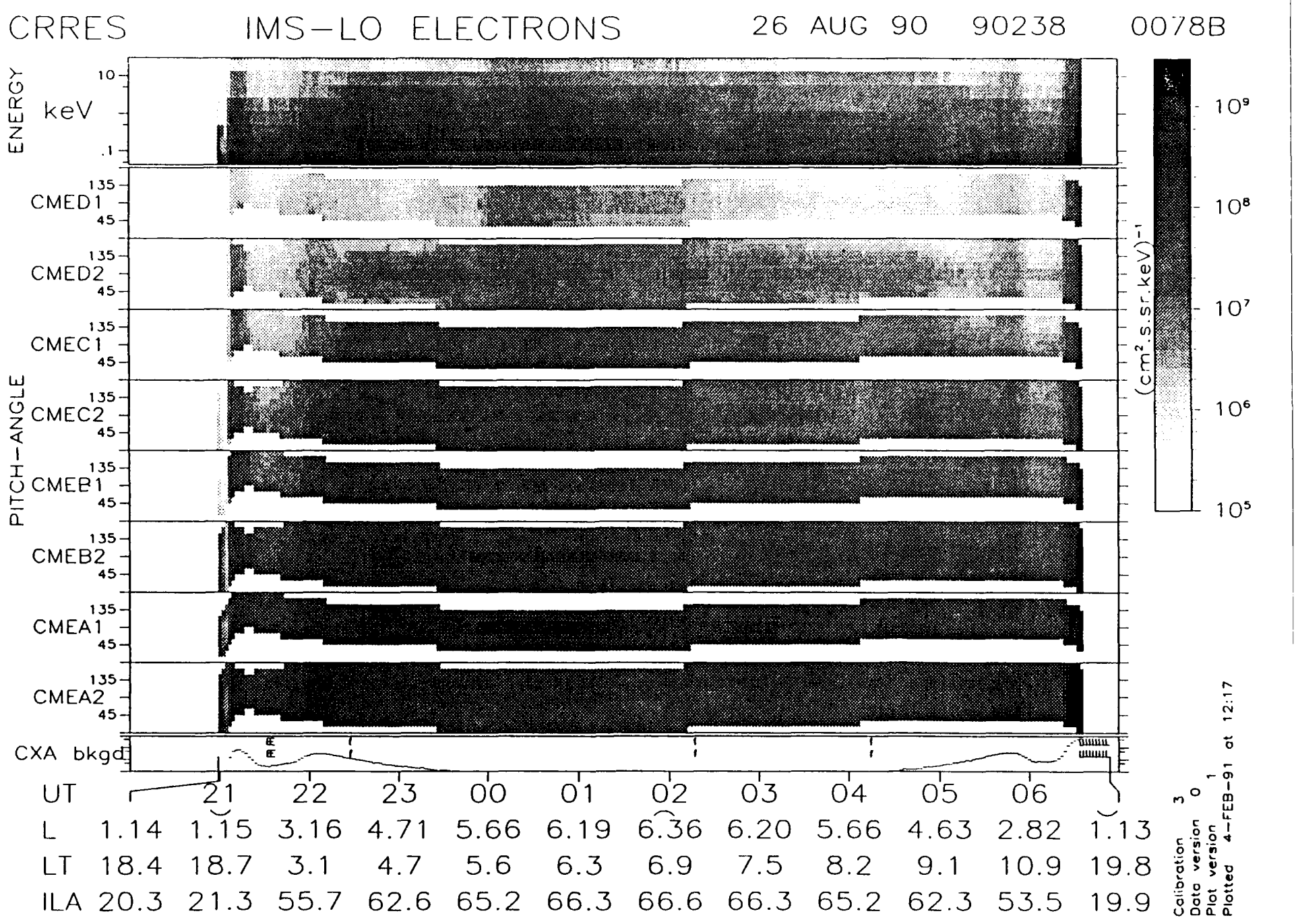
CRRES IMS–LO ELECTRONS 26 AUG 90 90238 0078B
ENERGY keV 10 .1
PITCH–ANGLE
CMED1 135 45
CMED2 135 45
CMEC1 135 45
CMEC2 135 45
CMEB1 135 45
CMEB2 135 45
CMEA1 135 45
CMEA2 135 45
CXA bkgd
(cm².s.sr.keV)⁻¹
10⁹
10⁸
10⁷
10⁶
10⁵
UT 21 22 23 00 01 02 03 04 05 06
L 1.14 1.15 3.16 4.71 5.66 6.19 6.36 6.20 5.66 4.63 2.82 1.13
LT 18.4 18.7 3.1 4.7 5.6 6.3 6.9 7.5 8.2 9.1 10.9 19.8
ILA 20.3 21.3 55.7 62.6 65.2 66.3 66.6 66.3 65.2 62.3 53.5 19.9
Calibration 3
Data version 0
Plot version 1
Plotted 4-FEB-91 at 12:17

Figure 24

APPENDIX 3

THE MEDIUM ENERGY ION MASS SPECTROMETER (ONR-307-8-3)

DRAFT

THE MEDIUM ENERGY ION MASS AND NEUTRAL ATOM SPECTROMETER (ONR-307-8-3)

H.D. Voss, E. Hertzberg, A.G. Ghielmetti
S.J. Battel, K.L. Appert, B. Higgins, D. O. Murray,
and R.R. Vondrak

Lockheed Palo Alto Research Laboratory
Space Sciences Laboratory
Dept. 91-20, B/255
3251 Hanover Street

March 22, 1991

Abstract

The primary objective of the medium energy ion mass spectrometer (ONR 307-8-3) on the CRRES satellite is to obtain the necessary data to contruct models of the energetic ion (10 to 2000 keV-AMU/q^2) and neutral atom (10 to 1500 keV) environment of the Earth's radiation belts. The spectrometer measures the energetic ion composition, energy spectrum, charge, and pitch angle distribution with good mass,temporal, and spatial resolution. The ion rejection in the neutral detector is <100 MeV-AMU/q^2. The instrument principle of operation is based on ion momentum separation in a 7000 gauss magnetic field followed by energy and mass defect analysis using an array of cooled silicon solid-state detectors. The architecture is parallel with simultaneous mass and energy analysis at relatively high sensitivity (100% duty cycle). The instrument is performing as designed in orbit with the major groups of hydrogen, helium, oxygen, and neutrals clearly resolved. The energetic ion composition during the 26 August 1990 storm illustrates the instrument performance.

1. SCIENTIFIC OBJECTIVES

The primary objective of the ONR-307 instrument complement is to obtain the necessary data to construct models of the energetic particle and plasma environment of the Earth's radiation belts. The instrument is part of the Combined Release and Radiation Effects Satellite (CRRES) which launched on 25 July 1990 into a geosynchronous transfer orbit (?600 x ? km) at an inclination of 18 degrees?. The Medium Energy Ion Mass Spectrometer (IMS-HI) measures both the energetic ion composition, energy spectra and pitch angle distributions and the energetic neutral particle energy spectra and pitch angle distributions with good mass, temporal, and spatial resolution. The IMS-HI is located at an angle of 75° to the spin axis to maximize pitch angle sampling. The ion energy range is approximately 10 to 2000 keV-AMU/q^2. The ion rejection in the neutral detector is < 100 MeV-AMU/q^2. In the innerbelt it is found that the integral ion flux > 100 MeV can be effectively measured with the neutral detector .

The IMS-HI instrument extends the energy range of ion composition measurements well above that of the traditional IMS-LO instruments, which are also part of the ONR-307 Experiment. The principle of the IMS-HI is based on ion momentum separation in a magnetic field (m/q^2 device) followed by energy and mass defect analysis using an array of cooled silicon solid state sensors. The incident energy on a solid state detector is equal to $(qRB)^2/2m$ (where R is the gyroradius in the magnetic field B). The IMS-HI features a parallel architecture with simultaneous mass and energy analysis at relatively high sensitivity (100% duty cycle).

The instrument is performing well in orbit according to the desired design specifications. The IMS-HI measurements will be used in concert with the other CRRES sensors to investigate the physical processes involved in the dynamics of the Radiation Belts.

2. APPLICATIONS

One of the key uncertainties in the radiation belt models is the medium energy ($30 < E < 600$ keV) ion composition of the Earth's ring current (Williams, 1979). The reason is that the major part of the ring current plasma falls in the gap between measurements of ion composition by traditional electrostatic and magnetic deflection systems ($E < \sim 30$ keV) and measurements by differential energy loss in solid state detector instruments ($E > \sim 600$ keV). The IMS-HI incorporates elements of these two traditional techniques to measure directly this important energy/mass range that is not accessible by application of either traditional technique independently.

A knowledge of the ring current ion composition is important from a geophysical standpoint and for obtaining an accurate radiation belt model to correctly predict electronic component and material irradiation effects. It is known, for example, that the irradiation effects on materials such as thermal control surfaces on long-lived satellites is strongly dependent on the mass and energy of the impinging ions. This is particularly important at geosynchronous altitudes.

Lyons and Evans (1976), Spjeldvik and Fritz (1978), and Tinsley (1978) have demonstrated the importance of including ions and neutrals other than protons to explain the decay rates observed in the ring current recovery phase. The ions of the ring current, by charge exchange with thermal hydrogen atoms, become neutrals and can thus escape from the Earth's environment. This is a significant loss process of the ring current medium energy ions. A relatively small percentage of these ions are directed toward the Earth, where they ionize the low latitude atmosphere. These can be used as tracers of the ring current composition.

Low altitude satellite measurements of energetic ions associated with the ring current have been reported by Moritz (1972), Mizera and Blake (1973).

Measuring the ring current energetic neutrals over the regions of space covered by the CRRES orbit will provide additional information on the ring current decay rates, spatial geometry, and temporal changes

weighted by the appropriate cross sections and neutral hydrogen density. Both the direct medium energy ion composition and the indirect neutral atom tracers can by analyzed with the IMS-HI Spectrometer.

3. MEASURING TECHNIQUES

The IMS-HI instrument is based on ion momentum separation in a magnetic field followed by energy and mass defect analysis using an array of cooled silicon solid state sensors as shown in Figure 1a. A photogragh of the instrument is shown in figure 1b. The entrance collimator defines the ion beam angular resolution using a series of rectangular baffles and includes a broom magnet to reject electrons with energy less than 1 MeV.

At the collimator exit the ions enter a 7000 gauss magnetic field and gyrate (mv/qB) onto a set of six passively cooled (-50°C) silicon surface barrier detectors. The technique of cooling solid state detectors for high resolution (< 2 keV FWHM) energetic ion measurements in spacecraft instruments was discussed by Voss et al. (1982) and was successfully demonstrated in the Stimulated Emission of Energetic Particles (SEEP) experiment on the S81-1 satellite (Imhof et al.,1983). The energy range, which varies with ion species, is approximately EM/q^2 = 10-2000 keV-AMU/q^2. A seventh sensor, located directly in line with the collimator, measures energetic neutrals and has an ion rejection of approximately 100 $MeV\text{-}AMU/q^2$. The instrument specifications are given in Table 1.

The instrument features simultaneous mass and energy analysis at relatively large geometrical factors (10^{-3} to 10^{-2} cm^2 ster). Simultaneous measurements of charge states can be identified for each M/q^2 and for the same M/q^2, in some cases, within the solid state detector due to dead zone and mass defect energy losses for equal M/q^2 (for example, O^{++} and He^{+}). Because of the multi sensor design and parallel processing electronics the dynamic range in flux covered is approximately six orders of magnitude.

A simulation of the ion separation in a 7000 gauss magnetic field is shown in the position-energy diagram of Figure 2. The image surface, S, is defined as the arc length, beginning at the collimator, for a radius, R=8 cm.

Solid-state detectors 1-7 are located at angle, Ø, of 40°, 65°, 90°, 115°, 140°, 165°, and 179°, respectively. Solid state detectors 1-6 are n-type silicon having either 20 or 40 grams cm^{-2} of gold surface deposit. The neutral detector is of p-type silicon to improve light rejection and radiation damage sensitivity. The mass defect in solid state detectors results from energy loss of non-ionizing nuclear collisions within the solid that reduce the efficiency of electronic signal generation. The mass defect increases with atomic weight of the nuclei in a well understood way (Forcinal et al., 1968), and causes further mass separation, with commensurate energy scatter, for the heavier nuclei.

The magnet section consists of a yoke, pole pieces, and a SmCo permanent magnet. To produce a homogeneous magnetic field of about 7 kG in the 5-mm gap and minimize weight, the best commercially available magnetic material (SmCo5 with 25 MGOe energy product) is used. The yoke completely surrounds the magnetic field, permitting one to reduce the magnetic resistivity in the return flux section and to minimize the magnetic stray fields. Shape and dimensions are optimized to save weight and to assure a uniform magnetic induction anywhere within the yoke. The resultant complex shape necessitates the use of commercial machining methods to meet the weight requirement and design goal of <~100nT magnetic stray field at a distance of 1 meter. A yoke material (Hyperco 50) that possesses relatively high permeability (2000-4000) at high induction levels (20 kG) was chosen. The weight of the flight magnet assembly is about 5.7 kilograms.

4. FUNCTION BLOCK DIAGRAM

A function block diagram of the IMS-HI is shown in Figure 3. Variable pulse height signals from the ion sensors are each routed for analysis to a peak detector circuit and analog multiplexer. Each peak detector circuit is allowed to track and hold the highest peak value for input pulses below the programmable threshold, V_T, and to hold and stop sampling for input pulses above V_T. The sample interval for each detector is 45 μ sec. The read and reset of each peak detector circuit is controlled by the master clock strobes so that a continuous and sequential scan is made of each detector.

Simultaneous with the reset command, the 256-channel analog-to-digital converter is activated, and the resulting digital pulse height (8 bits) is placed on the address bus of the energy look-up table. Also placed on the address bus of the RAM are the 3 bits that specify which detector is being processed. The content of this memory cell (16 bits) is read into the accumulator, incremented by one, and then read back into the memory cell. An address counter is then used to sequentially step through the entire RAM for telemetry readout. A data compressor packs the 16-bit sum into an 8-bit byte for serial interface with the satellite telemetry.

The two basic modes of instrument operation are Mass Lock and Mass Scan. In the Mass Scan mode, each of the seven solid state sensors is pulse height analyzed into 256 levels of which 64 intervals are accumulated in memory and read out every eight seconds. This mode is used to scan all mass peaks within the range of the sensor relative to the background continuum. In the Mass Lock mode, each of the seven solid state sensors is pulse height analyzed into 256 levels, of which four intervals (typically, four ions) are accumulated in memory and read out every half second. This mode is used for making rapid spectral snapshots of four ions as a function of pitch angle. Baseline operation of the instrument will be a toggle mode (32.768 sec) between the Mass Lock mode and the Mass Scan mode.

5. CALIBRATION

The IMS-HI instrument was calibrated at Goddard Space Flight Center (GSFC) using the low-energy accelerator for ions up to 150 keV. The instrument was mounted on a scan platform in a vacuum chamber at the output end of the accelerator beam line. At a bend in the beam line an electro-magnet was used to select the desired mass after the electrostatic acceleration. A solid-state detector at the entrance to the vacuum test chamber was used to monitor the beam stability. The instrument was calibrated using H^+, He^+, He^{++}, N^+, N^{++} O^+, and O^{++} ions. The neutral detector was calibrated using energetic neutral hydrogen atoms.

To illustrate the instrument performance during calibration the angular and energy scans for H^+ impinging on detector 2 are shown in figure 4. The calibration data are currently being compared to the instrument computer model and to the flight data to arrive at the best-fit calibrations. As indicated in figure 3 the energy passbands are very clean and scattering from the pole pieces is less than 0.2%.

In addition to the accelerator calibrations the instrument was tested with radioactive sources at -30°C in its final flight configuration. Six Tl-204 sources of varying intensities were used to saturate the sensors in a known fashion to calibrate flux rate effects. An internal electronic pulser was also included in the instrument to give several pulse heights of each detector to calibrate gain, linearity, and resolution variations on orbit. It has also been observed in-orbit that when the instrument is illuminated with high fluxes of MeV electrons in the outer belt that K-alpha lines are present and associated with high atomic number materials near the sensors.

Preliminary Flight Results

The instrument design temperatures were achieved in-orbit; -55°C for the magnet and sensors, -12°C for the preamps, and O°C for the electronics box. The sensors noise thresholds were therefore well within specifications. This is shown in figure 5 for detector 1 on orbit 77. Here the primary hydrogen peak is at 18 keV with a noise threshold of about 4 keV and a noise resolution of about 1.5 keV FWHM.

The scaler data for the seven detectors are illustrated in figure 6 for the ring current region (L~2.5) during quite times (orbit 64). At this time the ring current is dominated by medium energy E>100 keV ions. The ion spin modulation is evident in detectors 3 to 6. The background of 20 counts/sec is associated with multi-MeV electrons in the outer belt and cosmic rays. The background rate can be subtracted using an algorithm based on the differential spectrum in each of the seven detectors and the omni-directional MeV electron flux.

The final example of instrument performance is shown in figure 7 for the 64 channel mass spectrum of detectors 2, 3, and 4. These data were obtained on day 238 over a 5 minute interval at L= x.x. The distributions shown are for the raw count rates and do not have noise filtering, efficiencies, and other corrections included. The energy scale is preliminary and represents the deposited energy of the ions in the solid state detector.

The H^+ and He^+ peaks are conspicuous in each of the detectors as noted. The importance of mass defect in the solid state detector is illustrated well in detector 4 for He^+ and O^{++}. Both ions have the same m/q^2 and thus the same energy incident upon the detector (95 keV). Because the oxygen is less efficient at generating electron hole pairs its peak is shifted down from the He^+ peak by about 30 keV. It is well separated from the He^+ and N^+/O^+ peaks. Thus over certain energy and mass intervals the mass defect is an effective method of separating ion beams in a magnetic spectrometer. To obtain the ion flux the penetrating backgrounds and skirts of the strong ion peaks must be properly subtracted using peak analysis software.

ACKNOWLEDGEMENTS

The authors wish to thank F.Hilsenrath, L.A. Hooker, T.C. Sanders, D.A. Simpson, and V.F. Waltz for their efforts in the design, development, and fabrication of this instrument and J. Mobilia, R. A. Baraze, and R. McDonald for their efforts in data analysis. Appreciation is extended to Mr. R.G. Joiner for his program management role of our instruments at ONR. We also deeply appreciate the assistance of Drs. W. L. Imhof, J. M. Quinn, J. B. Reagan, R. M. Robinson, R.D. Sharp, and E.G. Shelley.

The assistance of S. Brown of GSFC was critical to the final calibration of this instrument.

This effort was supported by the Office of Naval Research under contract N00014-83-C-0476 and by the Lockheed Independent Research Program.

Figure Captions

Figure 1. (a) Illustration of ion trajectories in IMS-HI. (b) Photograph of the instrument showing the aperture, semi-circular magnetic field analyzer, and electronics.

Figure 2. Energy of various ions detected by the six detectors in IMS-HI.

Figure 3a. Calibration data for IMS-HI showing the energy (a) and angular resolution (b) for detector 2.

Figure 4. Early flight data from detector 1 showing a strong peak from 18 keV H+.

Figure 5. High time resolution data from IMS-HI showing pitch angle variations of H+ ions at six different energies.

Figure 6. Mass peaks in three different detectors measured by IMS-HI in August 1990.

References

Forcinal, G., Siffert, P., and Coche, A. (1968), Pulse height defects due to nuclear collisions measured with thin window silicon surface barrier detector, *IEEE Trans. Nucl. Sci. (NS-15)*, 475.

Imhof, W.L., Reagan, J.B., Voss, H.D., Gaines, E.E., Datlowe, D.W., Mobilia, J., Helliwell, R.A., Inan, U.S., Katsufrakis, J., and Joiner, R.G. (1983), The modulated precipitation of radiation belt electrons by controlled signals from VLF transmitters, *Geophys, Res. Lett., 10:8*, 615.

Lyons, L.R., and Evans, D.S. (1976), The inconsistency between proton charge exchange and the observed ring current decay, *J. Geophys. Res., 81*:6197.

Meier, R.R., and Weller, C.S. (1975), Observations of equatorial EUV bands: Evidence for low-altitude precipitation of ring current helium, *J. Geophys. Res., 80*:2813.

Mizera, P.F., and Blake, J.B. (1973), Observations of ring current protons at low altitudes, *J. Geophys, Res., 28*:1058.

Mortiz, J. (1972), Energetic protons at low equatorial altitudes: A newly discovered radiation belt phenomenon and its explanation, *J. Geophys, Res., 38*:701.

Spjeldvik, W.N., and Fritz, T.A. (1978), Energetic ionized helium in the quiet time radiation belts: Theory and comparison with observations, J. *Geophys. Res., 83*:654.

Tinsley, B.A. (1978), Effects of charge exchange involving H and H^+ in the upper atmosphere, *Planet. Space Sci., 26*:847.

Voss, H.D., Reagan, J.B., Imhof, W.L., Murray, D.O., Simpson, D.A., Cauffman, D.P., and Bakke, J.C (1982), Low temperature characteristics of solid state detectors for energetic x-ray, ion and electron spectrometers, *IEEE Trans. Nucl. Sci., (NS-29)*:164.

Voss, H.D., and Smith, L.G. (1980), Rocket observations of energetic ions in the nighttime equatorial precipitation zone, *Space Res., 20*:149.

Williams, D.J. (1979), Ring current composition and sources, in *Dynamics of the Magnetosphere*, S.I. Akasofu, Ed., R. Reidel, Dordrecht, Holland, pp. 407-424.

Table 1

Medium Energy Ion Mass Spectrometer (IMS-HI)
Specifications

Analyzer	7KG Magnet (q^2/m) and Mass Defect
Sensors	Silicon Surface Barrier (-55°C)
Number of Imaging Sensors	7 at 0.5 cm^2 each
Look Direction from Spin Axis	75°
Particles and Energy Range:	
Neutrals	10 - 1500 keV
Protons	15 - 2000 keV
Helium	4 - 500 keV
Oxygen	20 - 130 keV
Oxygen ++	20 - 500 keV
Other Ions	E > 20 keV
Number of Differential Mass Channels	64
Number of High Rate Mass Channels	4
Number of Differential Energy Channels	6
Pitch Angle Resolution	4° FWHM
Geometrical Factor	10^{-2} - 10^{-3} cm^2sr
Duty Cyle	100%

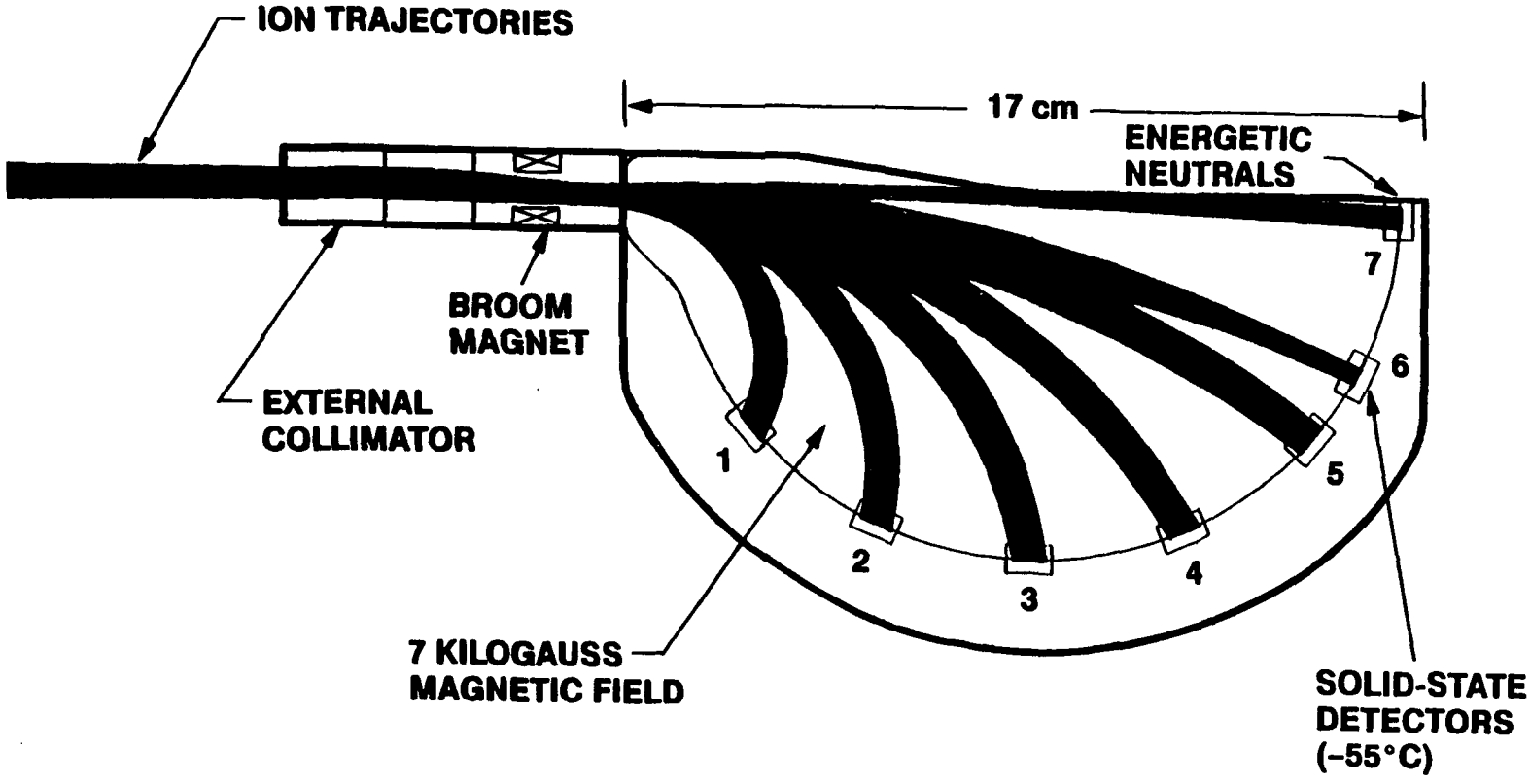
ION TRAJECTORIES
17 cm
ENERGETIC
NEUTRALS
BROOM
MAGNET
EXTERNAL
COLLIMATOR
1
2
3
4
5
6
7
7 KILOGAUSS
MAGNETIC FIELD
SOLID-STATE
DETECTORS
(-55°C)

Figure 1a

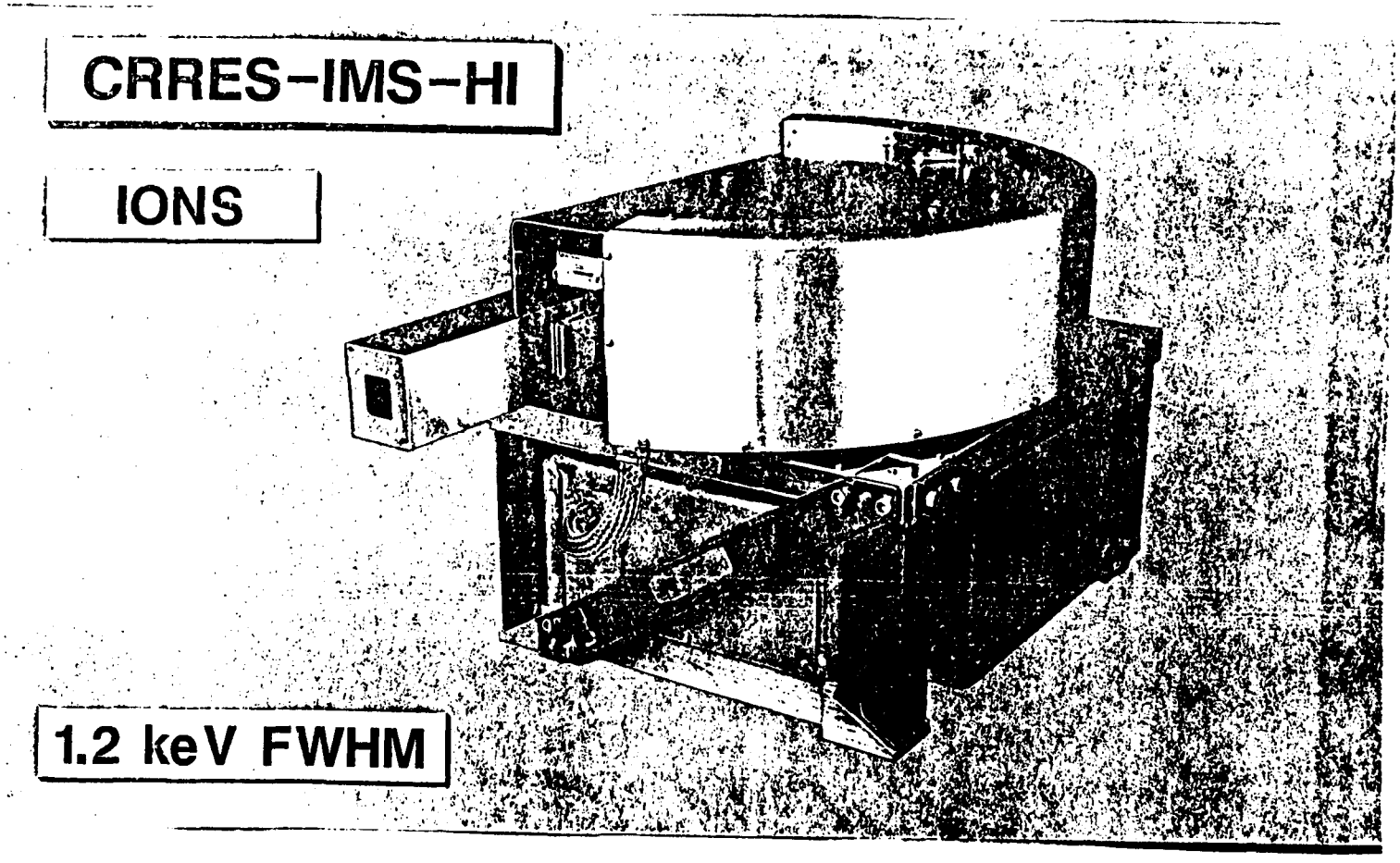

Figure 1b

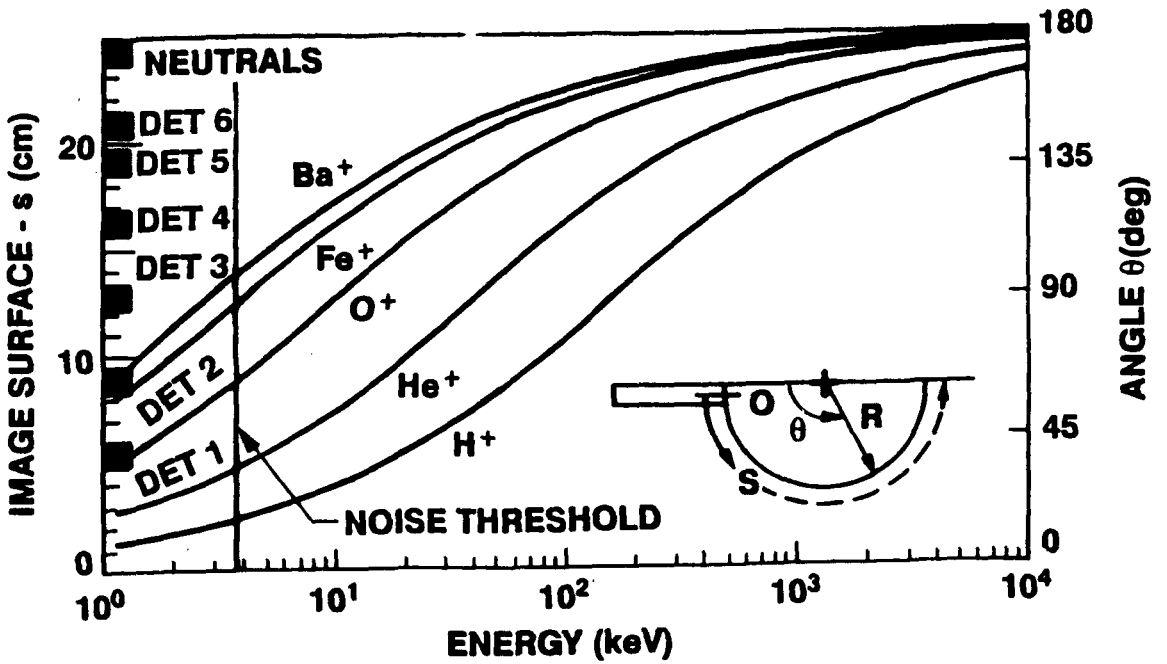
NEUTRALS
DET 6
DET 5
DET 4
DET 3
DET 2
DET 1
Ba+
Fe+
O+
He+
H+
NOISE THRESHOLD
O
θ
R
S
IMAGE SURFACE - s (cm)
20
10
0
ANGLE θ(deg)
180
135
90
45
0
10^0
10^1
10^2
10^3
10^4
ENERGY (keV)

Figure 2

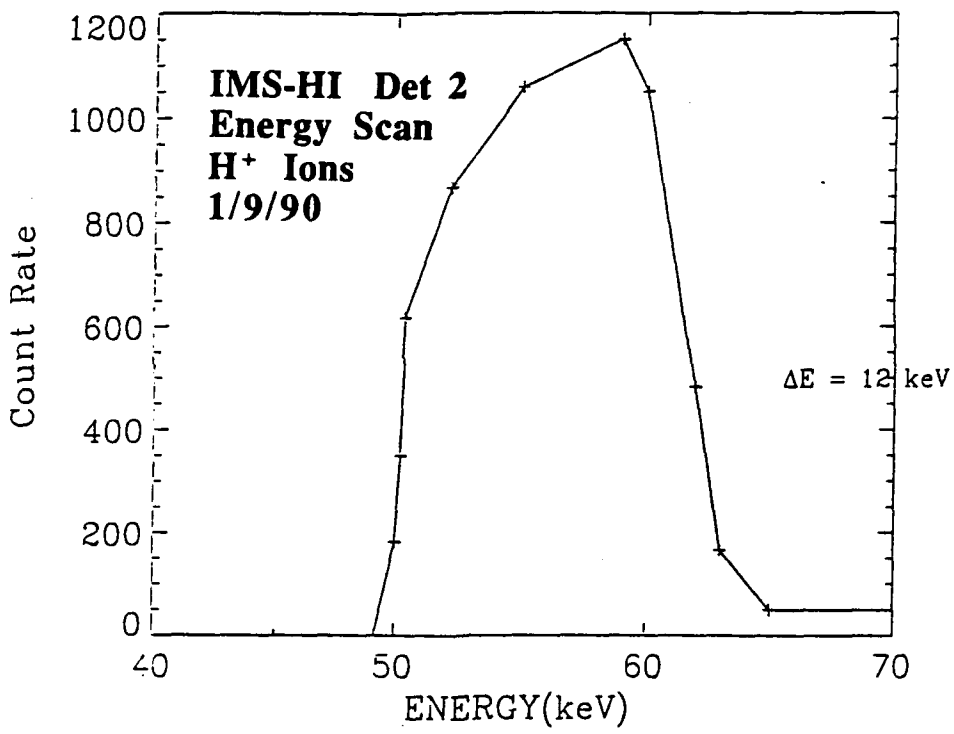
IMS-HI Det 2
Energy Scan
H+ Ions
1/9/90
Count Rate
1200
1000
800
600
400
200
0
40
50
60
70
ENERGY(keV)
ΔE = 12 keV

Figure 3a

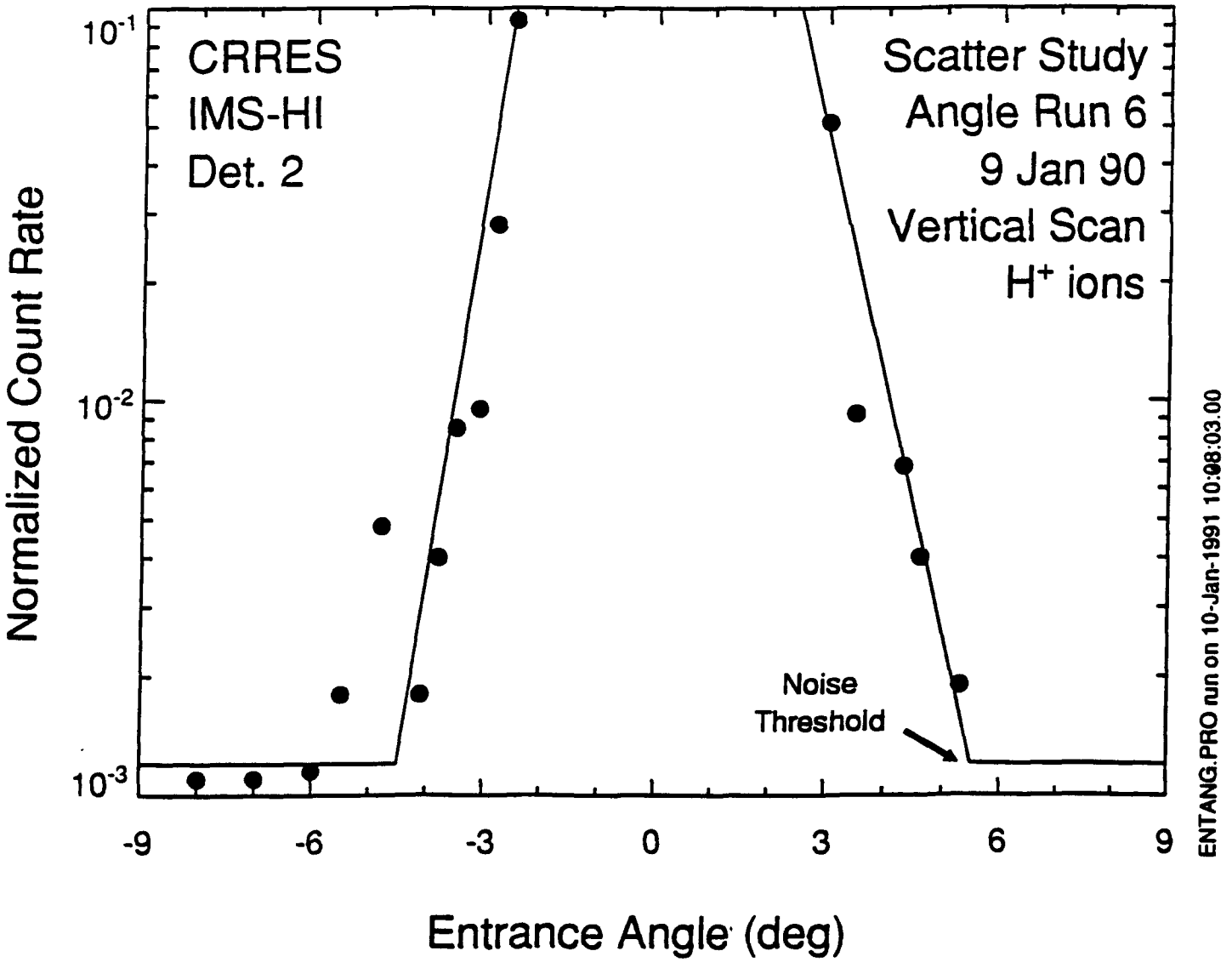
CRRES
IMS-HI
Det. 2
Scatter Study
Angle Run 6
9 Jan 90
Vertical Scan
H+ ions
Noise
Threshold
Normalized Count Rate
Entrance Angle (deg)
10-1
10-2
10-3
-9
-6
-3
0
3
6
9
ENTANG.PRO run on 10-Jan-1991 10:08:03.00

Figure 3b

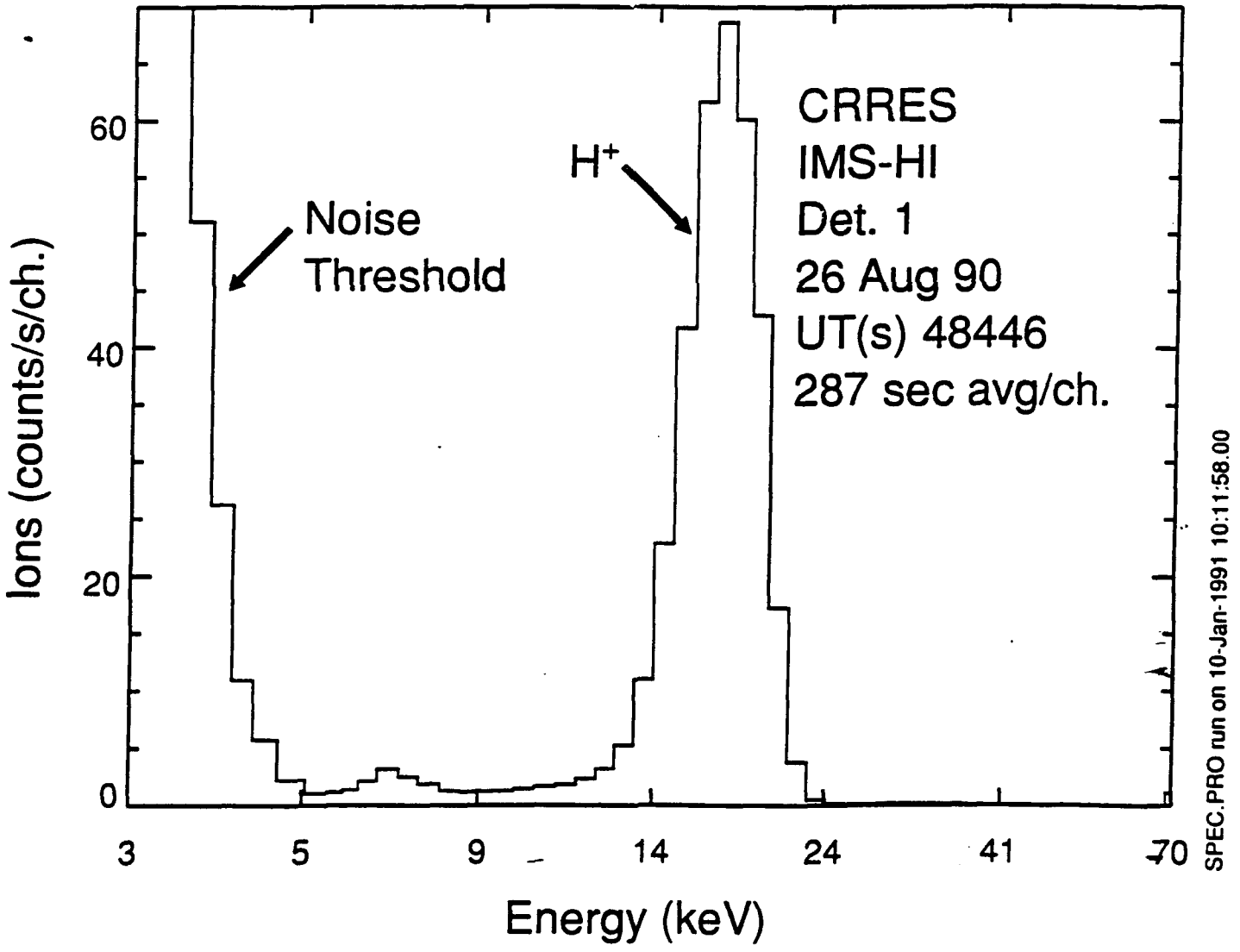
Ions (counts/s/ch.)
60
40
20
0
3
5
9
14
24
41
70
Energy (keV)
Noise
Threshold
H+
CRRES
IMS-HI
Det. 1
26 Aug 90
UT(s) 48446
287 sec avg/ch.
SPEC.PRO run on 10-Jan-1991 10:11:58.00

Figure 4

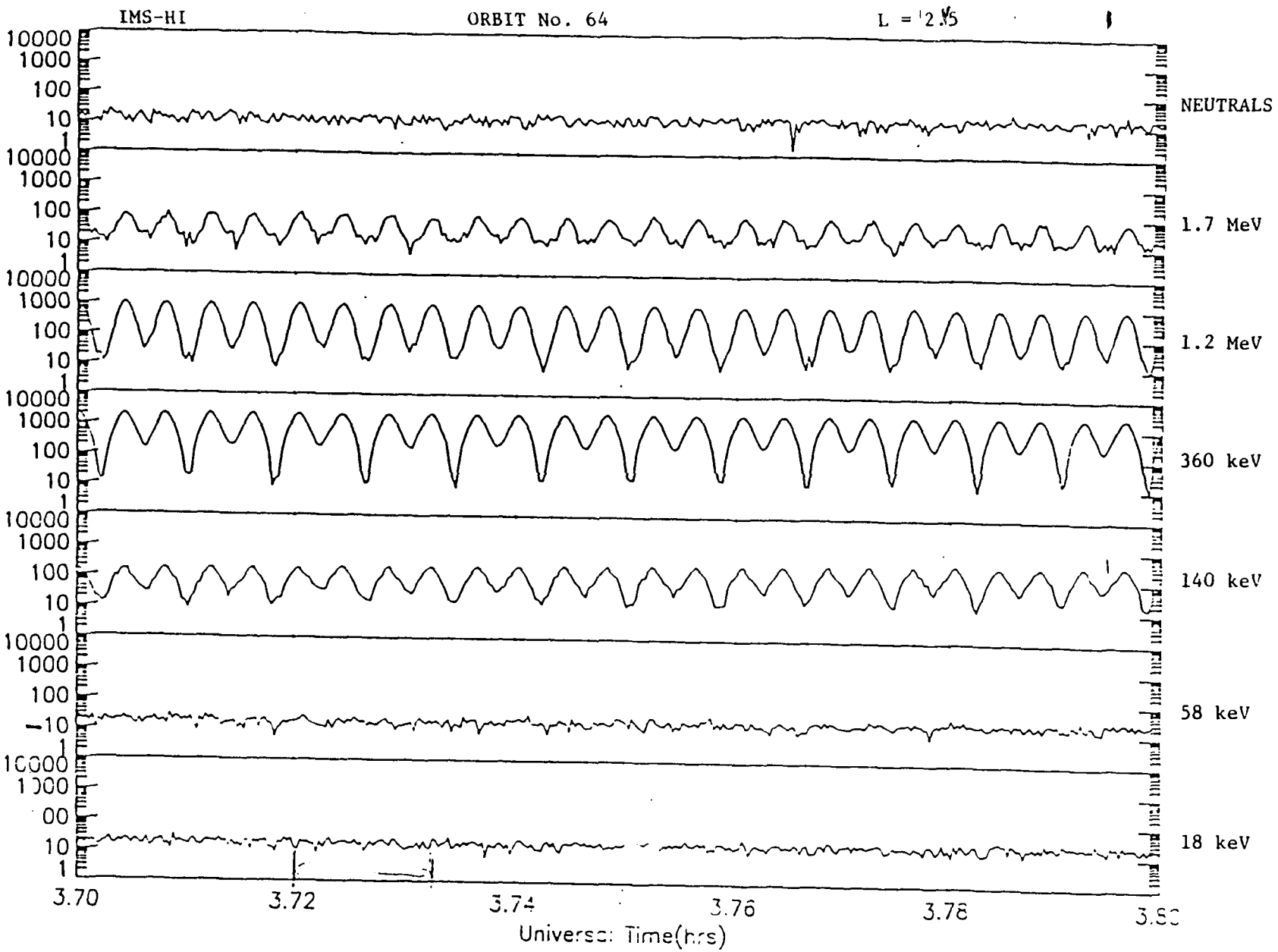
IMS-HI
ORBIT No. 64
L = 12.5
NEUTRALS
1.7 MeV
1.2 MeV
360 keV
140 keV
58 keV
18 keV
3.70
3.72
3.74
3.76
3.78
Universal Time(hrs)

Figure 5

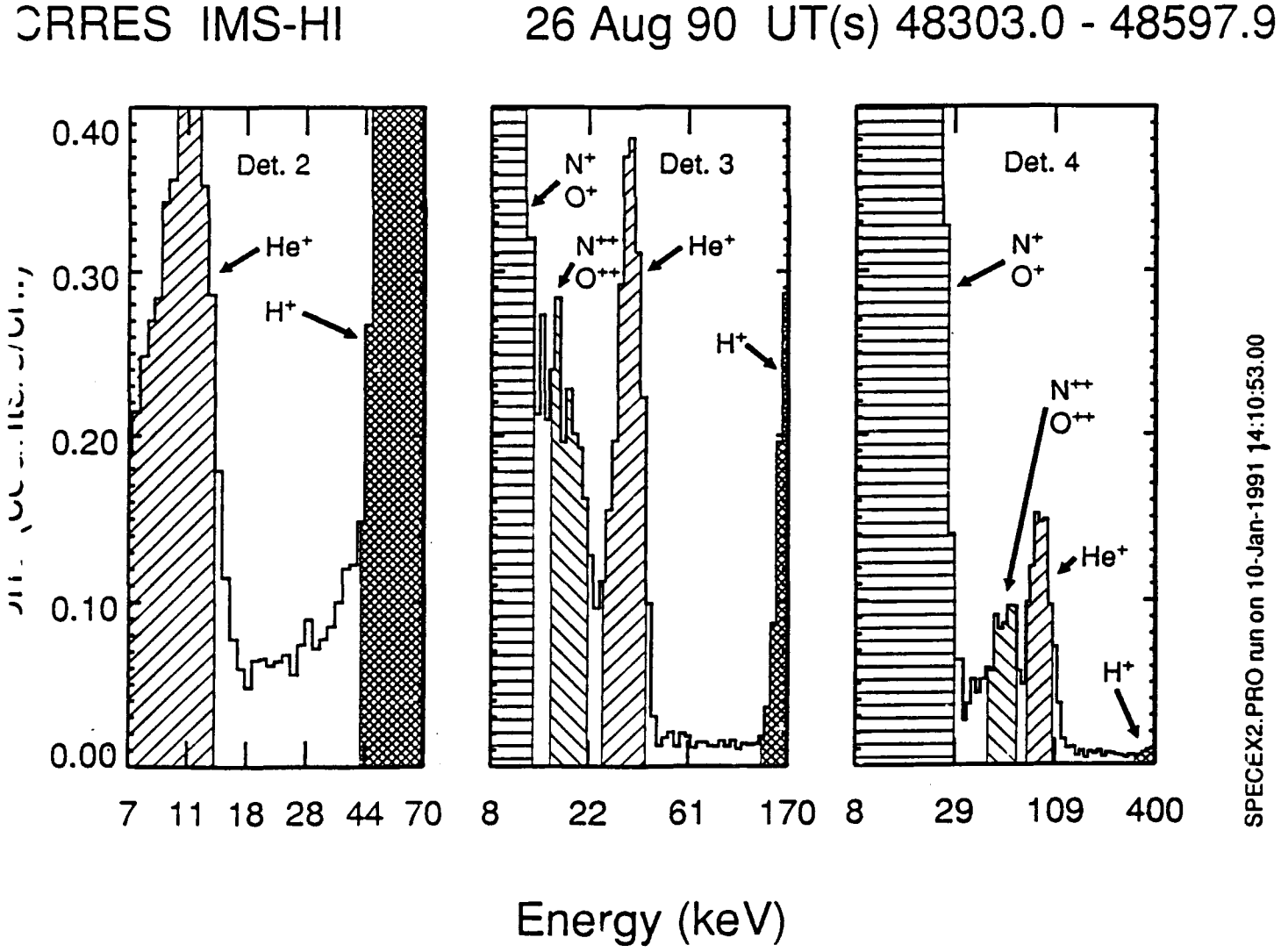
CRRES IMS-HI
26 Aug 90 UT(s) 48303.0 - 48597.9
0.40
0.30
0.20
0.10
0.00
Det. 2
He+
H+
Det. 3
N+
O+
N++
O++
He+
H+
Det. 4
N+
O+
N++
O++
He+
H+
7 11 18 28 44 70
8 22 61 170
8 29 109 400
Energy (keV)
SPECEX2.PRO run on 10-Jan-1991 14:10:53.00

Figure 6

END